Spring 5-15-2016

Superoxide Dismutase 1: Novel Insights on Disease Models and Tissue Specificity in Amyotrophic Lateral Sclerosis

Matthew James Crisp
Washington University in St. Louis

WASHINGTON UNIVERSITY IN ST. LOUIS

Division of Biology & Biomedical Sciences
Neurosciences

Dissertation Examination Committee:
Timothy M. Miller, Chair
Randall Bateman
Marc Diamond
Paul T. Kotzbauer
Conrad C. Weihl
Kevin Yarasheski

Superoxide Dismutase 1: Novel Insights on Disease Models and Tissue Specificity in Amyotrophic Lateral Sclerosis

by
Matthew James Crisp

A dissertation presented to the
Graduate School of Arts & Sciences
of Washington University in
partial fulfillment of the
requirements for the degree
of Doctor of Philosophy

May 2016
St. Louis, Missouri

TABLE OF CONTENTS

LIST OF FIGURES

CHAPTER 2

CHAPTER 3

LIST OF TABLES

CHAPTER 2

CHAPTER 3

LIST OF ABBREVIATIONS

ALS	Amyotrophic lateral sclerosis
C9ORF72	Chromosome 9 open reading frame 72
CNS	Central nervous system
CSF	Cerebrospinal fluid
DM	Degenerative myelopathy
FCR	Fractional catabolic rate
FSR	Fractional synthetic rate
FTD	Frontotemporal dementia
FTR	Fractional turnover rate
FUS	Fused in sarcoma
GWAS	Genome-wide association study
LMN	Lower motor neuron
MFL	Mole fraction labeled
MTOR	Mammalian target of rapamycin
M/Z	Mass-to-charge ratio
NEDL1	NEDD4-like ubiquitin protein ligase-1
OPTN	Optineurin
PFN1	Profilin 1
RAN	Repeat-associated non-ATG
SILK	Stable isotope labeling kinetics
SOD1	Superoxide dismutase 1
SQSTM1	Sequestosome 1
TARDBP	TAR DNA binding protein 43
TDP-43	Transactive response DNA-binding protein 43
TTR	Tracer:tracee ratio
UBQLN2	Ubiquilin-2
UMN	Upper motor neuron
UPS system	Ubiquitin-proteasome
VCP	Valosin-containing protein
WT	Wild-type
YFP	Yellow fluorescent protein

ACKNOWLEDGMENTS

This dissertation contains work funded in part from the following sources: K08NS074194, NIH/NINDS/AFAR (to TMM), R01NS078398 NINDS (to T.M.M), R21NS078242 NIH/NINDS (to JRC), P41GM103422 to Washington University Biomed MS resources, and F31NS078818 NIH/NINDS (to MJC). Funding was also provided by AKC Canine Health Foundation Grants #821 and #1213A, ALS Association grant #6054, and CARS grant 5UL1 RR024992-02.

A consequence in choosing the long path that is MD/PhD training is the impressive number of people that have had an impact on me both professionally and personally. Some of these people have served very direct roles on my scientific development, some have been travelers on parallel roads, and some work their magic unseen to ease the passage. They have all been amazing.

Foremost, I must thank my mentor, Tim Miller. His optimism is pathological, probably enough to warrant an additional section in the next revision of the Diagnostic and Statistical Manual. Despite my intrinsic scientific pessimism, he always managed to excite me about science – no small feat, as my flavor of realism has been imbued with scintillating false starts and failures. He allowed me the autonomy I needed while simultaneously grounding my ideas. He taught me the value of politics in science (a once apprehensive subject) and that the best ideas aim big (and sometimes fail big). As I continue on with my career, I have no doubt that I will continue to find bits of his influence in who I have become, like grains of sand found long after a stay on the beach.

I must also thank my collaborators, without whom the projects detailed in this thesis would never have germinated. A large thank you goes out to Kwasi Mawuenyega

in the Bateman lab for his mass spec virtuosity, infectious laugh, and deep well of patience at my naïveté. I also owe many thanks to Bob Chott in the Yarasheski lab for processing over 500 samples over the course of a year and a half. I owe the salvation of the half-life project to Bruce Patterson, who took the data and the trends we were seeing and applied the rigors of kinetic modeling to turn visual observations into a cold, numerical output. For the canine SOD1 project, I must thank Joan Coates at the University of Missouri Columbia for providing valuable samples and input, as well as Jeff Beckett for sticking by me for a summer tirelessly counting cells.

Thanks are also necessary for the Miller Lab members, past and present, who have made lab like a second home. I must first thank Quan Li for being an amazing mentor to me when I first joined the lab. I must also thank Erica Koval and Sarah DeVos for taking the plunge with me into the then new Miller Lab and being excellent companions along the way. Together, as The First Ones, we hacked through graduate school with a dull machete, leaving an indelible track for those future souls who, like us, seek high risk autonomy, projects with potential to reach dizzying heights with foundations akin to a well-played game of Jenga, and a mentor with a Bill Gates propensity for funding our insane ideas. And of course I owe much to the succeeding generation of Miller Lab members – Wade Self, Mariah Lawler – who reminded me of my enjoyment of teaching (and A Song of Ice and Fire) on a frequent basis.

There are so many others involved in my training to acknowledge. The faculty and co-laboratories of the Neuromuscular Division were second-to-none in their collaborative efforts and pleasant demeanors. My thesis committee, many of who were intrinsic to the SOD1 turnover project, has been enormously helpful. Of course I cannot

forget the staff that run the Medical Scientist Training Program – Brian, Christy, Liz, Linda, Wayne. They are the soul of this program and, honestly, bare the most credit for it being the best MSTP in the country.

Lastly, my sincerest gratitude extends to family. My parents, Jim and Jennifer Crisp, have been unwavering in their support of all my decisions to pursue education indefinitely. My siblings, Mike and Tim, and their families serve as a constant reminder of the importance of family. Finally, and most importantly, I owe the most gratitude to my wife, Jennifer, and sons, Simon and Ian. No accomplishment in the pages to come could amount to the value they bring to my life. I love them and owe them everything.

Matthew J. Crisp

Washington University in St. Louis

May 2016

ABSTRACT OF THE DISSERTATION

Superoxide Dismutase 1: Novel Insights on Disease

Models and Tissue Specificity in Amyotrophic Lateral Sclerosis

by

Matthew James Crisp

Doctor of Philosophy in Biology and Biomedical Sciences

Neurosciences

Washington University in St. Louis, 2016

Professor Timothy Miller, Chairperson

Mutations in superoxide dismutase 1 (SOD1) are known to cause dominantly-inherited amyotrophic lateral sclerosis (ALS), a rapidly-fatal adult-onset neurodegenerative disorder defined by motor neuron loss and progressive paralysis. In the past twenty years, research into the disorder has been driven by the creation of numerous transgenic animal models that have yielded multiple theories on the pathogenesis of the disease. Patients and animal models with SOD1 mutations express the defective protein in every cell, yet the disease only affects tissues in the neuromuscular axis. In this dissertation, I present original work exploring two aspects of SOD1 ALS. The first details the biochemical characterization of recently discovered canine SOD1 mutations that have been found to cause canine degenerative myelopathy (DM), the only naturally occurring non-human ALS model. My research showed that, like in human ALS and transgenic rodent models, canine DM is accompanied by an increase in detergent-insoluble mutant SOD1 in the spinal cords of diseased animals.

Also, these mutations retained full enzymatic activity and aggregate in cell culture, confirming that a toxic gain-of-function mechanism is at play in this model. The second part of this dissertation describes research into the tissue specificity of the disease. By developing a novel stable isotope labeling kinetics (SILK) method to measure long-lived proteins, I was able to determine the turnover rate of wild-type, mutant, and misfolded SOD1 in rodent tissues both affected and unaffected in disease and in cerebral spinal fluid (CSF) from healthy human subjects. The results indicated that SOD1 is a long-lived protein with significantly slower turnover in the tissues most affected in ALS. In agreement with studies *in vitro*, the turnover rates for mutant and misfolded SOD1 were accelerated compared to wild-type protein, reflecting increased protein instability; yet a significant difference in turnover between affected and unaffected tissues remained. Finally, by applying this novel SILK method to human subjects, I was able to confirm that SOD1 is a long-lived protein in human CSF and, by extension, in the central nervous system. These results validate the first method for measuring SOD1 turnover *in vivo* and strongly suggest an important role for the slow turnover of SOD1 in the tissue specificity of the ALS.

PREFACE

The contents of this dissertation represent the culmination of four years as a graduate student, six years as an MD/PhD student, and, although unrelated in content, almost ten years as a scientist-in-training. Although united under the common theme of SOD1 and ALS, the original works described herein focus on a two very different pieces in the ever-expanding story of this disease. I have written this dissertation with the goal of carving out the places in the field where these different pieces fit. As such, this document is not an all-inclusive dossier of the literature (a herculean task), but a distillation of the relevant pieces needed to understand how these findings expand our knowledge in the field of SOD1 ALS. My hope is not only that the reader find conclusive evidence for the awarding of a doctoral degree, but that he or she leave with the inspiration needed to take this field further to its logical conclusion – an understanding and cure for ALS. The basis of this dissertation derives from the following original work. Published works have been reprinted with the publisher's permission.

Crisp, M. J., Beckett, J., Coates, J. R., & Miller, T. M. (2013). Canine degenerative myelopathy: Biochemical characterization of superoxide dismutase 1 in the first naturally occurring non-human amyotrophic lateral sclerosis model. *Experimental Neurology* (248):1–9. PMID 23707216

Crisp, M.J., Mawuenyega, K.G., Patterson, B.W., Reddy, N.C., Chott, R., Self, W.K., Weihl, C.C., Jockel-Balsarotti, J., Varadachary, A., Buccelli, R., Yarasheski, K.E., Bateman, R.J., & Miller, T.M. (2015). In vivo kinetic approach reveals slow SOD1 turnover in the CNS. *Journal of Clinical Investigation* 125(7):2772-80. PMID 26075819

“For me, I am driven by two main philosophies: know more today about the world than I knew yesterday and lessen the suffering of others. You’d be surprised how far that gets you.”

– Neil deGrasse Tyson

“Absorb what is useful, discard what is not, add what is uniquely your own.”

– Bruce Lee

Chapter 1

The Role of Superoxide Dismutase 1 in Amyotrophic Lateral Sclerosis

Amyotrophic lateral sclerosis (ALS), colloquially known as Lou Gehrig's disease, is an adult-onset neurodegenerative disorder characterized by the loss of motor neurons in the spinal cord and cortex, resulting in a progressive paralysis and death on average 2-3 years after symptom onset (Kiernan et al. 2011). With an incidence of 1.5 - 2.7 cases per 100,000 in North America and Western Europe, ALS is the third most common neurodegenerative disorder after Alzheimer's and Parkinson's diseases and the most common motor neuron disease (Worms 2001). Almost universally fatal, the only FDA-approved treatment is Riluzole, a drug that prolongs survival by 2-4 months (Cheah et al. 2010). Initially named in the medical literature in 1874 by the prominent French physician Jean-Martin Charcot, it was not until 1993 that the first genetic link to the disease was discovered in a gene coding for superoxide dismutase 1 (SOD1) (Rosen et al. 1993, Rowland 2001). This seminal discovery marked the beginning of an ever-accelerating period of biomedical research into the disease that has resulted in the discovery of additional causative genes, the creation of numerous animal models, and the development of hypotheses into molecular mechanisms and potential treatments. However, despite over two decades of fervent research, a cure remains elusive and no consensus has emerged on the pathogenesis of the disease.

This dissertation will introduce the clinical, pathological, and genetic features of SOD1-mediated ALS, discuss the information obtained from the creation and study of numerous animal models as well as their advantages and disadvantages, detail the tissue specificity of the disease, describe the mechanisms for SOD1 protein turnover, and introduce stable isotope labeling kinetics (SILK). It will then describe work performed by the author on the biochemical characterization of SOD1 in canine

degenerative myelopathy, the most recently discovered and only naturally occurring SOD1 ALS model. Then, it will detail studies on SOD1 protein turnover in both a rodent ALS model and in human subjects as a window into the tissue specificity of the disease. Finally, it will discuss implications of the research in the study of ALS and pertinent future directions.

Clinical, Pathological, and Genetic Features of ALS

ALS is an adult onset neurological disorder characterized by the progressive loss of motor neurons. The clinical presentation of the disorder involves both upper motor neuron (UMN) and lower motor neuron (LMN) signs. The site of initial weakness varies widely among patients, with approximately 70% of patients presenting with unilateral limb onset, approximately 25% presenting with bulbar onset, and 5% presenting with respiratory onset (Kiernan et al. 2011). From there, the disease spreads to neighboring segments along the neuraxis as additional motor neurons die, resulting in an expanding paralysis that eventually affects the muscles of respiration. Most patients ultimately succumb to respiratory failure or sequelae from voluntary placement on a respirator approximately 2-3 years after disease onset. Sensory deficits can occur in about 32% of patients, but these manifestations arise late in the disease and may be complications of immobility (Hammad et al. 2007). Interestingly, certain motor neuron populations are generally resistant to degeneration until late in the disease, such as those that control the pelvic sphincter (Onuf's nucleus) and extraocular muscles. It has been recently shown that these resistant neurons lack the expression of metalloproteinase-9 (Kaplan et al. 2014).

Studies have revealed that between 35 and 51 percent of ALS patients display cognitive impairment (Lomen-Hoerth et al. 2003, Massman et al. 1996, Ringholz et al. 2005). Due to overlap between disorders, many have proposed that ALS exists on a spectrum with frontotemporal dementia (FTD), a disorder characterized by changes in social behavior, personality, or language that accompany degeneration of the frontal and temporal lobes (McKhann 2001). The strongest evidence for the ALS-FTD spectrum is genetic, with mutations in C9ORF72, TARDBP, FUS, OPTN, and UBQLN2 causing familial cases of both ALS and FTD (Robberecht & Philips 2013). Both disorders can also share similar pathology, dominated by ubiquitinated inclusions that contain the mutant protein. The fact that ALS and FTD can coexist is a double-edged sword in terms of understanding the mechanism of disease. On one side, unification of two previously separate disorders has the potential to extend biological findings to a wider set of patients. Conversely, the spectrum of ALS-FTD presentations, disease courses, and genetic factors greatly increases the complexity of the disease and decreases the likelihood of finding a sole mechanism.

The pathology of ALS is characterized by the loss of UMN and LMN in the motor cortex and spinal cord, respectively. Reactive gliosis, most evident in the corticospinal tracts, occurs concomitantly as neurons are lost. Histologically, a percentage of the remaining LMNs possess skein-like inclusions, Lewy body-like round inclusions, basophilic inclusions, and, more specific to the disease, Bunina bodies, which are eosinophilic inclusions composed of the proteins cystatin C and transferrin (Okamoto et al. 2008). With the exception of Bunina bodies, intracellular inclusions stain positive for ubiquitin and p62. The presence of additional proteins found in the inclusions, such as

SOD1, C9ORF72, TDP-43, FUS, OPTN, UBQLN2, and others, depends on the specific genetic or pathological subtype of the disease (Fecto & Siddique 2011). Many of these proteins are present in inclusions in FTD as well. As the genetic or pathological causes of ALS are clinically indistinguishable and are universally marked by intracellular inclusions, many have speculated to a common mechanism of disease.

Approximately 90% of ALS is sporadic with no known family history. Inherited forms comprise the remaining 10% of cases and have been the major driving force behind research (Mitchell & Borasio 2007). The first gene linked to ALS, SOD1, was initially described in 1993 and remained the only known causative locus for over a decade, accounting for approximately 20% of familial ALS at the time (Rosen et al. 1993). However, the past eight years have witnessed an explosion in the number of discovered genetic causes of ALS to the point where a known genetic etiology accounts for about 68% and 11% of familial and sporadic cases, respectively (Renton et al. 2014). Currently, nine genes have been found to cause ALS, with an additional thirteen implicated in the disease. These genes have a diverse set of functions, including RNA metabolism (TDP-43 and FUS), protein clearance (SQSTM1, VCP, and UBQLN2), vesicle trafficking and cytoskeletal dynamics (OPTN and PFN1), and superoxide metabolism (SOD1). Hexanucleotide repeat expansions in C9ORF72, a gene of unknown function, were recently discovered and account for the largest portion of familial ALS at 40% (DeJesus-Hernandez et al. 2011, Renton et al. 2011). As noted above, with the exception of SOD1, many of these genes have also been found to cause familial forms of FTD. If ALS and FTD exist on a spectrum, then SOD1-mediated

disease marks the purely motor, classically described ALS at one edge of this continuum.

Superoxide Dismutase 1: The First Genetic Link to ALS

Rosen and colleges initially described 11 different mutations in the SOD1 gene responsible for autosomal dominant familial ALS in 1993, revealing the first genetic cause of the disease (Rosen et al. 1993). Since that time, the number of mutations that have been described number greater than 160 (for an updated list of mutations, see http://alsod.iop.kcl.ac.uk/). SOD1 is a 153 amino acid Cu,Zn-metalloenzyme whose physiological function is the detoxification of superoxide free radicals into hydrogen peroxide and molecular oxygen. Dimerization is required for its function. The protein itself contains eight beta sheets interspersed with connecting loops, two intrachain disulfide bonds, and metal binding regions. Mutations occur at random throughout the protein and impart various degrees of insult to SOD1 structure and function. Some mutations disrupt the ability of the protein to bind cations or form dimers, rendering it enzymatically inactive and relatively unfolded, while others fall in regions with no functional enzymatic deficit. All mutations demonstrate a decrease in protein stability, as measured by numerous *in vitro* studies with recombinant SOD1 (Münch & Bertolotti 2010, Rodriguez et al. 2002, Tiwari & Hayward 2003). However, there is currently no relationship between the degree of protein instability or enzyme function and disease course (Ratovitski et al. 1999).

SOD1 mutations remain the second most common cause of familial ALS after the recently discovered hexanucleotide repeat in C9ORF72. The most recent figures

estimate that SOD1 mutations account for 12-20% of familial ALS (Renton et al. 2014, Robberecht & Philips 2013). Among the handful of genes that cause ALS, mutations in SOD1 are unique in that they present with a purely motor, classical type of ALS with no cognitive deficits. Pathologically, the intracellular inclusions in SOD1 ALS motor neurons do not stain positive for TDP-43, FUS, OPTN, or the RAN translation products of C9ORF72 that are shared by the majority of familial and sporadic cases. Conversely, the SOD1 inclusions that characterize SOD1 ALS are almost never seen in familial or sporadic cases involving those other proteins. These clinical and pathological differences indicate that SOD1 ALS falls on the extreme end of the ALS-FTD spectrum, offering a unique window into the purely motor aspect of the disease.

Since SOD1 was a well-known protein involved in reducing oxidative stress, the logical hypothesis that followed the initial discovery of SOD1 was that ALS resulted from a loss of enzymatic function (McNamara & Fridovich 1993). The development of ALS animal models soon put this hypothesis to rest. The first transgenic ALS mouse model was created in 1994 and overexpressed the human SOD1 mutation G93A (Gurney et al. 1994). This mouse developed progressive motor deficits that recapitulated those seen in human ALS, including weight loss, muscle spasticity, hindlimb weakness, and muscle atrophy that ultimately resulted in death around four months of age. These motor deficits were accompanied by pathological changes in the spinal cord that included loss of motor neurons, gliosis, and the presence of SOD1 G93A aggregates (Dal Canto & Gurney 1995). The G93A mouse was created with endogenous levels of mouse SOD1 with an enzymatically active mutant, indicating that a loss of activity was not responsible for disease. Furthermore, the SOD1 knockout mouse did not display

any signs of disease (Reaume et al. 1996). The results from these studies directed the field to focus on a toxic gain-of-function as the pathogenic mechanism of SOD1-mediated ALS.

Modeling Disease

In the twenty years since mutations in SOD1 were found to cause ALS, numerous animal models expressing a wide range of SOD1 mutants have been created. These models have proven invaluable in learning about the pathogenesis of the disease and in screening potential treatments. Although the most common SOD1 ALS model is the original Gurney mouse overexpressing the human SOD1 G93A transgene, the field has borne witness to the development of additional models in the mouse, rat, zebrafish, fly, worm, and the discovery of SOD1-mediated naturally occurring disease in the dog. Each model carries its own advantages and disadvantages that range from the more general (e.g. size, lifespan, ease of creation) to more disease specific (e.g. presentation, course, pathology) (Joyce et al. 2011). As SOD1 ALS is an autosomal dominant disease that takes decades to manifest, an interesting way to look at the available ALS models is to categorize them based on a spectrum of most artificial to most physiological. Models thus fall into three distinct categories: artificial human transgenic models, artificial endogenous transgenic models, and naturally occurring models. Each has offered valuable information into the nature of the disease.

Artificial human SOD1 transgenic models

The logical first step in developing an animal model of most autosomal dominant diseases is the insertion of the mutant human transgene into an animal. Thus, the first ALS models were constructed in mice and expressed transgenic human SOD1 in addition to endogenous mouse SOD1. Currently, over sixteen transgenic mouse models have been created with ubiquitous SOD1 expression, twelve of which express naturally occurring SOD1 mutations, two that express double or quadruple mutations, and two that express human SOD1 WT (Turner & Talbot 2008). Most of these models include the full genomic sequence of human SOD1 with its endogenous promoter and requires multiple copies for disease onset. However, cDNA driven expression has been shown to cause disease in SOD1 G37R mice bred to homozygosity (Wang et al. 2005). Both the onset and progression of disease in each mouse model vary depending on the nature and expression level of the mutation. For example, mice overexpressing SOD1 G93A, G37R, and H46R mutations begin to show signs of disease onset at 3-5 months of age that progresses to end stage in 1-2 months (Chang-Hong et al. 2005, Gurney et al. 1994, Wong et al. 1995). SOD1 G85R and G127X models express lower levels of the mutant protein despite multiple copies of the transgene and show signs of disease onset at 8 to 14 months with very rapid progression (Bruijn et al. 1997, Jonsson et al. 2004).

Although uncommon, rats overexpressing human SOD1 WT, G93A, or H46R transgenes have also been created (Aoki et al. 2005, Chan et al. 1998, Nagai et al. 2001). The relative size of these animals over mice allows for experiments involving surgical manipulations or CSF collection. While the SOD1 WT rats show no signs of

disease, the mutant animals recapitulate the disease phenotype seen in the corresponding mouse models quite well, with the exception that limb involvement can begin with either the hindlimb or forelimb. Like their murine counterparts, disease onset is dependent on transgene copy number and the nature of the mutation.

Modeling ALS in lower organisms with human SOD1 transgenes has reproduced the motor deficits seen in rodent models and human disease. Insertion and overexpression of a CMV driven human SOD1 G93A transgene in zebrafish resulted in swimming deficits and motor neuron loss preceded by neuromuscular junction and axonal damage (Sakowski et al. 2012). In flies, selective overexpression of human SOD1 WT, A4V, and G85R resulted in climbing defects, conduction defects, and an increased stress response in glia (Watson et al. 2008). However, no motor neuron loss or reduction in lifespan were observed, which may be due to the non-cell autonomous nature of the disease; mouse studies with selective pan-neuronal or motor neuron expression also failed to demonstrate motor neuron loss (Lino et al. 2002, Pramatarova et al. 2001, Wang et al. 2008). In worms, ubiquitous expression of human SOD1 mutant transgenes, but not SOD WT, imparts a greater sensitivity to oxygen free radical damage produced by paraquat (Oeda et al. 2001). Pan-neuronal expression of SOD1 demonstrated mutant specific neuronal aggregates, locomotion impairments, and defects in synaptic transmission (Wang et al. 2009). Others have used selective expression in worm body wall muscles to show aggregation propensity of particular SOD1 mutants is modulated by genetic background or environmental stress (Gidalevitz et al. 2009, Oeda et al. 2001).

Overall, ALS animal models overexpressing transgenic human SOD1 mutants have been the major driving force for research. For example, the SOD1 G93A mouse model remains the tried and true standard for the disease to this day due to its relatively rapid, predictable, and uniform disease onset and progression. One fundamental caveat with these models is the artificial nature of their existence. This artificiality is evident in that multiple copies of the transgene are required for disease and that the number of copies dictates disease course. This is in stark contrast to human ALS, where pathogenesis only requires a single mutant copy. Another consideration is the insertion of a human gene into a model background. This was a concern in the development of the SOD1 A4V mouse, which failed to develop disease unless it was crossed with a transgenic SOD1 WT mouse (Deng et al. 2006). The existence of a few studies where overexpression of human SOD1 WT also resulted in pathology suggest that high levels of the SOD1 protein itself is toxic (Graffmo et al. 2013, Jaarsma 2006, Jaarsma et al. 2000). Regardless, transgenic human SOD1 mutant models offer the most reliable, well characterized, and translatable disease model for laboratory research.

Artificial endogenous SOD1 transgenic models

Though not nearly as numerous as ALS models expressing the human SOD1 transgene, a couple animal models have been developed that overexpress mutations in endogenous SOD1. The most noteworthy case is the SOD1 G86R mouse, which overexpressed a missense mutation in murine SOD1 (mSOD1) at a residue conserved in human SOD1. This was actually the first ALS model mouse created but published a few months after the Gurney SOD1 G93A mouse (Ripps et al. 1995). Like its human

transgenic SOD1 G93A counterpart, it developed hindlimb paralysis and tail spasticity around 3-4 months of age accompanied by motor neuron loss, SOD1 aggregates, and reduced survival. The other example was in zebrafish that overexpressed native SOD1 WT or a SOD1 G93R mutation under the SOD1 promoter. These fish displayed mutant-dependent motor deficits, SOD1 aggregates, early NMJ loss, progressive motor neuron loss, and reduced survival (Ramesh et al. 2010).

These models offer insight into the role that SOD1 plays in motor neuron degeneration across species. SOD1 is highly conserved in eukaryotes, implying that changes in its primary sequence have not been well tolerated throughout evolution. Indeed, the fact that over 160 mutations in more than 70 out of 153 residues have been discovered to cause protein misfolding in human ALS suggests that the folded structure of SOD1 is intolerant to perturbation. In the least, the fact that mutations in the endogenous SOD1 of mice and zebrafish replicate human disease raises the possibility of an evolutionarily conserved mechanism for motor neuron degeneration. Such a finding offers strong validation for both human and endogenous SOD1 transgenic models of disease. Interestingly, however, crossing the mSOD1 G86R mouse with the transgenic hSOD1 WT mouse does not increase disease progression, unlike studies with hSOD1 mutant and WT double transgenic mice (Audet et al. 2010). Biochemically, mSOD1 and hSOD1 do not interact as indicated by the lack of detectable chimeric heterodimers or aggregates in these double transgenic animals. Recent evidence shows that the primary sequence divergence, specifically the tryptophan-32 residue unique to hSOD1, may account for this phenomenon (Grad et al. 2011). Overall, species-specific SOD1 mutations offer a unique angle into some of the more recently

proposed mechanisms of disease, such as cellular uptake of the mutant and the propagation of misfolded species.

Naturally occurring models

While the transgenic ALS models described above have contributed important information to the potential mechanisms of SOD1 ALS in the timescales required for typical laboratory research, they remain artificial in their dependence on the expression of multiple transgene copies. Transgenic models are also poor choices in trying to model the effects of age or environment on ALS in the background of short lifespans. After all, a major risk factor for the development of ALS is age. Specifically, the incidence of ALS increases with age, especially after the 4^{th} decade, and peaks at age 74, indicating that environment or age-related factors play a significant role in developing disease (Worms 2001).

In 2009, genome-wide association studies (GWAS) linked a mutation in canine SOD1 (cSOD1) to cases of canine degenerative myelopathy (DM) in multiple dog breeds (Awano et al. 2009). Two years later, another group found a second cSOD1 mutation in a Bernese Mountain dog with canine DM (Wininger et al. 2011). Canine DM affects multiple dog breeds toward the latter half of their lifespan and is characterized by an often asymmetric onset of paraparesis and ataxia in the hind limbs that progresses to paraplegia and muscle atrophy within one year from onset of signs. Although the entire course of the disease can last as long as 3 years, many owners elect for euthanasia. However, those dogs that have been allowed to progress show ascension of the disease to include the forelimbs, ultimately resulting in flaccid tetraplegia and

dysphagia (Coates & Wininger 2010, Shelton et al. 2012). Histopathology of spinal cords from affected dogs show a similar pattern of myelin and axonal loss and astrogliosis seen in human ALS, and immunohistochemistry reveals the same SOD1 aggregates in motor neurons that are present in humans and rodent models with hSOD1 mutations. Interestingly, unlike human ALS, canine DM is mostly autosomal recessive – a small amount of dogs heterozygous for SOD1 mutations did display disease – and incompletely penetrant (Zeng et al. 2014). Also, the disease differs from human ALS in that proprioceptive pathways are affected, dorsal root ganglion neurons degenerate, motor neuron loss is less severe, and muscle atrophy occurs irrespective of denervation (Morgan et al. 2013, 2014).

The significance of linking SOD1 to canine DM is that canine DM marks the first naturally occurring SOD1 ALS model. This opened up many questions into the nature of cSOD1 mutants. For example, as a majority of canine DM is autosomal recessive, an important question was whether this disease was a result of a loss of enzymatic function or a toxic gain-of-function. It was also unknown if cSOD1 mutants formed the same detergent-insoluble aggregates in the spinal cord of affected dogs as seen in human ALS and transgenic models. Additionally, no one had cloned cSOD1 WT or the E40K and T18S mutations to study their aggregation propensities in relation to hSOD1. Chapter 2 of this dissertation details work addressing each of these questions. The results confirm many biochemical similarities between the cSOD1 and hSOD1 mutants and lend further credence to canine DM as an ALS model organism.

Tissue Specificity in SOD1 ALS

As previously stated, ALS is clinically and pathologically defined by a loss of motor neurons in the spinal cord and cortex accompanied by atrophy of skeletal muscles. However, when one considers the ubiquitous expression of SOD1 throughout an organism, the tissue and cellular specificity of the disease are puzzling. After all, intracellular SOD1 concentrations are substantial, comprising up to 1% of all protein in the CNS, yet can reach higher absolute concentrations in the liver and kidney (Jonsson et al. 2008, Pardo et al. 1995, Zetterström et al. 2007). This relative difference between tissues is also seen with endogenous mSOD1 and transgenic hSOD1 in normal and ALS mice, respectively (Jonsson et al. 2006, Wang et al. 2002). The general lack of pathology in unaffected tissues presents an interesting question as to how these tissues handle mutant SOD1 differently from the CNS.

While SOD1 aggregates are generally not reported in tissues unaffected in disease (i.e. liver, kidney), there have been a few reports in the literature that suggest even these tissues may be susceptible to pathogenesis. One case report of a 34-year-old woman with Downs Syndrome and SOD1 ALS described finding SOD1 immunopositive inclusions in hepatocytes at autopsy (Marucci et al. 2007). Interestingly, Downs Syndrome patients have higher levels of SOD1, as the SOD1 genetic locus is on the 21st chromosome (Gulesserian et al. 2001). This case was unique in that this woman possessed two SOD1 S134N missense mutations and one wild-type copy. The fact that her 70-year-old mother was heterozygous for the mutation but unaffected by disease implied that increased gene dosage played a role in pathogenesis in a similar manner to how disease onset and severity correlate with gene dosage in numerous

animal models. It also argued for the existence of a general susceptibility to SOD1 aggregation in other tissues as a result of increased mutant protein burden. Another case report analyzed autopsy tissues from a SOD1 G127X patient using a mutant-specific antibody and found high molecular weight species in the liver and kidney via density-gradient centrifugation as well as SOD1 immunopositive inclusions in kidney tubular epithelium and hepatocytes (Jonsson et al. 2008). Although the antibody used was more sensitive and specific for the G127X mutant, the novelty of this finding is probably a result of many groups failing to look at SOD1 pathology outside of the neuromuscular axis. In animals, one study looking at the accumulation of hydrophobic, misfolded SOD1 species in affected and non-affected tissues of a G93A mouse model confirmed that these species exist and also accumulate in the liver and kidney, albeit to a significantly lesser degree than the spinal cord and brain (Zetterström et al. 2007). In these studies, the level of aggregated SOD1 found in these non-affected tissues was still a fraction of that found in the CNS, yet they suggest a common mechanism for SOD1 aggregation that may be modulated by the intrinsic ability for a tissue to clear toxic SOD1 species.

Disease specificity also extends to the cellular level within the CNS, as motor neurons are lost and other cell types are spared despite ubiquitous SOD1 expression. Even within motor neuron pools, the selective degradation does not extend to those in the occulomotor nuclei and Onuf's nucleus. This observation was recently linked to differential expression of metalloproteinase-9 in motor neuron pools and suggests a heterogeneity even among motor neurons (Kaplan et al. 2014). Traditionally, motor neurons are the cells most affected in ALS, yet studies have demonstrated that the

development of disease in SOD1 ALS is at least partially non-cell autonomous (Ilieva et al. 2009). Numerous conditional mouse models have been created with expression of mutant SOD1 restricted to specific cell types, including astrocytes, pre- and post-natal neurons, and microglia, yet not one of these models developed disease (Beers et al. 2006, Gong et al. 2000, Lino et al. 2002, Pramatarova et al. 2001). Mice with selective expression of mutant SOD1 in motor neurons and interneurons failed to develop weakness, but did show weight loss and some motor neuron loss with ubiquitinated inclusions (Wang et al. 2008). Muscle specific expression of SOD1 was shown to induce muscle pathology, weakness, and, in one study, motor neuron loss in mice (Dobrowolny et al. 2008, Wong & Martin 2010). However, this was likely due to an artifact of SOD1 overexpression, as SOD1 WT animals also showed the same pathology. Only animals with homozygous PrP-driven SOD1 G37R in neurons, astrocytes, and muscle displayed a neuromuscular phenotype, implying that the interplay between these cell types is required (Wang et al. 2005).

Interestingly, SOD1 transgenic mice with Cre-mediated excision of mutant SOD1 from specific cells types develop disease, but on a modified timeline. Removal of mutant SOD1 from microglia or astrocytes has been shown to delay disease progression, while removal from motor neuron pools resulted in a delay in disease onset (Boillée et al. 2006, Yamanaka et al. 2008). These data suggest that motor neurons may be responsible for the initial manifestations of the disease, while microglia and astrocytes play a larger role during later stages. Despite these observations, how this ubiquitously expressed mutant protein is selectively toxic to certain cells of the neuromuscular system has been a long-standing question in the field.

A Role for Protein Turnover

Protein turnover is a collective term that involves both the production and clearance rates of a protein in a cell and has important implications for many diseases. Turnover is a basic characteristic of proteins that dictates their steady-state levels in a cell or tissue. How long a synthesized protein remains in a cell is influenced by many factors. At the level of the protein itself, structural stability and biochemical properties (e.g. amino terminal residue, sequence motifs, hydrophobicity) influence protein turnover (Bachmair et al. 1986, Dice & Goldberg 1975a,b; Tompa et al. 2008). For example, it is well documented that many misfolded proteins are rapidly degraded, such as mutant cystic fibrosis transmembrane conductance regulator (CFTR) responsible for cystic fibrosis (Sun et al. 2006). Forces beyond individual protein structure are also at play in dictating turnover rate. These include transcriptional and translational regulation, the presence of interacting chaperones, subcellular sequestration of proteins, and the activities of the ubiquitin-proteasome system and autophagy. Dynamic interplay between these forces is responsible for the lifespan of a protein.

The susceptibility of the CNS in the development of many degenerative disorders involving protein aggregation may be a result of its intrinsically slower protein turnover rate. The best evidence for this comes from two studies utilizing stable isotope labeling and mass spectrometry to determine turnover rates for a multitude of proteins in rodents. The first study administered a diet of 100% ^{15}N-labeled amino acids to mice, which were incorporated into newly synthesized proteins over time (Price et al. 2010a). The extent of this incorporation was tracked by sacrificing the animals at different time points, collecting tissue, and detecting and analyzing the amount of incorporated label

into many proteins via mass spectrometry and a sophisticated data analysis algorithm (Guan et al. 2011). From this method, the turnover rates for over 1010, 1122, and 334 proteins in brain, liver, and blood, respectively, were calculated. The average half-life for brain proteins was about 9 days, while the average for liver and blood proteins were 3 and 3.5 days, respectively. When the turnover rates of identical proteins were compared between tissues, proteins in the brain were always longer lived than their counterparts in the liver. A second study administered a 100% ^{15}N-labeled diet to pregnant rats and their pups through 6 weeks of age, then switched to a normal diet and sacrificed the animals at six and twelve months (Savas et al. 2012). Using mass spectrometry, this group was able to detect the presence of ^{15}N-labeled proteins in the liver and brain and discovered that the lifespan of certain nucleoporins equaled the lifespan of the animal. Importantly, at each time point, the brain had significantly more labeled proteins than the liver, indicating its relatively reduced rate of turnover.

Turnover of SOD1 has been well studied in cell culture. Significantly increased clearance rates for mutants compared to wild-type protein have been repeatedly demonstrated using a radiolabel pulse-chase paradigm (Borchelt et al. 1994, Hoffman et al. 1996, Johnston et al. 2000, Ratovitski et al. 1999). The degree of accelerated turnover correlates with the general structural instability of the protein, with the dimer-interface (A4V) and metal binding site (G85R) mutants decaying significantly faster than the more benign enzymatically active mutants (G93A). The relatively increased turnover rate of mutant SOD1 seen in cell cultures has also been observed in a *C. elegans* model overexpressing mutant SOD1 as well as in the spinal cord of a SOD1 G85R-YFP mouse model using deuterium-exchange labeling kinetics (Farr et al. 2011, Oeda et al.

2001). In humans, examining the ratio of mutant to wild-type SOD1 in erythrocytes, which no longer synthesize protein, from numerous SOD1 ALS patients confirmed faster turnover of mutants in humans and correlated this accelerated turnover to disease progression (Sato et al. 2005).

Faster turnover of mutant SOD1 may be a result of its preferential targeting by protein clearance mechanisms. It has been shown that the mechanisms responsible for SOD1 clearance include both the ubiquitin-proteasome system (UPS) and autophagy (Di Noto et al. 2005, Hoffman et al. 1996, Kabuta et al. 2006, Puttaparthi et al. 2004, Urushitani et al. 2002). Interestingly, studies have demonstrated that SOD1 mutants are preferentially ubiquitinated by the E3 ligases Dorfin and NEDL1, and that the degree of ubiquitination correlates with the disease severity of the mutation (Miyazaki et al. 2004, Niwa et al. 2002). Overexpression of Dorfin reduced mutant SOD1 levels, ameliorated cellular toxicity, reduced the activation of the cytochrome-caspase system in mitochondria, and prolonged survival in both cell culture and SOD1 G93A mice (Sone et al. 2010, Takeuchi et al. 2004). Additionally, chemical inhibition of autophagy preferentially increased levels of mutant SOD1, indicating that the mutant forms are preferentially targeted by this pathway (Kabuta et al. 2006). It has been well established that chemical inhibition of either the UPS or autophagy results in an increase in SOD1 aggregates and cell death while enhancement reverses this toxicity, indicating that cells are exquisitely sensitive to perturbations in SOD1 protein clearance and subsequent increases in steady-state levels. This parallels the correlation between gene dosage and disease severity in many SOD1 ALS animal models.

Many groups have examined the role of the UPS and autophagy in animal models of SOD1 ALS. Proteasome activity has been shown to decrease with age in normal mice, suggesting a link between the UPS, age, and disease onset (Keller et al. 2000). However, limited attempts to globally reduce UPS activity in SOD1 mice via genetic crosses have yielded no significant differences in disease course. SOD1 G93A mice crossed with LMP2 knockout mice, which lack an essential subunit of the immunoproteasome, failed to exacerbate disease (Puttaparthi et al. 2007). Crosses between SOD1 G93A mice and mice overexpressing human ubiquitin or the dominant-negative Ub^{K48R} mutation also failed to modify disease (Gilchrist et al. 2005). Mutant SOD1 has been shown to accumulate in the spinal cord independent of gene expression as the disease progresses, indicating reduced clearance, yet is unaccompanied by reduced proteasome activity in the spinal cord (Cheroni et al. 2005). However, the failure to observe a deficit in proteasome activity in the spinal cord may be the result of cellular mixing with homogenization of the entire cord. By crossing SOD1 G93A mice with the UPS reporter Ub^{G76V}-GFP, one study demonstrated a reduction in proteasome activity late in the disease in motor neurons (Cheroni et al. 2009).

The role of autophagy manipulation in SOD1 ALS has been conflicting. Although one study reported a reduction in SOD1 levels and cellular toxicity in culture with the MTOR inhibitor rapamycin (Kabuta et al. 2006), two studies administering rapamycin to SOD1 mice showed no effect (Bhattacharya et al. 2012) or exacerbated the disease (Zhang et al. 2011) despite increased autophagy markers in the spinal cord. This may be due to the involvement of MTOR in many other cellular processes, such as cell growth, protein and lipid synthesis, and energy metabolism (Laplante & Sabatini 2012).

Indeed, activation of the MTOR-independent autophagy pathway with the disaccharide trehalose did reduce SOD1 mutant levels in cell culture and extend survival in ALS mice (Castillo et al. 2013, Gomes et al. 2010). Overall, these studies suggest a role for protein clearance in the pathogenesis of SOD1 and highlight the need develop methods to examine the kinetics of protein clearance *in vivo*.

Stable Isotope Labeling Kinetics (SILK)

Pulse-chase methodologies utilizing radiolabeled amino acids have been a reliable tool for calculating protein turnover for many decades (Toyama & Hetzer 2013). However, for safety and environmental reasons, the use of radiolabels is less than ideal for experimentation outside of cell culture. Measuring turnover rates of proteins in an immortalized, rapidly dividing cell culture model also has its limitations. For one, turnover rates are faster, as rapid cell division dilutes the labeled pool by half with each round of the cell cycle. Also, such rapid division requires a greater metabolic demand in terms of protein synthesis and degradation, resulting in an accelerated picture of protein turnover compared to much less active tissues. Indeed, this discrepancy is evident when turnover rates for identical proteins were compared between tissues and cell culture models (Price et al. 2010b). Therefore, to obtain the most physiological picture of protein turnover *in vivo*, the safest method is to use stable isotope labeling to monitor the production and clearance of proteins in tissue.

SILK requires the administration of a non-radioactive (i.e. stable) isotopically labeled amino acid over time that is incorporated into newly synthesized proteins. The carbon and nitrogen atoms in these tracer amino acids are replaced with ^{13}C or ^{15}N

isotopes, which results in an amino acid with increased mass but identical chemical properties. The choice of which tracer amino acid to use depends on a number of factors, such as cost, the presence of the amino acid in peptides generated from protease digestion of the target protein, and the metabolism of the amino acid (e.g. essential versus non-essential) (Wolfe & Chinkes 2005). Commonly used amino acids include $^{13}C_6$-leucine, $^{13}C_6$-lysine, $^{13}C_6$-arginine, $^{13}C_9$-phenylalanine, and their ^{15}N variants. The incorporation of the tracer amino acid into the target protein results in a positive shift in the mass/charge (m/z) ratio of proteolytic peptides, which can be detected and quantified via mass spectrometry to determine a tracer:tracee ratio (TTR) (Previs et al. 2012). The rate of change in TTR over time is then used to calculate the protein fractional turnover rate (FTR), expressed as the percent of a protein pool that is turned over per unit time. This number can be converted into a half-life by dividing the FTR from the natural log of 2, expressed in units of time. The FTR is a function of two different kinetic rates for a protein population: the fractional synthetic rate (FSR) and the fractional catabolic rate (FCR), or the rate of protein synthesis and degradation, respectively. Assuming no changes in the steady-state levels of a protein over time, FSR, FCR, and FTR are equivalent values.

The simplest models for stable isotope labeling involve a single compartment as the sole source of the tracer amino acid (also called the precursor pool for protein synthesis) at a steady-state level of tracer. For example, cells in a dish immediately exposed to fresh media containing 20% labeled amino acid. Newly synthesized proteins will begin to incorporate the stable labeled amino acid rapidly at first and then the rate will begin to taper off until the amount of labeled amino acid incorporated into a given

protein approaches 20%. On a graph of TTR versus time, the shape of this curve will be dictated by equation 1

$$\text{Protein label} = \text{precursor enrichment} \times (1 - e^{-\text{FTR} \times \text{time}}) \quad (1)$$

where precursor enrichment specifies the tracer concentration and FTR is the fractional turnover rate. The faster the FTR, the faster the TTR curve for a particular protein will reach a steady-state level of label. If a steady-state level of label incorporation is not achieved for a target protein, the FTR can be estimated using equation 2

$$\text{FTR} = \text{pseudo-linear change in protein labeling} / (\text{precursor enrichment} \times \text{time}) \quad (2)$$

where the pseudo-linear change in protein labeling represents the initial “linear” portion of the curve before tapering. This approach has been successfully applied to estimating an FSR for beta-amyloid in human CSF (Bateman et al. 2006, 2007; Mawuenyega et al. 2010).

In addition to measuring label incorporation into a protein of interest in the presence of a tracer, one can also measure the clearance of label from the protein of interest in the absence of tracer. This type of kinetic analysis is frequently employed in radiolabeled pulse-chase assays measuring the disappearance of radiolabeled protein over time. The goal for this type of analysis is to label a protein of interest in the presence of a tracer amino acid, then remove said tracer and measure the rate of disappearance of the labeled amino acid from the target protein (decay rate). For example, cells grown to confluence in the presence of 20% tracer followed by a switch to unlabeled media. Assuming first-order kinetics with no contribution of tracer recycling, equation 3 can be used to determine the FTR.

$$FTR = \ln (\Delta TTR / \Delta time) \quad (3)$$

The decision to measure tracer incorporation into a protein or its clearance depends on a number of factors, such as the turnover rate of the protein, toxicity of expression, changes in protein concentration, and cell culture lifespan. Again, assuming steady-state levels of a protein, equations 1 and 3 should yield equivalent measures of the FTR. However, if there is a disconnect between synthesis and degradation (e.g. increases or decreases in protein levels) then examining both equations is warranted. Indeed, such a discrepancy has been found for beta-amyloid clearance in the patients with Alzheimer's disease and presenilin mutations (Mawuenyega et al. 2010, Potter et al. 2013).

Measuring protein turnover becomes more complicated in the setting of animal or human studies due to less control over the kinetics of the tracer precursor pool. Unlike cell culture models where tracer availability is determined by media composition that can be rapidly changed, administering tracer amino acids to whole organisms involves a bolus, constant infusion, or a combination of both in order to increase and then maintain the concentration of tracer. This is because one cannot simply switch out all of the unlabeled amino acid with a labeled amino acid, but instead has to introduce the labeled amino acid in the setting of an existing unlabeled amino acid pool. Even when administering 100% tracer, there exists a gradual rise in the plasma concentration as the tracer diffuses through the animal and is exchanged among tissues. On the opposite end of the labeling curve, abatement of labeling does not result in instantaneous elimination from amino acid pools. Instead, the nature of first-order decay coupled with contributions from recycling of tracer from body stores results in some residual

concentration of tracer that contributes to protein synthesis. Thus, the kinetics of the tracer itself become a differential variable in equation 1 and must be accounted for in equation 3.

One important consideration in designing a SILK study to measure a long-lived protein is the method of tracer administration and sample collection. A protein with a short half-life (i.e. hours) can be measured by an intravenous tracer infusion with multiple sample collection points lasting a few hours. This is because a significant fraction of the protein pool will be turned over every hour (50% during one half-life). Such a design has been highly successful in measuring CSF β-amyloid turnover in human CSF, where subjects received a constant infusion of intravenous $^{13}C_6$-leucine and CSF was collected hourly via a catheter inserted over a 48 hour period (Bateman et al. 2006, 2007; Mawuenyega et al. 2010). However, for a longer-lived protein with a half-life on the order of days or weeks, an intravenous infusion would require days in order to ensure label uptake into newly synthesized protein and is unlikely to be tolerated. Additionally, sample collection would be required to be further out from the administration of tracer to allow for the full measurement of the kinetic curve (i.e. the increasing and decreasing components). As SOD1 is hypothesized to be a long-lived protein in the CNS, a novel labeling method was needed to deliver a sufficient dose of tracer over a long period and sample collection points taken days later. In Chapter 3 of this dissertation, I describe the development of a SILK method utilizing oral administration of the tracer $^{13}C_6$-leucine to both ALS animal models and healthy human subjects to show that SOD1 is relatively long-lived in the tissues most affected in disease.

Summary of Findings

The work detailed in the following pages represents new insights into two of the many facets of SOD1 ALS biology. Chapter 2 details the first biochemical characterization of the only two existing canine SOD1 mutants responsible for canine DM. This work found that cSOD1 mutants have multiple similarities with hSOD1 mutants, including the accumulation of detergent-insoluble aggregates in the spinal cord of affected dogs, an increased propensity to aggregate in the presence of denaturants and in cell culture, and the ability to form enzymatically active dimers, lending strong support to a similar toxic gain-of-function mechanism in the only naturally-occurring model of ALS. Chapter 3 describes original work developing a SILK method to measure long-lived protein SOD1 kinetics in both animal models and healthy human subjects. Using a rat ALS model, we found that SOD1 WT turnover is significantly slower in neuromuscular tissues (i.e. cortex, spinal cord, muscle) than tissues not affected by disease (i.e. liver and kidney). This relative difference was also true for the SOD1 G93A mutant. When we looked at the misfolded SOD1 mutant pool in the spinal cord and liver, we found a significantly accelerated turnover rate compared to total SOD1, but the same relative difference in turnover between the spinal cord and liver. We were able to successfully adapt our SILK method to measure SOD1 turnover in the CSF of healthy human subjects, marking the first time that an orally administered tracer amino acid has been used to measure long-lived proteins in humans. We found that SOD1 turnover in the CSF is approximately four-fold slower than the total CSF protein pool, replicating our results in CSF from ALS rats, confirming that SOD1 is a long-lived protein in the CNS,

and providing a foundation for future studies looking at SOD1 turnover in patients with SOD1 mutations.

REFERENCES

Aoki M, Kato S, Nagai M, Itoyama Y. 2005. Development of a rat model of amyotrophic lateral sclerosis expressing a human SOD1 transgene. *Neuropathology*. 25(4):365–70

Audet J-N, Gowing G, Julien J-P. 2010. Wild-type human SOD1 overexpression does not accelerate motor neuron disease in mice expressing murine Sod1 G86R. *Neurobiol. Dis.* 40(1):245–50

Awano T, Johnson GCGSCS, Wade CM, Katz ML, Taylor JF, et al. 2009. Genome-wide association analysis reveals a SOD1 mutation in canine degenerative myelopathy that resembles amyotrophic lateral sclerosis. *Proc Natl Acad Sci U S A*. 106(8):2794–99

Bachmair A, Finley D, Varshavsky A. 1986. In vivo half-life of a protein is a function of its amino-terminal residue. *Science (80-.).* 234(4773):179–86

Bateman RJ, Munsell LY, Chen X, Holtzman DM, Yarasheski KE. 2007. Stable isotope labeling tandem mass spectrometry (SILT) to quantify protein production and clearance rates. *J. Am. Soc. Mass Spectrom.* 18(6):997–1006

Bateman RJ, Munsell LY, Morris JC, Swarm R, Yarasheski KE, Holtzman DM. 2006. Human amyloid-beta synthesis and clearance rates as measured in cerebrospinal fluid in vivo. *Nat. Med.* 12(7):856–61

Beers DR, Henkel JS, Xiao Q, Zhao W, Wang J, et al. 2006. Wild-type microglia extend survival in PU.1 knockout mice with familial amyotrophic lateral sclerosis. *Proc. Natl. Acad. Sci. U. S. A.* 103:16021–26

Bhattacharya A, Bokov A, Muller FL, Jernigan AL, Maslin K, et al. 2012. Dietary restriction but not rapamycin extends disease onset and survival of the H46R/H48Q mouse model of ALS. *Neurobiol. Aging*. 33(8):1829–32

Boillée S, Yamanaka K, Lobsiger CS, Copeland NG, Jenkins N a, et al. 2006. Onset and progression in inherited ALS determined by motor neurons and microglia. *Science*. 312(5778):1389–92

Borchelt DR, Lee MK, Slunt HS, Guarnieri M, Xu ZS, et al. 1994. Superoxide dismutase 1 with mutations linked to familial amyotrophic lateral sclerosis possesses significant activity. *Proc Natl Acad Sci U S A*. 91(17):8292–96

Bruijn LI, Becher MW, Lee MK, Anderson KL, Jenkins NA, et al. 1997. ALS-Linked SOD1 Mutant G85R Mediates Damage to Astrocytes and Promotes Rapidly Progressive Disease with SOD1-Containing Inclusions. *Neuron*. 18(2):327–38

Castillo K, Nassif M, Valenzuela V, Rojas F, Matus S, et al. 2013. Trehalose delays the progression of amyotrophic lateral sclerosis by enhancing autophagy in motoneurons. *Autophagy*. 9:1308–20

Chan PH, Kawase M, Murakami K, Chen SF, Li Y, et al. 1998. Overexpression of SOD1 in transgenic rats protects vulnerable neurons against ischemic damage after global cerebral ischemia and reperfusion. *J. Neurosci.* 18:8292–99

Chang-Hong R, Wada M, Koyama S, Kimura H, Arawaka S, et al. 2005. Neuroprotective effect of oxidized galectin-1 in a transgenic mouse model of amyotrophic lateral sclerosis. *Exp. Neurol.* 194(1):203–11

Cheah BC, Vucic S, Krishnan A V, Kiernan MC. 2010. Riluzole, neuroprotection and amyotrophic lateral sclerosis. *Curr. Med. Chem.* 17:1942–1199

Cheroni C, Marino M, Tortarolo M, Veglianese P, De Biasi S, et al. 2009. Functional alterations of the ubiquitin-proteasome system in motor neurons of a mouse model of familial amyotrophic lateral sclerosis. *Hum. Mol. Genet.* 18(1):82–96

Cheroni C, Peviani M, Cascio P, Debiasi S, Monti C, Bendotti C. 2005. Accumulation of human SOD1 and ubiquitinated deposits in the spinal cord of SOD1G93A mice during motor neuron disease progression correlates with a decrease of proteasome. *Neurobiol. Dis.* 18(3):509–22

Coates JR, Wininger FA. 2010. Canine degenerative myelopathy. *Vet Clin North Am Small Anim Pr.* 40(5):929–50

Dal Canto MC, Gurney ME. 1995. Neuropathological changes in two lines of mice carrying a transgene for mutant human Cu,Zn SOD, and in mice overexpressing wild type human SOD: a model of familial amyotrophic lateral sclerosis (FALS). *Brain Res.* 676(1):25–40

DeJesus-Hernandez M, Mackenzie IR, Boeve BF, Boxer AL, Baker M, et al. 2011. Expanded GGGGCC Hexanucleotide Repeat in Noncoding Region of C9ORF72 Causes Chromosome 9p-Linked FTD and ALS. *Neuron*. 72:245–56

Deng H-XX, Shi Y, Furukawa Y, Zhai H, Fu R, et al. 2006. Conversion to the amyotrophic lateral sclerosis phenotype is associated with intermolecular linked insoluble aggregates of SOD1 in mitochondria. *Proc Natl Acad Sci U S A*. 103(18):7142–47

Di Noto L, Whitson LJ, Cao X, Hart PJ, Levine RL. 2005. Proteasomal degradation of mutant superoxide dismutases linked to amyotrophic lateral sclerosis. *J. Biol. Chem.* 280:39907–13

Dice JF, Goldberg AL. 1975a. A statistical analysis of the relationship between degradative rates and molecular weights of proteins

Dice JF, Goldberg AL. 1975b. Relationship between in vivo degradative rates and isoelectric points of proteins. *Proc. Natl. Acad. Sci. U. S. A.* 72:3893–97

Dobrowolny G, Aucello M, Rizzuto E, Beccafico S, Mammucari C, et al. 2008. Skeletal muscle is a primary target of SOD1G93A-mediated toxicity. *Cell Metab.* 8(5):425–36

Farr GW, Ying Z, Fenton W a, Horwich AL. 2011. Hydrogen-deuterium exchange in vivo to measure turnover of an ALS-associated mutant SOD1 protein in spinal cord of mice. *Protein Sci*. 20(10):1692–96

Fecto F, Siddique T. 2011. Making connections: Pathology and genetics link amyotrophic lateral sclerosis with frontotemporal lobe dementia

Gidalevitz T, Krupinski T, Garcia S, Morimoto RI. 2009. Destabilizing protein polymorphisms in the genetic background direct phenotypic expression of mutant SOD1 toxicity. *PLoS Genet.* 5:

Gilchrist CA, Gray DA, Stieber A, Gonatas NK, Kopito RR. 2005. Effect of ubiquitin expression on neuropathogenesis in a mouse model of familial amyotrophic lateral sclerosis. *Neuropathol. Appl. Neurobiol.* 31:20–33

Gomes C, Escrevente C, Costa J. 2010. Mutant superoxide dismutase 1 overexpression in NSC-34 cells: effect of trehalose on aggregation, TDP-43 localization and levels of co-expressed glycoproteins. *Neurosci Lett*. 475(3):145–49

Gong YH, Parsadanian a S, Andreeva A, Snider WD, Elliott JL. 2000. Restricted expression of G86R Cu/Zn superoxide dismutase in astrocytes results in

astrocytosis but does not cause motoneuron degeneration. *J. Neurosci.* 20(2):660–65

Grad LI, Guest WC, Yanai A, Pokrishevsky E, O'Neill M a, et al. 2011. Intermolecular transmission of superoxide dismutase 1 misfolding in living cells. *Proc. Natl. Acad. Sci. U. S. A.* 108(39):16398–403

Graffmo KS, Forsberg K, Bergh J, Birve A, Zetterström P, et al. 2013. Expression of wild-type human superoxide dismutase-1 in mice causes amyotrophic lateral sclerosis. *Hum. Mol. Genet.* 22(1):51–60

Guan S, Price JC, Prusiner SB, Ghaemmaghami S, Burlingame AL. 2011. A Data Processing Pipeline for Mammalian Proteome Dynamics Studies Using Stable Isotope Metabolic Labeling

Gulesserian T, Seidl R, Hardmeier R, Cairns N, Lubec G. 2001. Superoxide dismutase SOD1, encoded on chromosome 21, but not SOD2 is overexpressed in brains of patients with Down syndrome. *J. Investig. Med.* 49:41–46

Gurney ME, Pu H, Chiu AY, Dal Canto MC, Polchow CY, et al. 1994. Motor neuron degeneration in mice that express a human Cu,Zn superoxide dismutase mutation. *Science (80-.).* 264(5166):1772–75

Hammad M, Silva A, Glass J, Sladky JT, Benatar M. 2007. Clinical, electrophysiologic, and pathologic evidence for sensory abnormalities in ALS. *Neurology*. 69:2236–42

Hoffman EK, Wilcox HM, Scott RW, Siman R. 1996. Proteasome inhibition enhances the stability of mouse Cu/Zn superoxide dismutase with mutations linked to familial amyotrophic lateral sclerosis. *J Neurol Sci*. 139(1):15–20

Ilieva H, Polymenidou M, Cleveland DW. 2009. Non-cell autonomous toxicity in neurodegenerative disorders: ALS and beyond. *J. Cell Biol.* 187(6):761–72

Jaarsma D. 2006. Swelling and vacuolisation of mitochondria in transgenic SOD1-ALS mice: a consequence of supranormal SOD1 expression? *Mitochondrion*. 6(1):48–9; author reply 50–1

Jaarsma D, Haasdijk ED, Grashorn JA, Hawkins R, van Duijn W, et al. 2000. Human Cu/Zn superoxide dismutase (SOD1) overexpression in mice causes mitochondrial vacuolization, axonal degeneration, and premature motoneuron death and accelerates motoneuron disease in mice expressing a familial amyotrophic lateral sclerosis mutant SO. *Neurobiol. Dis.* 7(6 Pt B):623–43

Johnston J a, Dalton MJ, Gurney ME, Kopito RR. 2000. Formation of high molecular weight complexes of mutant Cu,Zn-superoxide dismutase in a mouse model for familial amyotrophic lateral sclerosis. *Proc. Natl. Acad. Sci.* 97(23):12571–76

Jonsson PA, Bergemalm D, Andersen PM, Gredal O, Brännström T, Marklund SL. 2008. Inclusions of amyotrophic lateral sclerosis-linked superoxide dismutase in ventral horns, liver, and kidney. *Ann. Neurol.* 63(5):671–75

Jonsson PA, Ernhill K, Andersen PM, Bergemalm D, Brännström T, et al. 2004. Minute quantities of misfolded mutant superoxide dismutase-1 cause amyotrophic lateral sclerosis. *Brain*. 127(Pt 1):73–88

Jonsson PA, Graffmo KS, Andersen PM, Brännström T, Lindberg M, et al. 2006. Disulphide-reduced superoxide dismutase-1 in CNS of transgenic amyotrophic lateral sclerosis models. *Brain*. 129(Pt 2):451–64

Joyce PI, Fratta P, Fisher EMC, Acevedo-Arozena A. 2011. SOD1 and TDP-43 animal models of amyotrophic lateral sclerosis: Recent advances in understanding disease toward the development of clinical treatments. *Mamm. Genome*. 22:420–48

Kabuta T, Suzuki Y, Wada K. 2006. Degradation of amyotrophic lateral sclerosis-linked mutant Cu,Zn-superoxide dismutase proteins by macroautophagy and the proteasome. *J. Biol. Chem.* 281(41):30524–33

Kaplan A, Spiller KJ, Towne C, Kanning KC, Choe GT, et al. 2014. Neuronal matrix Metalloproteinase-9 is a determinant of selective Neurodegeneration. *Neuron*. 81:333–48

Keller JN, Hanni KB, Markesbery WR. 2000. Possible involvement of proteasome inhibition in aging: implications for oxidative stress. *Mech. Ageing Dev.* 113(1):61–70

Kiernan MC, Vucic S, Cheah BC, Turner MR, Eisen A, et al. 2011. Amyotrophic lateral sclerosis. *Lancet*. 377(9769):942–55

Laplante M, Sabatini DM. 2012. MTOR signaling in growth control and disease

Lino MM, Schneider C, Caroni P. 2002. Accumulation of SOD1 mutants in postnatal motoneurons does not cause motoneuron pathology or motoneuron disease. *J. Neurosci.* 22:4825–32

Lomen-Hoerth C, Murphy J, Langmore S, Kramer JH, Olney RK, Miller B. 2003. Are amyotrophic lateral sclerosis patients cognitively normal? *Neurology*. 60:1094–97

Marucci G, Morandi L, Bartolomei I, Salvi F, Pession A, et al. 2007. Amyotrophic lateral sclerosis with mutation of the Cu/Zn superoxide dismutase gene (SOD1) in a patient with Down syndrome. *Neuromuscul. Disord.* 17(9-10):673–76

Massman PJ, Sims J, Cooke N, Haverkamp LJ, Appel V, Appel SH. 1996. Prevalence and correlates of neuropsychological deficits in amyotrophic lateral sclerosis. *J. Neurol. Neurosurg. Psychiatry*. 61:450–55

Mawuenyega KG, Sigurdson W, Ovod V, Munsell L, Kasten T, et al. 2010. Decreased Clearance of CNS b -Amyloid in Alzheimer ' s Disease. . 330(December):2010

McKhann GM. 2001. Clinical and Pathological Diagnosis of Frontotemporal Dementia. *Arch. Neurol.* 58(11):1803

McNamara JO, Fridovich I. 1993. Human genetics. Did radicals strike Lou Gehrig? *Nature*. 362(6415):20–21

Mitchell JD, Borasio GD. 2007. Amyotrophic lateral sclerosis. *Lancet*. 369:2031–41

Miyazaki K, Fujita T, Ozaki T, Kato C, Kurose Y, et al. 2004. NEDL1, a novel ubiquitin-protein isopeptide ligase for dishevelled-1, targets mutant superoxide dismutase-1. *J. Biol. Chem.* 279(12):11327–35

Morgan BR, Coates JR, Johnson GC, Bujnak AC, Katz ML. 2013. Characterization of intercostal muscle pathology in canine degenerative myelopathy: a disease model for amyotrophic lateral sclerosis. *J. Neurosci. Res.* 91(12):1639–50

Morgan BR, Coates JR, Johnson GC, Shelton GD, Katz ML. 2014. Characterization of thoracic motor and sensory neurons and spinal nerve roots in canine degenerative myelopathy, a potential disease model of amyotrophic lateral sclerosis. *J. Neurosci. Res.* 92(4):531–41

Münch C, Bertolotti A. 2010. Exposure of Hydrophobic Surfaces Initiates Aggregation of Diverse ALS-Causing Superoxide Dismutase-1 Mutants. *J. Mol. Biol.* 399(3):512–25

Nagai M, Aoki M, Miyoshi I, Kato M, Pasinelli P, et al. 2001. Rats expressing human cytosolic copper-zinc superoxide dismutase transgenes with amyotrophic lateral sclerosis: associated mutations develop motor neuron disease. *J. Neurosci.* 21:9246–54

Niwa J-I, Ishigaki S, Hishikawa N, Yamamoto M, Doyu M, et al. 2002. Dorfin ubiquitylates mutant SOD1 and prevents mutant SOD1-mediated neurotoxicity. *J. Biol. Chem.* 277(39):36793–98

Oeda T, Shimohama S, Kitagawa N, Kohno R, Imura T, et al. 2001. Oxidative stress causes abnormal accumulation of familial amyotrophic lateral sclerosis-related mutant SOD1 in transgenic Caenorhabditis elegans. *Hum. Mol. Genet.* 10(19):2013–23

Okamoto K, Mizuno Y, Fujita Y. 2008. Bunina bodies in amyotrophic lateral sclerosis

Pardo CA, Xu Z, Borchelt DR, Price DL, Sisodia SS, Cleveland DW. 1995. Superoxide dismutase is an abundant component in cell bodies, dendrites, and axons of motor neurons and in a subset of other neurons. *Proc. Natl. Acad. Sci. U. S. A.* 92:954–58

Potter R, Patterson BW, Elbert DL, Ovod V, Kasten T, et al. 2013. Increased in vivo amyloid-β42 production, exchange, and loss in presenilin mutation carriers. *Sci. Transl. Med.* 5:189ra77

Pramatarova A, Laganière J, Roussel J, Brisebois K, Rouleau G a. 2001. Neuron-specific expression of mutant superoxide dismutase 1 in transgenic mice does not lead to motor impairment. *J. Neurosci.* 21(10):3369–74

Previs SF, Zhou H, Wang S-P, Herath K, Johns DG, et al. 2012. Proteome Kinetics: Coupling the Administration of Stable Isotopes with Mass Spectrometry-Based Analysis. In *Integrative Proteomics*, pp. 233–56

Price JC, Guan S, Burlingame A, Prusiner SB, Ghaemmaghami S. 2010a. Analysis of proteome dynamics in the mouse brain. . 2010:

Price JC, Guan S, Burlingame A, Prusiner SB, Ghaemmaghami S. 2010b. Analysis of proteome dynamics in the mouse brain. *Proc Natl Acad Sci U S A*. 107(32):14508–13

Puttaparthi K, Van Kaer L, Elliott JL. 2007. Assessing the role of immuno-proteasomes in a mouse model of familial ALS. *Exp. Neurol.* 206(1):53–58

Puttaparthi K, Wojcik C, Rajendran B, DeMartino GN, Elliott JL. 2004. Aggregate formation in the spinal cord of mutant SOD1 transgenic mice is reversible and mediated by proteasomes. *J. Neurochem.* 87(4):851–60

Ramesh T, Lyon AN, Pineda RH, Wang C, Janssen PML, et al. 2010. A genetic model of amyotrophic lateral sclerosis in zebrafish displays phenotypic hallmarks of motoneuron disease. *Dis Model Mech*. 3(9-10):652–62

Ratovitski T, Corson LB, Strain J, Wong P, Cleveland DW, et al. 1999. Variation in the biochemical/biophysical properties of mutant superoxide dismutase 1 enzymes and the rate of disease progression in familial amyotrophic lateral sclerosis kindreds. *Hum Mol Genet*. 8(8):1451–60

Reaume AG, Elliott JL, Hoffman EK, Kowall NW, Ferrante RJ, et al. 1996. Motor neurons in Cu/Zn superoxide dismutase-deficient mice develop normally but exhibit enhanced cell death after axonal injury. *Nat Genet*. 13(1):43–47

Renton AE, Chiò A, Traynor BJ. 2014. State of play in amyotrophic lateral sclerosis genetics. *Nat. Neurosci.* 17:17–23

Renton AE, Majounie E, Waite A, Sim??n-S??nchez J, Rollinson S, et al. 2011. A hexanucleotide repeat expansion in C9ORF72 is the cause of chromosome 9p21-linked ALS-FTD. *Neuron*. 72:257–68

Ringholz GM, Appel SH, Bradshaw M, Cooke NA, Mosnik DM, Schulz PE. 2005. Prevalence and patterns of cognitive impairment in sporadic ALS. *Neurology*. 65:586–90

Ripps ME, Huntley GW, Hof PR, Morrison JH, Gordon JW. 1995. Transgenic mice expressing an altered murine superoxide dismutase gene provide an animal model of amyotrophic lateral sclerosis. *Proc Natl Acad Sci U S A*. 92(3):689–93

Robberecht W, Philips T. 2013. The changing scene of amyotrophic lateral sclerosis. *Nat. Rev. Neurosci.* 14:248–64

Rodriguez J a, Valentine JS, Eggers DK, Roe JA, Tiwari A, et al. 2002. Familial amyotrophic lateral sclerosis-associated mutations decrease the thermal stability of distinctly metallated species of human copper/zinc superoxide dismutase. *J. Biol. Chem.* 277(18):15932–37

Rosen DR, Siddique T, Patterson D, Figlewicz DA, Sapp P, et al. 1993. Mutations in Cu/Zn superoxide dismutase gene are associated with familial amyotrophic lateral sclerosis. *Nature*. 362(6415):59–62

Rowland LP. 2001. How amyotrophic lateral sclerosis got its name: the clinical-pathologic genius of Jean-Martin Charcot. *Arch. Neurol.* 58:512–15

Sakowski S a, Lunn JS, Busta AS, Oh SS, Zamora-Berridi G, et al. 2012. Neuromuscular effects of G93A-SOD1 expression in zebrafish. *Mol. Neurodegener.* 7(1):44

Sato T, Nakanishi T, Yamamoto Y, Andersen PM, Ogawa Y, et al. 2005. Rapid disease progression correlates with instability of mutant SOD1 in familial ALS. *Neurology*. 65(12):1954–57

Savas JN, Toyama BH, Xu T, Yates 3rd JR, Hetzer MW, Yates JR. 2012. Extremely long-lived nuclear pore proteins in the rat brain. *Science (80-.).* 335(6071):942

Shelton GD, Johnson GC, O'Brien DP, Katz ML, Pesayco JP, et al. 2012. Degenerative myelopathy associated with a missense mutation in the superoxide dismutase 1 (SOD1) gene progresses to peripheral neuropathy in Pembroke Welsh Corgis and Boxers. *J Neurol Sci*. 318(1-2):55–64

Sone J, Niwa J, Kawai K, Ishigaki S, Yamada S, et al. 2010. Dorfin ameliorates phenotypes in a transgenic mouse model of amyotrophic lateral sclerosis. *J. Neurosci. Res.* 88:123–35

Sun F, Zhang R, Gong X, Geng X, Drain PF, Frizzell RA. 2006. Derlin-1 promotes the efficient degradation of the cystic fibrosis transmembrane conductance regulator (CFTR) and CFTR folding mutants. *J Biol Chem*. 281(48):36856–63

Takeuchi H, Niwa J, Hishikawa N, Ishigaki S, Tanaka F, et al. 2004. Dorfin prevents cell death by reducing mitochondrial localizing mutant superoxide dismutase 1 in a neuronal cell model of familial amyotrophic lateral sclerosis. *J. Neurochem.* 89:64–72

Tiwari A, Hayward LJ. 2003. Familial amyotrophic lateral sclerosis mutants of copper/zinc superoxide dismutase are susceptible to disulfide reduction. *J Biol Chem*. 278(8):5984–92

Tompa P, Prilusky J, Silman I, Sussman JL. 2008. Structural disorder serves as a weak signal for intracellular protein degradation. *Proteins Struct. Funct. Genet.* 71:903–9

Toyama BH, Hetzer MW. 2013. Protein homeostasis: live long, won't prosper. *Nat. Rev. Mol. Cell Biol.* 14(1):55–61

Turner BJ, Talbot K. 2008. Transgenics, toxicity and therapeutics in rodent models of mutant SOD1-mediated familial ALS. *Prog Neurobiol*. 85(1):94–134

Urushitani M, Kurisu J, Tsukita K, Takahashi R. 2002. Proteasomal inhibition by misfolded mutant superoxide dismutase 1 induces selective motor neuron death in familial amyotrophic lateral sclerosis. *J. Neurochem.* 83(5):1030–42

Wang J, Farr GW, Hall DH, Li F, Furtak K, et al. 2009. An ALS-linked mutant SOD1 produces a locomotor defect associated with aggregation and synaptic dysfunction when expressed in neurons of Caenorhabditis elegans. *PLoS Genet.* 5:

Wang J, Xu G, Borchelt DR. 2002. High Molecular Weight Complexes of Mutant Superoxide Dismutase 1: Age-Dependent and Tissue-Specific Accumulation. *Neurobiol. Dis.* 9(2):139–48

Wang J, Xu G, Slunt HH, Gonzales V, Coonfield M, et al. 2005. Coincident thresholds of mutant protein for paralytic disease and protein aggregation caused by restrictively expressed superoxide dismutase cDNA. *Neurobiol. Dis.* 20(3):943–52

Wang L, Sharma K, Deng H-X, Siddique T, Grisotti G, et al. 2008. Restricted expression of mutant SOD1 in spinal motor neurons and interneurons induces motor neuron pathology. *Neurobiol. Dis.* 29(3):400–408

Watson MR, Lagow RD, Xu K, Zhang B, Bonini NM. 2008. A drosophila model for amyotrophic lateral sclerosis reveals motor neuron damage by human SOD1. *J. Biol. Chem.* 283(36):24972–81

Wininger FA, Zeng R, Johnson GS, Katz ML, Johnson GC, et al. 2011. Degenerative myelopathy in a Bernese Mountain Dog with a novel SOD1 missense mutation. *J Vet Intern Med*. 25(5):1166–70

Wolfe RR, Chinkes DL. 2005. *Isotope Tracers in Metabolic Research*. Hoboken, NJ: Wiley-Liss

Wong M, Martin LJ. 2010. Skeletal muscle-restricted expression of human SOD1 causes motor neuron degeneration in transgenic mice. *Hum. Mol. Genet.* 19(11):2284–2302

Wong PC, Pardo CA, Borchelt DR, Lee MK, Copeland NG, et al. 1995. An adverse property of a familial ALS-linked SOD1 mutation causes motor neuron disease characterized by vacuolar degeneration of mitochondria. *Neuron*. 14(6):1105–16

Worms PM. 2001. The epidemiology of motor neuron diseases: a review of recent studies. *J. Neurol. Sci.* 191(1-2):3–9

Yamanaka K, Chun SJ, Boillee S, Fujimori-Tonou N, Yamashita H, et al. 2008. Astrocytes as determinants of disease progression in inherited amyotrophic lateral sclerosis. *Nat. Neurosci.* 11:251–53

Zeng R, Coates JR, Johnson GC, Hansen L, Awano T, et al. 2014. Breed distribution of SOD1 alleles previously associated with canine degenerative myelopathy. *J. Vet. Intern. Med.* 28(2):515–21

Zetterström P, Stewart HG, Bergemalm D, Jonsson PA, Graffmo KS, et al. 2007. Soluble misfolded subfractions of mutant superoxide dismutase-1s are enriched in spinal cords throughout life in murine ALS models. *Proc. Natl. Acad. Sci. U. S. A.* 104(35):14157–62

Zhang XX, Li L, Chen S, Yang D, Wang Y, et al. 2011. Rapamycin treatment augments motor neuron degeneration in SOD1 G93A mouse model of amyotrophic lateral sclerosis. *Autophagy*. 7(4):412–25

Chapter 2

Canine Degenerative Myelopathy: Biochemical Characterization of Superoxide Dismutase 1 in the First Naturally Occurring Non-human Amyotrophic Lateral Sclerosis Model

ABSTRACT

Mutations in canine superoxide dismutase 1 (SOD1) have recently been shown to cause canine degenerative myelopathy, a disabling neurodegenerative disorder affecting specific breeds of dogs characterized by progressive motor neuron loss and paralysis until death, or more common, euthanasia. This discovery makes canine degenerative myelopathy the first and only naturally occurring non-human model of amyotrophic lateral sclerosis (ALS), closely paralleling the clinical, pathological, and genetic presentation of its human counterpart, SOD1-mediated familial ALS. To further understand the biochemical role that canine SOD1 plays in this disease and how it may be similar to human SOD1, we characterized the only two SOD1 mutations described in affected dogs to date, E40K and T18S. We show that a detergent-insoluble species of mutant SOD1 is present in spinal cords of affected dogs that increases with disease progression. Our *in vitro* results indicate that both canine SOD1 mutants form enzymatically active dimers, arguing against a loss of function in affected homozygous animals. Further studies show that these mutants, like most human SOD1 mutants, have an increased propensity to form aggregates in cell culture, with 10-20% of cells possessing visible aggregates. Creation of the E40K mutation in human SOD1 recapitulates the normal enzymatic activity but not the aggregation propensity seen with the canine mutant. Our findings lend strong biochemical support to the toxic role of SOD1 in canine degenerative myelopathy and establish close parallels for the role mutant SOD1 plays in both canine and human disorders.

INTRODUCTION

For two decades, data from human studies and transgenic animal models have shown that mutations in superoxide dismutase 1 (SOD1) cause a form of dominantly-inherited amyotrophic lateral sclerosis (ALS), a progressive neurodegenerative disorder resulting in motor neuron loss, paralysis, and death 3-5 years after symptom onset (Kiernan et al 2011; Rosen et al 1993; Turner & Talbot 2008). To date, over 160 mutations have been identified in SOD1, which normally functions as a Cu,Zn-metalloenzyme that converts superoxide anions to molecular oxygen and H_2O_2 (for a list of mutations, see http://alsod.iop.kcl.ac.uk/). Although SOD1 mutations occur throughout the protein and result in a range of disease durations, they are united in their reduced stability and increased ability to aggregate. In fact, SOD1 aggregates in motor neurons are the histopathological hallmark of SOD1 ALS, a property that extends to animal models, cell culture overexpression systems, and experiments with recombinant protein. As SOD1-mediated ALS is a dominantly-inherited disease, this toxic gain of function becomes important in the setting of the remaining functional copy of wild-type (WT) SOD1, yet the mechanism responsible for how this toxic gain of function contributes to disease is unknown.

Until recently, with the exception of the artificial G86R and G93R mutations created in mouse and zebrafish SOD1, respectively, humans were the only organisms in which ALS occurred, and the only organisms where mutations in SOD1 responsible for causing this disease have been described (Ramesh et al 2010; Ripps et al 1995). That changed with GWAS data linking a mutation in canine SOD1 (cSOD1) to canine degenerative myelopathy (DM), a progressive neurodegenerative disorder in dogs with striking similarities to the clinical progression of human ALS (Awano et al 2009).

Specifically, canine DM affects multiple dog breeds toward the latter half of their lifespan and is characterized by an often asymmetric onset of paraparesis and ataxia in the hind limbs that progresses to paraplegia and muscle atrophy within one year from onset of signs. Although elective euthanasia occurs for a majority of these dogs by this stage, those that have been allowed to progress show ascension of the disease to include the forelimbs, ultimately resulting in flaccid tetraplegia and dysphagia. The entire course of the disease can last as long as 3 years (Coates & Wininger 2010). Histopathology of spinal cords from affected dogs show a similar pattern of myelin and axonal loss replaced with astrogliosis seen in human ALS, and immunohistochemistry reveals the same SOD1 aggregates in motor neurons that are present in humans and rodent models with human SOD1 (hSOD1) mutations (Awano et al 2009; Bruijn 1998).

Dog models of human disease offer specific advantages over traditional rodent models. For example, many human diseases occur naturally in dogs that would otherwise need to be artificially induced in rodent models. Furthermore, the limited genetic diversity of dog breeds, faster aging, shared environment with humans, and availability of advanced medical care facilitate expedited clinical trials for promising pharmacological agents targeting human disease. One example is that many canine models of human cancers, which develop sporadically in dogs, have been found to share several genetic similarities with human cancers and have been successfully used in clinical trials (Rankin et al 2012; Rowell et al 2011). Therefore, with these advantages in mind, further characterization of the canine model of ALS is warranted. Here, we report the first biochemical characterization of the only two cSOD1 mutations known to be associated with canine DM – the E40K mutation originally described in a number of

breeds and the T18S mutation from a case report detailing a Bernese Mountain dog with canine DM (Awano et al 2009; Wininger et al 2011). We show that spinal cords of DM dogs contain detergent-insoluble mutant SOD1 that correlates with disease severity and that both mutants are enzymatically active dimers that possess an increased aggregation propensity *in vitro*. Our results elucidate important similarities between human and canine SOD1 with respect to enzymatic function and aggregation propensity, adding a biochemical dimension to the clinical and histopathological similarities between canine DM and SOD1-mediated human ALS.

METHODS

Detergent extraction of SOD1 aggregates

Frozen thoracic spinal cord sections were obtained from age-matched control dogs and dogs with increasing severity of canine DM. Detergent extraction of SOD1 aggregates was preformed as previously described (Prudencio et al 2010). Briefly, 100 mg of frozen tissue was thawed on ice and homogenized via hand blender in 10 w/v TEN buffer (10 mM Tris, pH 8, 1 mM EDTA, 100 mM NaCl) with protease inhibitors (Sigma). The homogenate was then mixed with an equal volume of 2X Extraction Buffer (10 mM Tris, pH 8, 1 mM EDTA, 100 mM NaCl, 1% NP-40, protease inhibitors), mixed via sonication, and spun cold at 100,000xg for 10 minutes in a Beckman Ultracentrifuge. The supernatant, representing the detergent soluble fraction S1, was transferred to a new tube. The pellet was washed twice by resuspension in 1X extraction buffer via sonication and spun at 100,000xg for 10 minutes, cold. After the final wash, the supernatant was discarded and the pellet, designated as P2, resuspended via sonication in Buffer 3 (10 mM Tris, pH 8, 1 mM EDTA, 100 mM NaCl, 0.5% NP-40, 0.25% SDS, 0.5% Na-deoxycholate, protease inhibitors). Protein concentration for the S1 and P2 fractions was determined by BCA assay (Pierce). The experiment was repeated once.

Generation of SOD1 Constructs

Total RNA was extracted with TRIzol (Invitrogen) from frozen brain tissue obtained from control and DM-affected dogs according to the manufacturer's protocol. Total RNA was then reverse transcribed using oligo dT primers to generate cDNA (SuperScript III First-Strand Synthesis System for RT-PCR, Invitrogen). Wild-type (WT)

and E40K cSOD1 were amplified via PCR using primers with engineered restriction endonuclease sites at the 5' ends. To subclone cSOD1 cDNA into pGEX4T-1 (GE Healthcare) using EcoRI and NotI, the forward primer was 5'-agtcgaattcATGGAGATGAAGGCCGTGTGC-3' and the reverse primer was 5'-atcggcggccgcTTATTGGGCGATCCCAATGACA-3'. To subclone into pEYFP-C1 (Clontech) using EcoRI and BamHI, the forward primer was 5'-agtcgaattcaATGGAGATGAAGGCCGTGTGC -3'and the reverse primer was 5'-atcgggatccTTATTGGGCGATCCCAATGACA-3'. The T18S mutant was obtained by site-directed mutagenesis of the wild-type SOD1 using the primers 5'-GTGGAGGGC**T**CCATCCACTTCGTGCAGAAG-3' and 5'-CTTCTGCACGAAGTGGATGG**A**GCCCTCCAC-3'. Positive clones were verified by sequencing and subcloned into pGEX4T-1 and pEYFP-C1 using primers previously described. The human E40K mutant was generated via site-directed mutagenesis of wild-type hSOD1 using the primers 5'-GCATTAAAGGACTGACT**A**AAGGCCTGCATGGATTC-3' and 5'-GAATCCATGCAGGCCTT**T**AGTCAGTCCTTTAATGC-3'. The human E40G mutant was similarly generated using the primers 5'-GCATTAAAGGACTGACTG**G**AGGCCTGCATGGATTC-3' and 5'-GAATCCATGCAGGCCT**C**CAGTCAGTCCTTTAATGC-3'. Positive clones were verified by sequencing and subcloned into pEYFP-C1 with the primers 5'-agtcgaattcaGCCACGAAGGCCGTGT-3' and 5'-atcgggatccTTATTGGGCGATCCCAATTACACC-3' and the restriction endonucleases EcoRI and BamHI.

Untagged versions of the above plasmids for mammalian expression were created by subcloning human and canine SOD1 constructs into pCI-NEO (Promega) with a forward primer containing an EcoRI site and a Kozak sequence and a reverse primer containing a NotI site. For cSOD1, the primers were 5'-agtcgaattcgccaccATGGAGATGAAGGCCGTGTGC-3' and 5'-atcggcggccgcTTATTGGGCGATCCCAATGACA-3'. For hSOD1, the primers were 5'-agtcgaattcgccaccATGGCGACGAAGGCCGTG-3' and 5'-atcggcggccgcTTATTGGGCGATCCCAATTACACC-3'. Positive clones were verified by sequencing.

Cell Culture, Transfection, and Microscopy

NSC34 cells were grown in DMEM containing 10% fetal bovine serum with 10 U/mL penicillin and 10 µg/mL streptomycin. Cells were split into 12-well plates at $5X10^5$ cells/well 18 hours prior to transfection with media lacking antibiotics. Cells were transiently transfected with 900 ng of midi-prep DNA (Promega) and 6 µL Lipofectamine 2000 (Invitrogen) according to the manufacturer's protocol. Twenty-four hours later, cells were split into 24-well plates at varying densities for microscopy, with a small aliquot taken for protein analysis. Forty-eight hours after transfection, cells were washed once with phosphate buffered saline (PBS) and fixed in 4% paraformaldehyde for 30 minutes at room temperature, followed by three PBS washes. Cells were counterstained with DAPI in PBS containing 0.1% Triton X-100 for 10 minutes, followed by three PBS washes. Images were captured on a Nikon Eclipse TE300 inverted microscope using Metamorph software (Molecular Devices). Observers were blinded during cell counts, and at least 120 cells were counted for each condition in three separate experiments.

Recombinant SOD1 Production

Rosetta 2 *E. coli* (Novagen) containing GST-tagged cSOD1 WT, E40K, and T18S and hSOD1 WT, G85R, or E40K in pGEX4T-1 were grown in LB media with 100 µg/mL ampicillin and 25 µg/mL chloramphenicol at 37°C overnight, then diluted 1:10 in pre-heated LB with antibiotics and grown for two hours at 37°C. Protein production was induced for a further four hours after the addition of 1.0 mM IPTG. Cells were pelleted by centrifugation at 3500xg for 25 minutes, washed with 1X PBS, centrifuged again, and frozen until needed for purification.

Cell pellets were thawed on ice and resuspended in lysis buffer (10 mM Tris, 1 mM EDTA, 150 mM NaCl, 1% Triton X-100, 5 mM DTT, pH 8.0). Cells were incubated with 4 mg/mL lysozyme (Sigma) for 15 minutes at room temperature, followed by sonication and centrifugation at 10,000xg for 15 minutes. 600 µL of a 50% slurry of pre-equilibrated glutathione sepharose 4B beads (GE Healthcare) was then added to each supernatant and incubated with end-over-end rotation for 18 hours at 4°C. Beads were then washed three times with PBS and the bound SOD1 proteins cleaved from GST with the Thrombin Cleavage Capture Kit (Novagen) as per manufacturer's instructions. SOD1 proteins were metallated by dialysis against 100 mM Tris (pH 8.0), 300 mM NaCl, and 200 µM $CuCl_2$ for 3.5 hours, followed by dialysis against 100 mM Tris, 300 mM NaCl, and 200 µM $ZnCl_2$ for 3.5 hours as previously described (Chia et al 2010). Metallated proteins were then dialyzed overnight at 4°C against 20 mM Tris (pH 7.8), 10 mM NaCl, and concentrated using Amicon Ultra centrifugal filters with a 10K membrane. SOD1 concentrations were determined using the Bradford assay.

SOD1 Dismutase Activity Assay

SOD1 enzymatic activity was determined using the SOD Determination Kit (Sigma) according to manufacturer's protocol. Recombinant cSOD1 WT, E40K, T18S and hSOD1 WT, G85R, and E40K were diluted to 50 ng/μL with 20 mM Tris (pH 7.8), 10 mM NaCl, then 10-fold serially diluted down to 50 pg/μL. SOD1 from bovine erythrocytes (Sigma) was used to generate a standard curve from 0.1 U/mL to 50 U/mL. The assay was performed a total of three times.

Denaturing and Partially Denaturing SDS-PAGE and Immunoblotting

For denaturing gels, boiled samples were run on a 14% acrylamide Tris gel and transferred to nitrocellulose membranes. Membranes were blocked in PBS with 0.05% Tween (PBS-T) containing 5% milk for 1 hour at room temperature and incubated with anti-SOD1 (FL-154) antibody (Santa Cruz) in 5% milk PBS-T overnight at 4°C. Following three washes, membranes were incubated with donkey anti-rabbit IgG, horseradish peroxidase-linked whole antibody (GE Healthcare) at 1:5000 in 5% milk PBS-T for 2 hours at room temperature. Blots were developed with ECL 2 Western Blotting Substance (Pierce) and visualized on a G:Box Chemi XT4 imager (Syngene). Unless otherwise indicated, Western blots were repeated twice.

Partially denaturing PAGE was performed as previous described (Tiwari & Hayward 2003). Briefly, 1 μg of recombinant cSOD1 WT, E40K, T18S and hSOD1 WT and G85R were mixed with partially denaturing sample buffer without a reducing agent (62 mM Tris, 10% glycerol, 0.05% bromophenol blue, 0.4% SDS, pH 6.8) and incubated at 37°C for 30 minutes. Samples were then run on a 14% acrylamide Tris gel (both the

gel and the running buffer contained 0.1% SDS) and stained with Gel Code Blue (Pierce) according to the manufacturer's protocol. This protocol was repeated for recombinant hSOD1 E40K. The experiments were repeated once with a fresh preparation of recombinant canine SOD1.

Filter Trap Assay

For TFE-treated recombinant protein, 2 µg of recombinant cSOD1 WT, E40K, and T18S were incubated in 0%, 10%, and 20% trifluoroethanol (TFE) for 6 hours at 37°C with agitation. Samples were then dialyzed against 20 mM Tris (pH 7.8), 10 mM NaCl overnight at 4°C. For untagged human and canine SOD1 constructs expressed in NSC34 cells, cells were washed once in PBS, collected, and lysed via sonication in PBS containing protease inhibitors. Samples were spun at 800xg for 10 minutes to remove large cell debris without removing SOD1 aggregates. Protein concentration was determined via Bradford assay and adjusted to 1 µg/µL. The dialyzed TFE-treated recombinant SOD1 proteins or 150 µg of cell lysate were then run over a 0.2 µM cellulose acetate membrane on a Minifold II Slot Blot System (Whatman) and washed once with PBS. Membranes were blocked in 5% milk PBS-T for 1 hour at room temperature and incubated with anti-SOD1 (FL-154) antibody (Santa Cruz) in 5% milk PBS-T overnight at 4°C. Following three washes, membranes were incubated with donkey anti-rabbit IgG, horseradish peroxidase-linked whole antibody (GE Healthcare) at 1:5000 in 5% milk PBS-T for 2 hours at room temperature. Blots were developed with ECL 2 Western Blotting Substance (Pierce) and visualized on a G:Box Chemi XT4 imager (Syngene). Experiments were repeated a total of three times.

RESULTS

Spinal cords of DM dogs contain detergent-insoluble mutant SOD1 that increases with disease severity

The presence of detergent-insoluble mutant SOD1 species in spinal cords of SOD1 transgenic mice and patients with SOD1 A4V mutations has been well characterized (Deng et al 2006; Wang et al 2003). To determine if this biochemical property was also found in DM, we fractionated spinal cords from two non-affected dogs and four homozygous SOD1 E40K dogs with DM of increasing disease grade (See (Shelton et al 2012) for details on DM grade) into detergent-soluble (designated S1) and –insoluble (designated P2) fractions. We included non-affected dogs of different ages to control for age-related SOD1 accumulation, which has been shown in SOD1 WT transgenic mouse and rat models, as many dogs with Grade 3 and 4 DM are >14 years old (Prudencio et al 2009a). Spinal cords from transgenic rats overexpressing SOD1 WT or G93A were used as controls. Western blot analysis revealed the presence of detergent-insoluble SOD1 in DM-affected dog spinal cords that increased with disease severity, despite approximately identical levels of detergent-soluble SOD1 between control and DM-affected dogs (Figure 1). As expected, a small amount of detergent-insoluble WT cSOD1 was found in the older non-affected spinal cord, but this level was below that of even Grade 1 DM. While advanced age may result in some degree of detergent-insoluble SOD1 accumulation in canine spinal cords, it does not account for the significant increase seen in DM-affected spinal cords. Thus, we conclude that the E40K mutation shares the same accumulation of detergent-insoluble aggregates as seen in human ALS and rodent models.

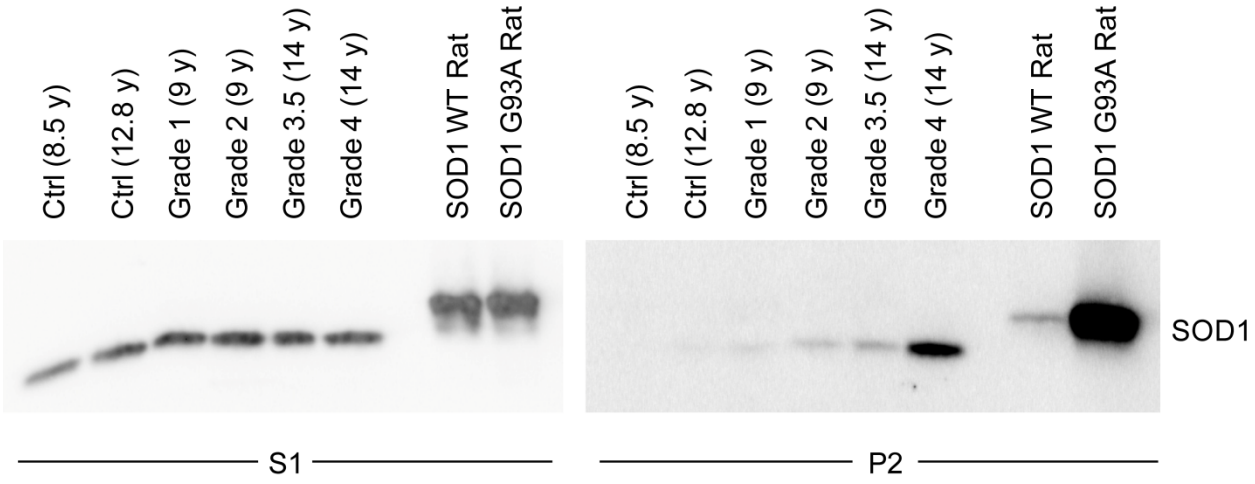

FIGURE 1. Canine DM spinal cords contain detergent-insoluble SOD1 that correlates with disease severity. Detergent extraction of cSOD1 from thoracic spinal cord sections of non-affected dogs (Ctrl) and DM-affected dogs of increasing disease severity (Grades 1-4, with Grade 1 mild and Grade 4 severe) show increasing levels of detergent-insoluble mutant SOD1 (P2 fraction) with increasing DM Grade. Age is indicated in parentheses. As controls, transgenic rats overexpressing hSOD1 WT or SOD1 G93A were included. The S1 lanes contain 16 µg protein, except for the transgenic rat samples at 4 µg, and the P2 lanes contain 18.6 µg protein.

Properties of canine SOD1 mutations

To date, only two mutations in cSOD1 have been described in the literature, as compared to the >120 mutations known for hSOD1 (Awano et al 2009; Wininger et al 2011). The sequence for cSOD1 was originally determined from a study looking for mutations in dogs with a form of spinal muscular atrophy and is hypothesized to contain eight beta sheets and a metal-binding active site similar to its human counterpart (Green et al 2002). As can be seen from the primary amino acid sequence, the E40K mutation falls within connecting loop III and results in a +2 charge shift, while the T18S mutation occurs in the second beta strand and does not change overall protein charge (Figure 2). Both mutations result in minor changes in hydrophobicity. Such varying characteristics reflect the inconsistencies seen in trying to correlate protein charge, hydrophobicity, and even aggregation propensity to disease onset and progression in familial ALS (Prudencio et al 2009b). As neither canine mutation disrupts the metal binding region of the enzyme, we predicted that both mutations retain dismutase activity, which lends credibility to a gain of toxic function and not loss of function in the dog model where a majority of dogs homozygous for mutant SOD1 show the DM phenotype.

A

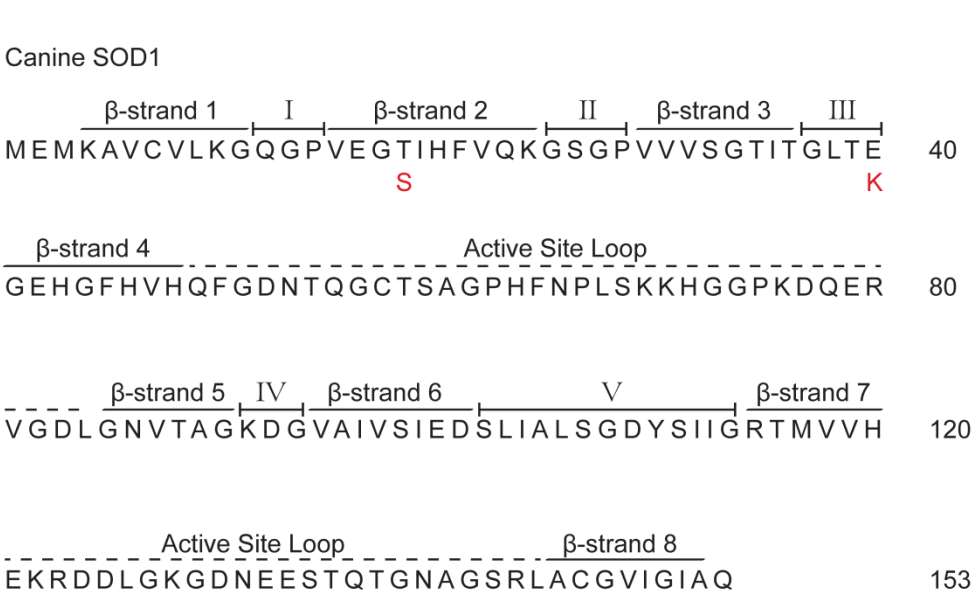

B

Mutation	Location	ΔCharge	ΔHydrophobicity
E40K	Connecting Loop III	+2	0.14
T18S	Beta strand 2	0	-0.24

FIGURE 2. Canine SOD1 primary sequence and known SOD1 mutations. (A) Similar to hSOD1, cSOD1 contains 8 beta sheets interspersed by connecting loops and surrounding an active site that binds copper. Known cSOD1 mutations are depicted in red below the primary sequence. (B) Location, Δcharge, and Δhydrophobicity for known cSOD1 mutations. Δcharge calculation performed with PROTEIN CALCULATOR v3.3 (Scripps). Δhydrophobicity calculated according to (Chiti et al 2003).

To measure enzymatic activity, a commercially available superoxide dismutase activity kit was used with recombinant cSOD1 WT, E40K, and T18S proteins. As controls, we compared dismutase activity with recombinant hSOD1 WT and G85R, a metal binding region mutant with significantly reduced activity (Borchelt et al 1994). As predicted from the structural location of these mutants (i.e. outside of the metal binding region), both cSOD1 mutants retain full enzymatic activity (Figure 3A), providing evidence in favor of a toxic gain of function in dogs homozygous for these mutations.

Since both canine mutants were dismutase active, we predicted that they would remain as structural dimers under partially denaturing polyacrylamide gel electrophoresis as consistent with previous reports of human mutations (Tiwari & Hayward 2003). Using a lower SDS concentration (0.4%) and no reducing agent or boiling, this prediction was confirmed (Figure 3B). Both the E40K and T18S cSOD1 mutants migrated predominantly as dimers, while the hSOD1 G85R mutant migrated mostly as a monomer, reflecting its well documented monomeric state.(Zetterstrom et al 2007) The shifted position of the E40K mutant on the gel reflects its +2 charge shift as compared to the WT or T18S proteins (Figure 2B). This is in agreement with our data reflecting full enzymatic activity in these mutants indicating the existence of a functional dimer. Thus, our data confirm that both cSOD1 mutants form enzymatically active dimers and, more importantly, that affected dogs homozygous for either mutant do not experience a loss of dismutase activity.

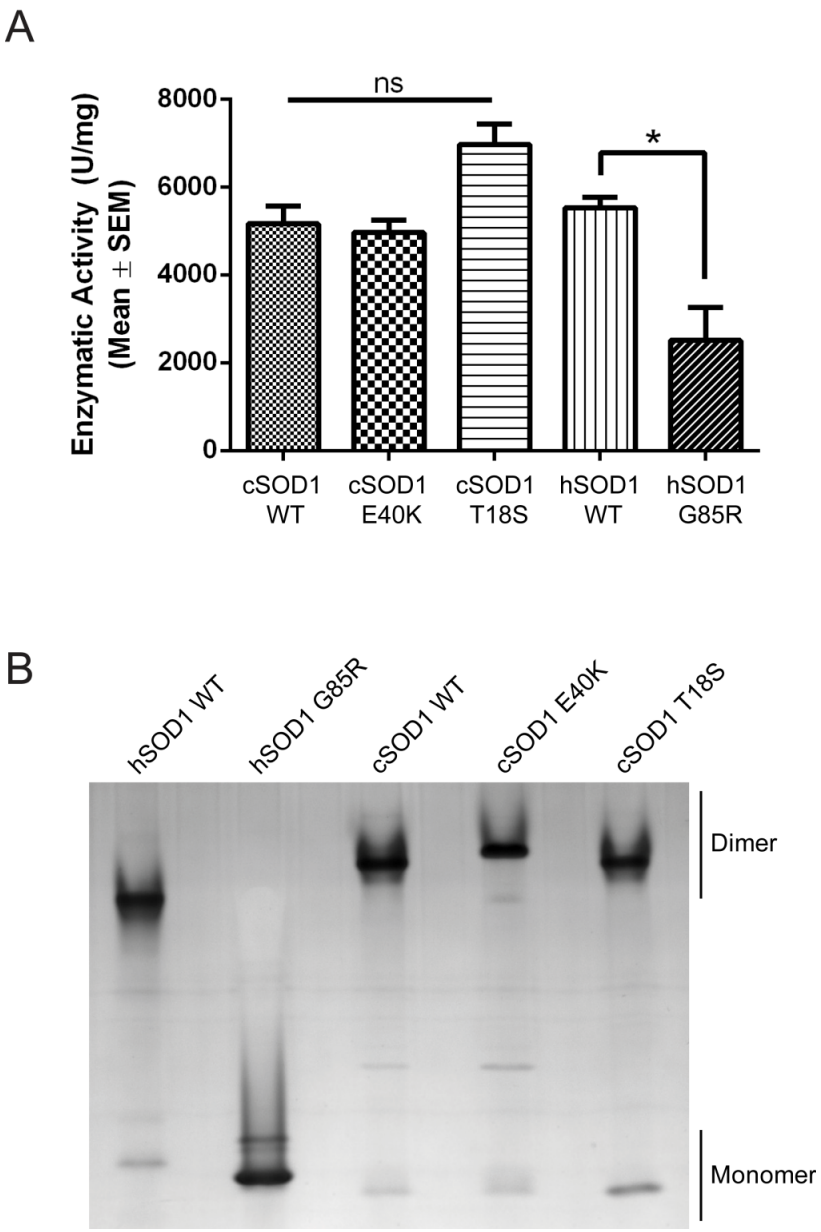

FIGURE 3. Canine SOD1 mutants form enzymatically active dimers. (A) Dismutase activity assay performed on recombinant canine and human SOD1 proteins. No significant difference between cSOD1 WT and E40K or T18S. * $p<0.05$ (B) Partially denaturating PAGE gel showing that cSOD1 WT, E40K, and T18S predominantly migrate as dimers, while the metal binding hSOD1 mutant G85R exists as a monomer.

Canine SOD1 mutations are unstable and prone to aggregation

As has been confirmed with hSOD1 mutants, we hypothesized that mutations in the cSOD1 protein would result in reduced stability and increased aggregation potential (Münch & Bertolotti 2010). We observed that treatment of the canine mutants, but not WT, with 20% TFE resulted in significant aggregation as detected by filter trap assay, indicating that the E40K and T18S mutants more readily expose their hydrophobic surfaces and aggregate than WT (Figure 4). Also, at lower concentrations of TFE, not only do both E40K and T18S show greater signal on the filter trap assay than WT, but E40K shows the most signal at 0% TFE indicating that it is relatively more unstable than T18S. This increased aggregation signal correlates with its greater degree of aggregation in cell culture (Figure 5A).

To visualize the degree of aggregation of cSOD1 mutants, we tagged WT, E40K, and T18S with an N-terminal YFP tag and transiently transfected each construct into NSC34 cells, an immortalized motor neuron-like cell line (Cashman et al 1992). After 48 hours, similar expression levels resulted in significant aggregation in 10-20% of cells for both mutants, while the WT protein remained soluble (Figure 5). Data show that the degree of aggregation for the E40K mutant was significantly more than the T18S mutant, which reflects its increased aggregation as seen by filter trap assay. The aggregates closely resemble SOD1 aggregates for hSOD1 proteins in cell culture (Gomes et al 2010).

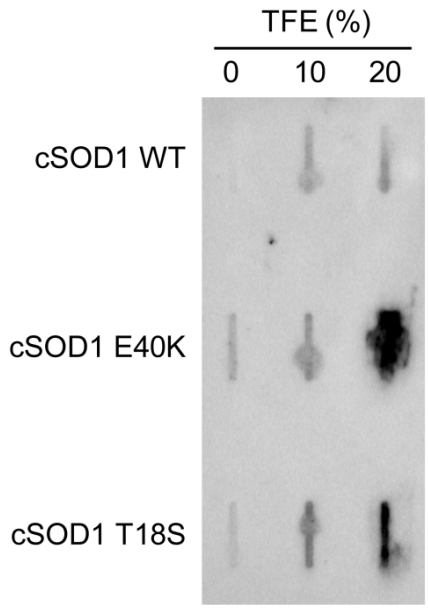

FIGURE 4. Canine SOD1 mutants are prone to aggregation *in vitro*. Filter trap assay of recombinant cSOD1 proteins exposed to increasing concentrations of TFE. The E40K and T18S mutants show heightened sensitivity to 20% TFE compared to WT, indicating an increased ability to aggregate.

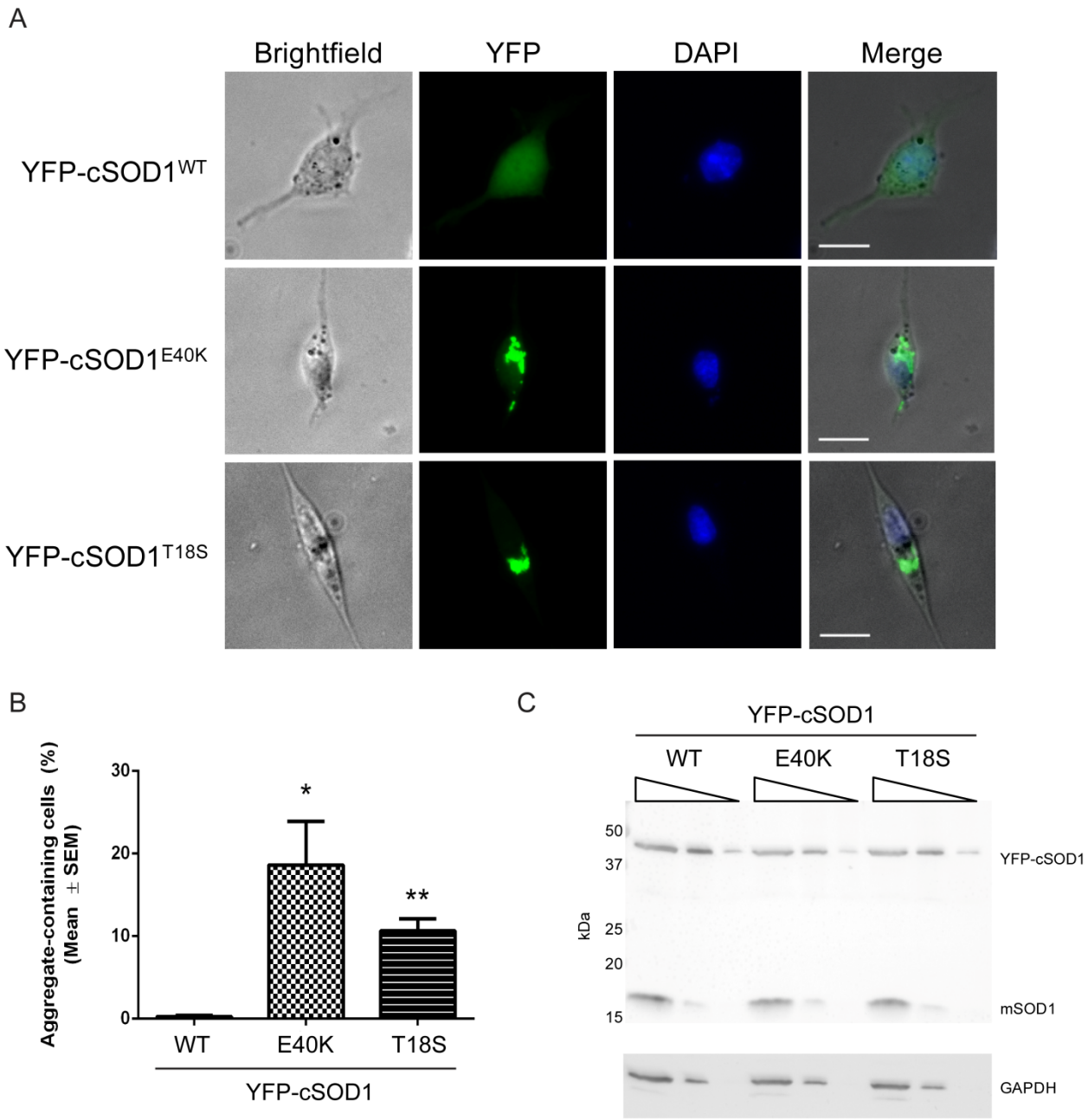

FIGURE 5. Canine SOD1 mutants aggregate in cell culture. (A) NSC34 cells transiently transfected for 48 hours with 900 ng of YFP-tagged cSOD1 WT, E40K, or T18S. Scale bar = 20 μm. (B) Quantification of A. At least 120 cells were counted in three separate experiments. * $p<0.05$; ** $p<0.01$ (C) Western blot of transfected NSC34 cell lysates (17.6 μg initial protein with 1:5 serial dilutions) probed with α-SOD1 (FL154) or α-GAPDH antibodies. YFP-cSOD1 and the endogenous mouse SOD1 (mSOD1) at 17 kDa are indicated on the blot.

The E40K mutation in hSOD1 fails to recapitulate the aggregation seen in the canine mutant

Since human and canine SOD1 share 79.1% identity, and since >160 mutations have been described for the human protein, it was no surprise that the canine E40K mutation occurred at a residue shared with hSOD1. In fact, an older review of SOD1 mutants points out the existence of an E40G mutation, but no primary description exists (Turner & Talbot 2008). To address any biochemical overlap between this mutation in humans and dogs, we created the E40K mutation in hSOD1 via site directed mutagenesis. As the location of this mutation in both human and canine SOD1 falls within one of the connecting loops and does not interfere with metal binding, we predicted that the human E40K mutant would, like its canine counterpart, be an enzymatically active dimer. A partially denaturing PAGE gel and dismutase activity confirm these predictions (Figure 6A, 6B). However, when we transiently transfected human SOD1 E40K into NSC34 cells, no aggregates were observed, even up to 72 hours after transfection (Figure 6C and data not shown). This is despite ample YFP-cSOD1 protein production in cells by Western blot (Figure 6D). To rule out any inhibitory effects that the YFP tag may have on aggregation, we transiently-transfected untagged hSOD1 WT, G85R, and E40K, as well as cSOD1 WT, E40K, and T18S, into NSC34 cells and looked for the presence of aggregates via a filter trap assay (Figure 6E). In agreement with previous observations with YFP-tagged SOD1 constructs, we found a significant aggregation signal from canine E40K and T18S and human G85R, but not human E40K. We subsequently created the hSOD1 E40G mutation to see if the lack of aggregation in human E40K was amino acid specific, but also found no aggregation in NSC34 or HEK293 cells (data not shown). Thus, despite the high sequence similarity

between species, the aggregation propensity of the E40K mutation is unique to cSOD1 under the conditions and with the cell types studied here.

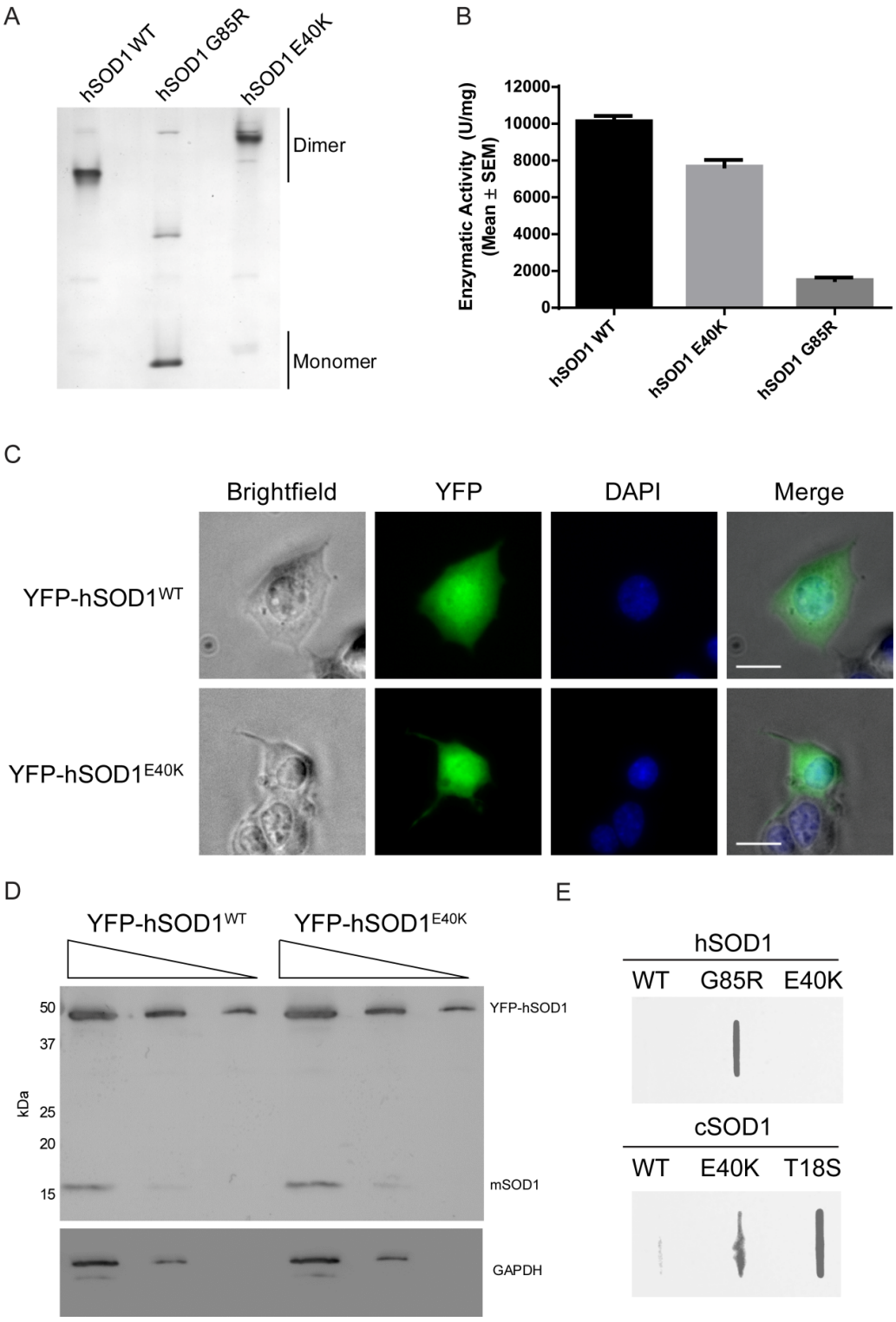

FIGURE 6. The human E40K mutation is a dismutase active dimer that fails to aggregate. (A) Partially denaturing PAGE gel showing that hSOD1 E40K migrates as a dimer with a positive charge shift. (B) Dismutase assay of hSOD1 WT, E40K, and G85R

mutations. No significant difference is seen between WT and E40K. (C) Representative images of NSC34 cells transiently transfection with 900 ng of YFP-tagged hSOD1 WT and E40K showing diffuse cytoplasmic and nuclear distribution with no aggregates. Scale bar = 20 μm (D) Western blot of transfected NSC34 cell lysates from C (1:5 serial dilutions) probed with α-SOD1 (FL154) or α-GAPDH antibodies. YFP-hSOD1 and the endogenous mouse SOD1 (mSOD1) at 17 kDa are indicated on the blot. (E) Filter trap assay of NSC34 cell lysates transiently transfected with human or canine SOD1 constructs lacking the N-terminal YFP tag confirm that hSOD1 E40K does not form aggregates.

DISCUSSION

The discovery that mutations in SOD1 are linked to canine DM opens many avenues for comparative studies between this disorder and human ALS, as well as a multitude of questions on the degree of similarity between these phylogenetically separated proteins. An important starting point for comparing the two disorders is understanding the biochemical characteristics of the only two known cSOD1 mutations linked to this disease as compared to hSOD1. Our results confirm that, like hSOD1 mutants, mutant cSOD1 forms detergent-insoluble aggregates in spinal cords of affected dogs that increase with disease severity. Further data show that both E40K and T18S mutations in cSOD1 are not loss of function mutations, but form enzymatically active dimers that are prone to aggregation *in vitro*. Finally, despite a high degree of sequence similarity to hSOD1, we show that the aggregation propensity of the conserved E40K mutation is unique to cSOD1.

One of the most striking differences between canine DM and human ALS is that, unlike the well documented toxic gain of function in dominantly-inherited SOD1-mediated human ALS, homozygosity at the SOD1 locus is frequently observed in most cases of canine DM (Awano et al 2009; Wininger et al 2011). Thus, unlike the heterozygous state found in the majority of ALS patients, a loss of function contributing to disease in these animals was a real possibility. In fact, SOD1 knock-out mice display mild age-related muscle denervation and degeneration that, depending on the genetic background, translate into impaired performance on motor tests (Flood et al 1999; Kostrominova 2010; Muller et al 2006; Shefner et al 1999). Therefore, we first needed to rule out SOD1 loss of function in these animals. As our data show that the canine E40K and T18S mutations form enzymatically active dimers, we are confident that the canine

DM model reflects the same toxic gain of function phenotype described for hSOD1 mutants. However, if it is true that a DM phenotype is most common in the presence of two copies of mutant SOD1, and if the >160 mutations in hSOD1 foreshadow the possibility of additional mutations in cSOD1 that render it enzymatically inactive, then an overlapping DM and SOD1 knock-out phenotype in dogs with such mutation remains an interesting possibility.

In hSOD1, one common feature among all mutants is increased aggregation propensity *in vitro* and *in vivo*. This is accompanied by decreased protein stability as measured by differential scanning fluoroscopy, susceptibility of many, but not all, mutants to proteinase K digestion, and abnormal migration under reducing conditions when compared to the remarkably stable WT protein (Münch & Bertolotti 2010; Ratovitski et al 1999; Tiwari & Hayward 2003). Our results with cSOD1 confirm that the E40K and T18S mutations are no exception. We consistently observed SOD1 aggregates in transiently-transfected NSC34 cells that, in our eyes, exceeded the degree of aggregation for many human SOD1 mutants. Coupled with its increased aggregation in the presence of TFE and the accumulation of detergent-insoluble SOD1 species in cases of canine DM, cSOD1 mirrors many of the properties of its human counterpart, and is predicted to recapitulate additional properties. However, the slight differences between the clinical presentations in canine DM and human ALS may reflect significant differences between the two proteins. For example, it has been shown that mutant hSOD1 aggregates possess prion-like properties in their ability to accelerate the misfolding and aggregation of additional SOD1 *in vitro*, as well as physically enter cells and cause the misfolding and aggregation of intracellular mutant and WT SOD1 (Chia et

al 2010; Grad et al 2011; Munch et al 2011). With SOD1 playing a role in canine DM, does this same mechanism hold true in dogs? One group elegantly elucidated the importance of the W32 residue in hSOD1 in maintaining species-specific cross-seeding of misfolded SOD1 (Grad et al 2011) As cSOD1 lacks this critical residue, does this impact its ability to seed? These questions highlight the significance that canine DM offers as an additional tool to pursue disease mechanisms of SOD1.

Canine and human SOD1 share approximately 80% identity. While the T18S mutation occurs at a unique amino acid found only in cSOD1, the E40K mutation occurs at a conserved residue between canine and human SOD1. When we created the E40K mutation in hSOD1 to explore the similarities with the canine mutant, we showed that this mutation, like canine E40K, is a dismutase active dimer. However, we were surprised to find that mutating this residue in hSOD1 does not result in an aggregation phenotype despite the prevalent aggregation seen in its canine counterpart and despite the appearance of an hSOD1 E40G mutation in the SOD1 literature (Turner & Talbot 2008). We also did not observe aggregation when we transiently transfected YFP-hSOD1 E40G into NSC34 cells (data not shown). The most recent edition of the online ALSod database (http://alsod.iop.kcl.ac.uk/, accessed February 22nd, 2013) no longer lists the hSOD1 E40G mutation, and no primary literature source exists, thus E40G may not represent a disease causing mutation in humans. As over 160 causative mutations spanning over 70 residues have been identified for hSOD1, the discovery of a mutation that causes aggregation in a species-specific manner is unique and raises interesting questions concerning the relationship between protein sequence, tertiary structure, and aggregation propensity. Perhaps hSOD1 contains a sufficiently different tertiary

structure that ameliorates the instability conferred by E40K. Or perhaps the structure of cSOD1 renders mutations at this residue particularly unstable.

What are the implications of another animal model of ALS, and what are the advantages of the canine DM model as compared to existing SOD1 models? Canine DM is not a perfect model of human ALS (Table 1). So far, a majority of dogs homozygous for SOD1 mutations develop disease, although some heterozygous dogs do develop canine DM and show intermediate levels of SOD1 aggregates in motor neurons (Joan Coates, personal communication). Additionally, the motor neuron loss that is the hallmark of human ALS is not seen to the same degree histopathologically and DM also involves proprioceptive pathways (Table 1) (Awano et al 2009; Coates et al 2007; Coates & Wininger 2010; Shelton et al 2012). Despite these differences, canine DM offers a naturally occurring, non-artificial system in which to study SOD1 and ALS. This differs from many of the mouse and rat transgenic models created so far, many of which require hSOD1 overexpression to non-physiological levels (e.g. G93A). In contrast, dogs with canine DM develop disease late in life with physiological levels of mutant cSOD1, thus providing a better picture of the natural disease progression. Our results show that, at the biochemical level, canine and human SOD1 are remarkably similar. Both aggregate readily when mutated, both display decreased protein stability, and both contain mutants that are functionally indistinct from WT protein (Table 1). Thus, it is reasonable to assume that human and canine SOD1 cause disease via a similar mechanism. In elucidating biochemical similarities between human ALS and canine DM, this study expands the research toolkit for understanding ALS and opens the door for developing novel therapies for ALS.

ACKNOWLEDGMENTS

We thank Dr. Gary S. Johnson of the Animal Molecular Genetic Diseases Laboratory for genotyping and Dr. Martin L. Katz in assisting with kit preparations for tissue collections. This work was supported by K08NS074194, NIH/NINDS/AFAR (to TMM), R01NS078398 NINDS (to T.M.M), R21NS078242 NIH/NINDS (to JRC), and F31NS078818 NIH/NINDS (to MJC). Funding was also provided by AKC Canine Health Foundation Grants #821 and #1213A and ALS Association grant #6054.

	Clinical and Genetic			Histopathology		Biochemistry		
	Clinical Onset	Inheritance	Proprioceptive involvement	MN loss	SOD1 aggregates in spinal cord	Detergent-insoluble SOD1 species in spinal cord	Recombinant SOD1 aggregates	SOD1 aggregates in cell culture
SOD ALS	Limb, Bulbar	Autosomal Dominant	No	++++	Yes	Yes[a]	Yes[b]	Yes[c]
Canine DM	Lower Limb	Mostly Autosomal Recessive	Yes	+	Yes	Yes*	Yes*	Yes*

[a](Deng et al., 2006; Wang et al., 2003)
[b](Münch and Bertolotti, 2010)
[c](Gomes et al., 2010; Matsumoto et al., 2005)
*This study

TABLE 1. Clinical, genetic, pathological, and biochemical differences between human ALS and canine DM.

[a](Deng et al 2006; Wang et al 2003) [b](Münch & Bertolotti 2010) [c](Gomes et al 2010; Matsumoto et al 2005) *This study

REFERENCES

Awano T, Johnson GS, Wade CM, Katz ML, Johnson GC, et al. 2009. Genome-wide association analysis reveals a SOD1 mutation in canine degenerative myelopathy that resembles amyotrophic lateral sclerosis. *Proc Natl Acad Sci U S A* 106:2794-9

Borchelt DR, Lee MK, Slunt HS, Guarnieri M, Xu ZS, et al. 1994. Superoxide dismutase 1 with mutations linked to familial amyotrophic lateral sclerosis possesses significant activity. *Proc Natl Acad Sci U S A* 91:8292-6

Bruijn LI. 1998. Aggregation and Motor Neuron Toxicity of an ALS-Linked SOD1 Mutant Independent from Wild-Type SOD1. *Science* 281:1851-4

Cashman NR, Durham HD, Blusztajn JK, Oda K, Tabira T, et al. 1992. Neuroblastoma x spinal cord (NSC) hybrid cell lines resemble developing motor neurons. *Dev Dyn* 194:209-21

Chia R, Tattum MH, Jones S, Collinge J, Fisher EM, Jackson GS. 2010. Superoxide dismutase 1 and tgSOD1 mouse spinal cord seed fibrils, suggesting a propagative cell death mechanism in amyotrophic lateral sclerosis. *PLoS One* 5:e10627

Chiti F, Stefani M, Taddei N, Ramponi G, Dobson CM. 2003. Rationalization of the effects of mutations on peptide and protein aggregation rates. *Nature* 424:805-8

Coates JR, March PA, Oglesbee M, Ruaux CG, Olby NJ, et al. 2007. Clinical characterization of a familial degenerative myelopathy in Pembroke Welsh Corgi dogs. *J Vet Intern Med* 21:1323-31

Coates JR, Wininger FA. 2010. Canine degenerative myelopathy. *Vet Clin North Am Small Anim Pract* 40:929-50

Deng HX, Shi Y, Furukawa Y, Zhai H, Fu R, et al. 2006. Conversion to the amyotrophic lateral sclerosis phenotype is associated with intermolecular linked insoluble aggregates of SOD1 in mitochondria. *Proc Natl Acad Sci U S A* 103:7142-7

Flood DG, Reaume AG, Gruner JA, Hoffman EK, Hirsch JD, et al. 1999. Hindlimb motor neurons require Cu/Zn superoxide dismutase for maintenance of neuromuscular junctions. *Am J Pathol* 155:663-72

Gomes C, Escrevente C, Costa J. 2010. Mutant superoxide dismutase 1 overexpression in NSC-34 cells: effect of trehalose on aggregation, TDP-43 localization and levels of co-expressed glycoproteins. *Neurosci Lett* 475:145-9

Grad LI, Guest WC, Yanai A, Pokrishevsky E, O'Neill MA, et al. 2011. Intermolecular transmission of superoxide dismutase 1 misfolding in living cells. *Proc Natl Acad Sci U S A* 108:16398-403

Green SL, Tolwani RJ, Varma S, Quignon P, Galibert F, Cork LC. 2002. Structure, chromosomal location, and analysis of the canine Cu/Zn superoxide dismutase (SOD1) gene. *J Hered* 93:119-24

Kiernan MC, Vucic S, Cheah BC, Turner MR, Eisen A, et al. 2011. Amyotrophic lateral sclerosis. *Lancet* 377:942-55

Kostrominova TY. 2010. Advanced age-related denervation and fiber-type grouping in skeletal muscle of SOD1 knockout mice. *Free Radic Biol Med* 49:1582-93

Matsumoto G, Stojanovic A, Holmberg CI, Kim S, Morimoto RI. 2005. Structural properties and neuronal toxicity of amyotrophic lateral sclerosis-associated Cu/Zn superoxide dismutase 1 aggregates. *J Cell Biol* 171:75-85

Muller FL, Song W, Liu Y, Chaudhuri A, Pieke-Dahl S, et al. 2006. Absence of CuZn superoxide dismutase leads to elevated oxidative stress and acceleration of age-dependent skeletal muscle atrophy. *Free Radic Biol Med* 40:1993-2004

Münch C, Bertolotti A. 2010. Exposure of Hydrophobic Surfaces Initiates Aggregation of Diverse ALS-Causing Superoxide Dismutase-1 Mutants. *Journal of Molecular Biology* 399:512-25

Munch C, O'Brien J, Bertolotti A. 2011. Prion-like propagation of mutant superoxide dismutase-1 misfolding in neuronal cells. *Proc Natl Acad Sci U S A* 108:3548-53

Prudencio M, Durazo A, Whitelegge JP, Borchelt DR. 2009a. Modulation of mutant superoxide dismutase 1 aggregation by co-expression of wild-type enzyme. *J Neurochem* 108:1009-18

Prudencio M, Durazo A, Whitelegge JP, Borchelt DR. 2010. An examination of wild-type SOD1 in modulating the toxicity and aggregation of ALS-associated mutant SOD1. *Hum Mol Genet* 19:4774-89

Prudencio M, Hart PJ, Borchelt DR, Andersen PM. 2009b. Variation in aggregation propensities among ALS-associated variants of SOD1: correlation to human disease. *Hum Mol Genet* 18:3217-26

Ramesh T, Lyon AN, Pineda RH, Wang C, Janssen PM, et al. 2010. A genetic model of amyotrophic lateral sclerosis in zebrafish displays phenotypic hallmarks of motoneuron disease. *Dis Model Mech* 3:652-62

Rankin KS, Starkey M, Lunec J, Gerrand CH, Murphy S, Biswas S. 2012. Of dogs and men: comparative biology as a tool for the discovery of novel biomarkers and drug development targets in osteosarcoma. *Pediatr Blood Cancer* 58:327-33

Ratovitski T, Corson LB, Strain J, Wong P, Cleveland DW, et al. 1999. Variation in the biochemical/biophysical properties of mutant superoxide dismutase 1 enzymes and the rate of disease progression in familial amyotrophic lateral sclerosis kindreds. *Hum Mol Genet* 8:1451-60

Ripps ME, Huntley GW, Hof PR, Morrison JH, Gordon JW. 1995. Transgenic mice expressing an altered murine superoxide dismutase gene provide an animal model of amyotrophic lateral sclerosis. *Proc Natl Acad Sci U S A* 92:689-93

Rosen DR, Siddique T, Patterson D, Figlewicz DA, Sapp P, et al. 1993. Mutations in Cu/Zn superoxide dismutase gene are associated with familial amyotrophic lateral sclerosis. *Nature* 362:59-62

Rowell JL, McCarthy DO, Alvarez CE. 2011. Dog models of naturally occurring cancer. *Trends Mol Med* 17:380-8

Shefner JM, Reaume AG, Flood DG, Scott RW, Kowall NW, et al. 1999. Mice lacking cytosolic copper/zinc superoxide dismutase display a distinctive motor axonopathy. *Neurology* 53:1239-46

Shelton GD, Johnson GC, O'Brien DP, Katz ML, Pesayco JP, et al. 2012. Degenerative myelopathy associated with a missense mutation in the superoxide dismutase 1 (SOD1) gene progresses to peripheral neuropathy in Pembroke Welsh Corgis and Boxers. *J Neurol Sci* 318:55-64

Tiwari A, Hayward LJ. 2003. Familial amyotrophic lateral sclerosis mutants of copper/zinc superoxide dismutase are susceptible to disulfide reduction. *J Biol Chem* 278:5984-92

Turner BJ, Talbot K. 2008. Transgenics, toxicity and therapeutics in rodent models of mutant SOD1-mediated familial ALS. *Prog Neurobiol* 85:94-134

Wang J, Slunt H, Gonzales V, Fromholt D, Coonfield M, et al. 2003. Copper-binding-site-null SOD1 causes ALS in transgenic mice: aggregates of non-native SOD1 delineate a common feature. *Hum Mol Genet* 12:2753-64

Wininger FA, Zeng R, Johnson GS, Katz ML, Johnson GC, et al. 2011. Degenerative myelopathy in a Bernese Mountain Dog with a novel SOD1 missense mutation. *J Vet Intern Med* 25:1166-70

Zetterstrom P, Stewart HG, Bergemalm D, Jonsson PA, Graffmo KS, et al. 2007. Soluble misfolded subfractions of mutant superoxide dismutase-1s are enriched in spinal cords throughout life in murine ALS models. *Proc Natl Acad Sci U S A* 104:14157-62

Chapter 3

Novel in Vivo Kinetic Approach Reveals

Slow CNS SOD1 Turnover

ABSTRACT

RNA targeted therapeutic strategies are being developed for neurodegenerative syndromes. Protein levels change as a function of protein half-life ($t_{1/2}$), critically influencing the timing and application of therapeutics. Protein kinetics and concentration may also play important roles in neurodegeneration. Thus, it is essential to understand in vivo protein kinetics including half-life. Using a stable isotope labeling technique combined with mass spectrometric detection, we determined the kinetics of superoxide dismutase 1 (SOD1), a protein that causes amyotrophic lateral sclerosis (ALS), in vivo. Application of this method to rats expressing human SOD1 demonstrated that SOD1 is a long-lived protein, that the $t_{1/2}$ of SOD1 in the CSF is similar to its $t_{1/2}$ in the CNS, and that SOD1 $t_{1/2}$ is longest in the CNS when compared to other tissues. Translation of this method to humans demonstrated successful label incorporation in the CSF and confirmed that SOD1 is a long-lived protein in the CSF of healthy subjects ($t_{1/2}$ 25 ± 7 days). The findings from this study provide important insights into the kinetics of SOD1 and can be translated into the design and implementation of clinical trials that target long-lived CNS proteins.

INTRODUCTION

Amyotrophic lateral sclerosis (ALS) is an adult-onset neurodegenerative disorder characterized by the loss of motor neurons in the spinal cord and cortex, resulting in progressive paralysis and death on average 2-3 years after symptom onset (Kiernan et al 2011). With an incidence of 1.5 - 2.7 cases per 100,000 in North America and Western Europe, ALS is the third most common neurodegenerative disorder after Alzheimer's and Parkinson's diseases and the most common motor neuron disease (Worms 2001). Almost universally fatal, the only FDA-approved treatment is Riluzole, a non-specific NMDA receptor antagonist that prolongs survival by 2-4 months (Cheah et al 2010). Moving forward, therapies that specifically target the proteins responsible for familial forms of ALS are being developed. For these and other targeted therapies in neurodegenerative disease, quantification of protein kinetics ($t_{1/2}$, production, and clearance) is a key factor in optimizing the frequency of delivery and determining the optimal time to assess for a biological response.

Measuring protein turnover has been routinely conducted in cell culture with radioisotopes that have provided important information regarding how protein characteristics (mutations, conformations, and post-translational modifications among others) affect protein turnover. However, measuring turnover rates of proteins in an immortalized, rapidly dividing cell culture model has limitations and shows discrepancies when turnover rates of identical proteins are compared between tissues and cell culture models (Price et al 2010). The development of stable isotope labeling kinetics (SILK) has enabled the study of protein turnover rates in vivo using a safe, stable isotope amino acid tracer that is incorporated into newly synthesized proteins and can be

quantitatively measured by mass spectrometry – a technique that has been highly successful in studies of amyloid-beta in human CSF and animal model brain (Bateman et al 2007, Bateman et al 2006, Bateman et al 2009, Castellano et al 2011, Elbert et al 2008, Mawuenyega et al 2013, Mawuenyega et al 2010, Potter et al 2013). In these studies a relatively short (9 hour) intravenous infusion of the stable isotope $^{13}C_6$-leucine resulted in adequate labeling of the rapidly turned over amyloid-beta ($t_{1/2}$ of 8 hours). However, the ability to measure the turnover of long-lived proteins is challenging, especially in humans. The labeling time needed becomes too long for an intravenous approach, and sample collection must be carried out over many days instead of hours. Indeed, D_2O-labeling studies in both animal models and human subjects have demonstrated that long-term labeling is necessary to measure proteins with a $t_{1/2}$ on the order of days (Fanara et al 2012, Price et al 2012). Here, we report the development of a SILK method using a stable isotope labeled amino acid to measure the turnover of a long-lived protein in rodents and in human CSF.

We applied our SILK method first to SOD1, a homodimeric metalloenzyme that catalyzes the conversion of superoxide anion to hydrogen peroxide and molecular oxygen (McCord & Fridovich 1969, Rosen et al 1993). Mutations in SOD1 cause dominantly inherited ALS via a toxic gain of function. Recent work by our group using antisense oligonucleotides (ASOs) against superoxide dismutase 1 (SOD1), a gene responsible for 20% of familial ALS cases, has shown great promise in animal models and has recently completed a Phase I clinical trial (Miller et al 2013). Our work and other targeted therapies highlight the need to understand SOD1 kinetics in order to effectively design clinical trials (Foust et al 2013, Gros-Louis et al 2010, Liu et al 2012,

Miller et al 2013, Wang et al 2014). Specifically, $t_{1/2}$ determines the predicted nadir for SOD1 levels in the CSF of patients treated with protein production inhibitors. Since SOD1 CSF levels correlate with SOD1 levels in the CNS, measurement of SOD1 CSF protein in humans offers the ability to determine pharmacodynamics for future clinical trial design (Winer et al 2013). We first developed our SILK method in rats expressing human SOD1 protein, from which we successfully measured the $t_{1/2}$ of SOD1 in tissues and in the CSF. Translating our findings in rats to human CSF demonstrated excellent labeling of SOD1, defined the $t_{1/2}$ of SOD1 in humans, and further validated this method for using stable isotopes to measure turnover of long-lived proteins.

METHODS

Stable Isotope Labeling in Rats

$^{13}C_6$-leucine labeling experiments were performed in 100-day-old male and female transgenic rats overexpressing human SOD1 WT or SOD1 G93A (Chan et al 1998, Nagai et al 2001). Animal protocols were approved by the Institutional Animal Care and Use Committee (IACUC) at Washington University and conducted according to the NIH Guide for Care and Use of Laboratory Animals. Both labeled L-leucine (U-$^{13}C_6$, 97-99%, CLM-2262) and unlabeled L-leucine (ULM-8203) were obtained from Cambridge Isotope Laboratories, Inc. (Andover, MA) and dissolved in water (5 mg/mL). To increase palatability, leucine solutions were sweetened with sucrose (20 mg/mL). During the course of the experiment, rats were fed *ad libitum* a modified Baker Amino Acid diet chow that contained no leucine (TestDiet). 50 mg of leucine (10 mL total volume) was orally administered twice daily (100 mg total daily dose) in accordance with published daily leucine requirements (Owens et al 1994). Before administration of the $^{13}C_6$-leucine label, rats were acclimated to the unlabeled leucine diet for 1-2 weeks. Rats were then labeled with $^{13}C_6$-leucine for 7 days and chased with unlabeled leucine for an additional 7, 19, 25, or 56 days. At the indicated time points, rats were anesthetized with isoflurane and approximately 200 µL of CSF was extracted from the cisterna magna, flash frozen, and stored at -80°C. Rats were then perfused (15 mL/min) with cold PBS containing 0.03% heparin sulfate for 15 minutes. Blood was collected from the mechanically ruptured vena cavae at the start of perfusion, spun at 1800xg for 10 minutes, and the supernatant flash frozen and stored at -80°C. After perfusion, spinal cord, cortex, liver, and kidney were harvested, flash frozen in liquid nitrogen, and stored

at -80°C. Three rats were sacrificed at each collection time point with the following exceptions: SOD1 WT Days 3 and 7 (n=6), SOD1 G93A Day 14 (n=2).

Fractionation of Tissue Lysates

Tissues were thawed on ice and homogenized in 5x v/w of TEN buffer (10 mM Tris, pH 8, 1 mM EDTA, 100 mM NaCl) containing the protease inhibitors AEBSF, aprotinin, bestatin E-64, leupeptin, and pepstain A (Sigma P8340). A portion of the tissue lysate was centrifuged at 100,000xg for 10 minutes (Beckman-Coulter Optima TLX-120 Ultracentrifuge) and the supernatant saved for misfolded SOD1 immunoprecipitation. Detergent-soluble SOD1 was extracted as described previously (Prudencio et al 2010). Briefly, the homogenate was mixed with an equal volume of 2X Extraction Buffer (10 mM Tris, pH 8, 1 mM EDTA, 100 mM NaCl, 1% NP-40, protease inhibitors), sonicated, and centrifuged at 100,000xg for 10 minutes at 4°C. The supernatant, representing the detergent soluble fraction, was transferred to a new tube and protein concentration was determined by BCA assay (Pierce).

Preparation of $^{13}C_6$-leucine labeled SOD1 standard curve

Labeled (containing $^{13}C_6$-leucine) and unlabeled media were prepared from RPMI-1640 medium without arginine, leucine, lysine, and phenol red (Sigma R-1780) supplemented with 10% dialyzed fetal bovine serum (Sigma F0392), 200 mg/L L-arginine, 40 mg/L lysine, and 50 mg/L of either $^{13}C_6$-leucine (labeled) or unlabeled leucine. HEK293T cells, which constitutively express human SOD1, were used to prepare $^{13}C_6$-leucine labeled SOD1 standards. Cells were grown to near confluence in complete RPMI-1640 medium supplemented with 10% fetal bovine serum, then split

into 10-cm dishes at a low concentration and allowed to settle overnight. Cells were then washed once with PBS and grown to near confluence (approximately 72 hours) in 0%, 0.08%, 0.17%, 0.34%, 0.68%, 1.25%, 2.5%, 5%, 10%, or 20% labeled/unlabeled media. Cells were then washed once with PBS and homogenized in cold lysis buffer (50 mM Tris pH 8, 150 mM NaCl, 1% NP-40, protease inhibitors) with sonication (20% power for 20 seconds). The lysate was spun at 15,000xg for 5 minutes, the supernatant collected, and protein quantified using the BCA Protein Assay (Pierce). Aliquots of lysate were frozen at -80°C.

Isolation and mass spectrometric analysis of $^{13}C_6$-leucine labeled SOD1, plasma free $^{13}C_6$-leucine, and $^{13}C_6$-leucine labeled total protein

M-270 Epoxy Dynabeads (Invitrogen) were crosslinked to either anti-SOD1 (mouse monoclonal; Sigma S2147) or anti-misfolded SOD1 (B8H10, mouse monoclonal, MM-0070 MédiMabs) antibodies using the Dynabeads Antibody Coupling Kit (Invitrogen) at a concentration of 25 μg antibody per mg of beads. Total soluble SOD1 was immunoprecipitated from the detergent soluble tissue fraction or standard curve HEK293T cell lysate (approximately 100 μg of protein) using 50 μL of α–SOD1 crosslinked Dynabeads overnight in 1X TEN buffer containing 0.1% Tween and protease inhibitors. Misfolded SOD1 was immunoprecipitated from tissue lysates taken prior to detergent fractionation, which had been spun at 100,000xg. The beads were washed three times in PBS and SOD1 was eluted from the beads with 50 μL of formic acid. The formic acid eluent was transferred to a new polypropylene tube and lyophilized via speed vacuum (Labconco CentriVap), resuspended with 100% methanol,

lyophilized again via speed vacuum, and resuspended in 25 µL of 25 mM $NaHCO_3$ buffer (pH 8.8). 600 ng of sequencing grade endoproteinase Glu-C (Roche) was added to each sample and digestion allowed to proceed at 25°C for 17 hours. Samples were again lyophilized via vacuum and resuspended in 20 µL of 5% acetonitrile/0.05% formic acid prior to liquid chromatography-triple quadrupole-mass spectrometry (UPLC/tandem MS) analysis (Xevo, Waters). The $^{13}C_6$-leucine/$^{12}C_6$-leucine ratio in SOD1 peptides was quantified by comparing the area under the curve for the SOD1 peptides KADDLGKGGNEE, GLHGFHVHE, and SNGPVKVWGSIKGLTE in the presence or absence of $^{13}C_6$-leucine. The full list of transition ions used to acquire the UPLC/tandem MS data is listed in Supplemental Table 1. Excellent correlations between these peptides enabled us to use the peptide with the most robust signal for kinetic analysis (Supplemental Figure 3).

Plasma free $^{13}C_6$-leucine abundance reflected the precursor pool enrichment for SOD1 protein synthesis. Plasma proteins were precipitated with 10% trichloroacetic acid overnight at 4°C, the protein pellet retained for quantification of bound $^{13}C_6$-leucine, and the supernatant removed after centrifugation at 21,000xg for 10 minutes. The supernatant was chemically derivatized to form the *N*-heptafluorobutyryl *n*-propyl esters of plasma-free amino acids, and $^{13}C_6$-leucine enrichment was quantified using capillary gas chromatography-negative chemical ionization-quadrupole mass spectrometry (GC-MS; Agilent 6890N Gas Chromatograph and Agilent 5973N Mass Selective Detecter) with the m/z of 355 as compared to 349 as described previously (Potter et al 2013, Reeds et al 2006). Protein bound $^{13}C_6$-leucine abundance was quantified in the TCA precipitated-proteins after sonicating the pellet in a cold 10% TCA solution, twice. The

pellets were hydrolyzed in 6 N HCl for 24 hours at 110°C. The hydrolysates were subjected to cation-exchange chromatography (50W-X8 resin, Sigma) to trap the protein bound amino acids that were eluted from the column with 6N NH_4OH. The samples were then dried under vacuum and processed for GC-MS analysis as described previously (Parise et al 2001). Labeled/unlabeled ratios from both the UPLC/tandem MS and GC-MS were obtained as tracer:tracee ratios (TTR) and converted to mole fraction label (MFL) to account for the bias that occurs at high stable tracer enrichments using the equation: $MFL = \frac{TTR}{1+TTR}$.

Human subjects

Studies involving human subjects were approved by the Washington University Human Studies Committee and the Clinical Research Unit (CRU) Advisory Committee (an Institute of Clinical and Translational Sciences (ICTS) Resource Unit). Informed consent was obtained from all participants. Demographics of the five participants are described in Supplemental Table 2. All participants underwent an initial screening visit that consisted of a physical and neurological examination and phlebotomy for a complete blood count, complete metabolic panel, prothrombin time, and partial thromboplastin time. Exclusion criteria included evidence of neurologic disorder by history or examination, inability to safely take food and drink by mouth, lab values greater than 2x upper limit of normal, special diets (e.g. gluten-free), pregnancy, allergy to lidocaine, history of bleeding disorders, or contraindications for lumbar puncture. Eligible participants consumed a prepackaged reduced leucine diet supplemented with $^{13}C_6$-leucine powder for 10 days. The reduced leucine diet (approximately 2000 mg

leucine/day) was prepared by dieticians in the Washington University Research Kitchen, handed to the subjects, and consumed at home. Food intake was monitored by a self-reported food journal. Participants consumed $^{13}C_6$-leucine (Cambridge Isotope Laboratories CLM-2262) after dissolving 330 mg $^{13}C_6$-leucine in 120 mL of tap water + Kool-Aid® flavored powder three times per day (total daily dose = 990 mg). During the $^{13}C_6$-leucine labeling period, overnight fasting blood was collected on days 1 and 10 of the research meal plan. On day 11, participants resumed consumption of their habitual diets. CSF (via lumbar puncture) and venous blood samples were collected approximately 14, 28, 42, and 67-84 days after $^{13}C_6$-leucine labeling was initiated (actual time points differed slightly between subjects). Approximately 20-25 mL of CSF was drawn with each lumbar puncture.

Blood was centrifuged at 1800xg for 10 minutes, the serum aliquoted into low-binding 1.5 mL tubes (Ambion AM12450), frozen on dry ice, and stored at -80°C. CSF (20-25 mL) was centrifuged at 1000xg for 10 minutes at 4°C, and 1 mL was aliquoted into several low-binding 1.5 mL tubes, frozen on dry ice, and stored at -80°C. Immunoprecipitation of SOD1 from 1 mL of CSF was carried out by adding 50 µL of α-SOD1 cross-linked M-270 Dynabeads, protease inhibitors, Tween (final concentration 0.1%), and rotating the tubes overnight at 4°C. SOD1 was eluted from the beads (99% 50 µL formic acid), digested (endoproteinase Glu-C), and prepared for LC/tandem MS analysis as described above for rodent CSF. Plasma free $^{13}C_6$-leucine enrichment was quantified as described above, and used to reflect the precursor pool enrichment for SOD1 protein synthesis. $^{13}C_6$-leucine abundance in human plasma (50 µL) and CSF (1 mL) protein precipitates (10% TCA) was quantified as described above.

Compartmental modeling of rodent and human kinetic data

Modeling was conducted using SAAM II (Resource for Kinetic Analysis, University of Washington, Seattle). For the animal studies, the kinetic data for plasma free $^{13}C_6$-leucine, tissue-specific SOD1 species, and total protein from liver, cortex, and spinal cord were incorporated into a compartmental model. The KADDLGKGGNEE peptide was used for modeling as it had the most robust LC/tandem MS signal. The model consisted of a central plasma leucine compartment that initially received the orally administered tracer and which exchanged tracer-labeled leucine with all proteins throughout the body (Supplemental Figure 2A,B). Arrows connecting the compartments of the model represent first order rate constants (units: pools day^{-1}) that describe the flux of leucine between compartments. The model describes the complete time course of tracer incorporation and clearance into each measured compartment; the fractional turnover rate (FTR, pools/d) for each compartment is the rate constant for the return of leucine from each compartment back to plasma. Note that isotopic enrichment time course data was available for plasma leucine and for all protein/tissue compartments highlighted in color in Supplemental Figure 2A,B. A “whole body protein” compartment was used to account for most of the shape information of plasma leucine as label exchanged with all other unsampled proteins. The SAAM program devised first-order linear differential equations as dictated by the structure of the model, and optimized the fit of the model-projected solution to the data for all sampled protein/tissue compartments simultaneously by adjusting the model rate constants through an iterative process. The model was set up in SAAM in a manner to simulate the appearance of

label into plasma as a result of the twice-daily tracer dosing scheme for the 7 days of oral tracer labeling. A similar model was used for the human studies to account for plasma free $^{13}C_6$-leucine, CSF total protein, and CSF SOD1 species for each subject following 10 days of thrice-daily oral tracer administration (Supplemental Figure 2C). The GLHGFHVHE peptide gave the most robust LC/tandem MS signal for the human in vivo tracer kinetics and was therefore used for modeling. Like the animal model, plasma leucine comprised the central compartment from which tracer was exchanged with all other compartments. $t_{1/2}$ was calculated as ln 2/FTR.

Statistics

Descriptive statistics for variables in each kinetic model described in this manuscript (FTR, 95% confidence intervals) were calculated using the SAAM II modeling software.

Study approval

Animal protocols were approved by the Institutional Animal Care and Use Committee (IACUC) at Washington University and conducted according to the NIH Guide for Care and Use of Laboratory Animals. Studies involving human subjects were approved by the Washington University Human Studies Committee and the Clinical Research Unit (CRU) Advisory Committee (an Institute of Clinical and Translational Sciences (ICTS) Resource Unit). Written informed consent was received from all participants prior to inclusion in the study.

RESULTS

Development of a $^{13}C_6$-leucine labeling approach and mass spectrometry-based method for quantifying labeled SOD1 in cell culture

The calculation of protein turnover by administering stable isotope labeled amino acids or D_2O over time has been demonstrated in numerous cell culture models and in human CSF and plasma proteins (Bateman et al 2007, Bateman et al 2006, Bateman et al 2009, Castellano et al 2011, Elbert et al 2008, Mawuenyega et al 2013, Mawuenyega et al 2010, Ong 2012, Potter et al 2013) (Fanara et al 2012, Price et al 2012). Stable isotope labeled amino acids are biologically identical to their naturally-occurring counterparts and, unlike radiolabeled amino acids, are innocuous to both the system being studied and the experimental environment. SILK utilizes the administration of a stable isotope labeled amino acid that is incorporated during protein translation. The labeled and unlabeled proteins are immuno-isolated, digested into peptides, and analyzed using LC- tandem MS to quantify incorporation of the tracer into specific peptides (Figure 1A). Using $^{13}C_6$-leucine labeled HEK293T cells, we identified three leucine-containing peptides that reliably and accurately determined incorporation of label (Figure 1C-E, Supplemental Figure 1). These data confirmed our ability to label, isolate, and measure tracer-incorporated SOD1 using LC/tandem MS.

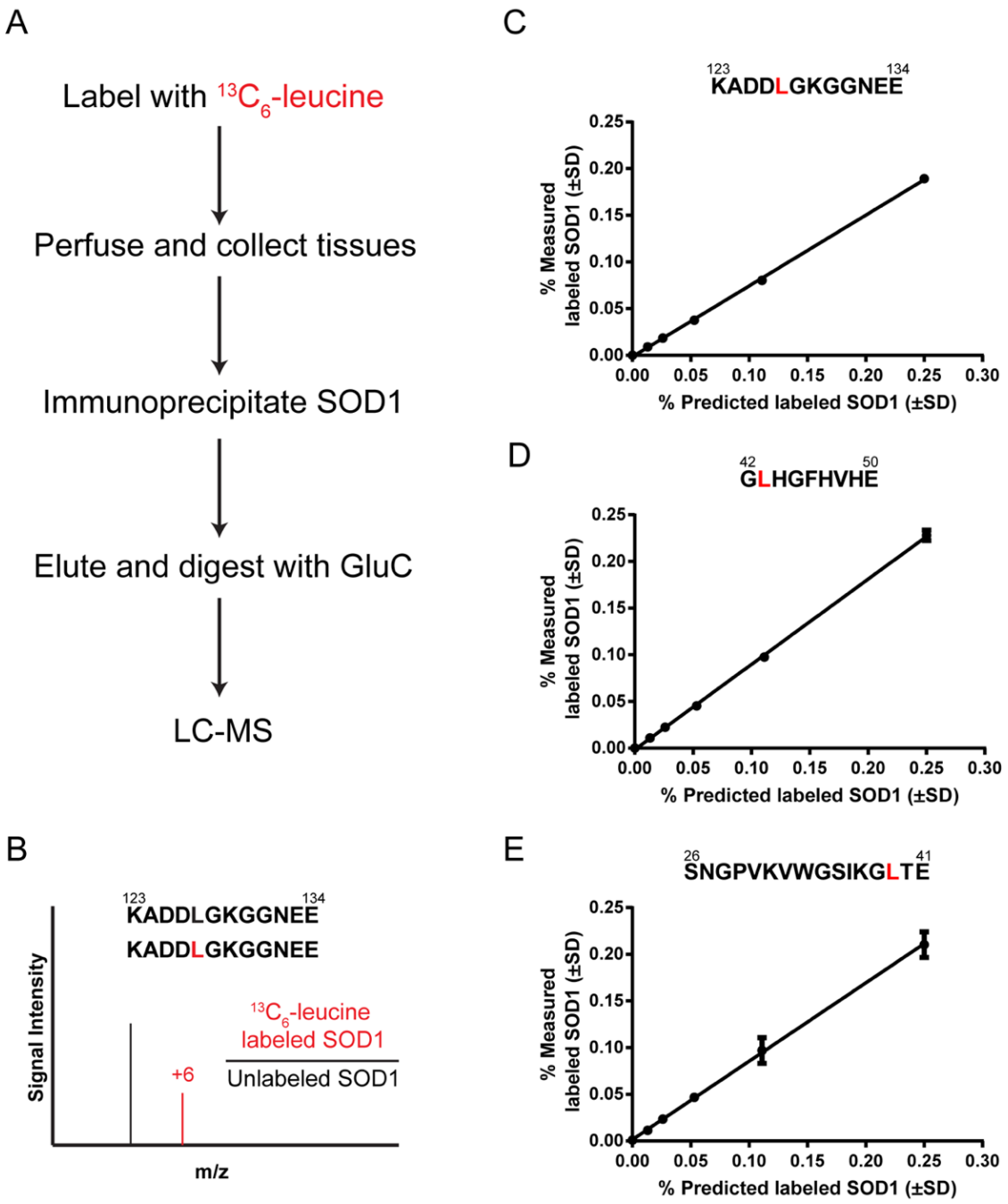

Figure 1. Schematic of SOD1 isolation and MS detection method. A) Flow chart detailing the isolation, processing, and detection of leucine-containing SOD1 peptides. B) Schematic representing LC/tandem MS detection of $^{13}C_6$-leucine containing peptides. The +6 Da shift in the leucine containing peptide KADDLGKGGNEE reflects the incorporation of $^{13}C_6$-leucine. C-E) LC/tandem MS standard curves for the three leucine containing peptides used in quantifying labeled SOD1.

Development of a SILK method to measure SOD1 turnover in vivo

Preliminary experiments revealed insufficient labeling in human CSF SOD1 during a 9-hour intravenous infusion of $^{13}C_6$-leucine (data not shown). Based on this observation, we concluded that CSF SOD1 $t_{1/2}$ in vivo was likely on the order of days to weeks rather than hours. To develop the method, we labeled human SOD1 expressing rats by oral administration of $^{13}C_6$-leucine. We used rats expressing either wild-type human SOD1 (WT) or mutant human SOD1 G93A protein, a well-studied mutation that is known to cause ALS in humans and is characterized by a predictable disease onset in animal models (Aoki et al 2005, Gurney et al 1994). Approximately 100-day-old transgenic rats overexpressing human wild-type SOD1 or G93A were orally administered $^{13}C_6$-leucine for 7 days followed by unlabeled leucine for an additional 56 days. Plasma, spinal cord, cortex, CSF, liver, and kidney were collected at indicated time points (Figure 2A) in order to model plasma free $^{13}C_6$-leucine and SOD1 kinetics in vivo. Following detergent fractionation to immunoprecipitate soluble SOD1 from tissues, we used our LC/tandem MS method to detect and analyze leucine-containing SOD1 peptides and quantify SOD1 fractional turnover rates (FTR) and $t_{1/2}$ in each tissue.

The shape of the plasma free $^{13}C_6$-leucine curve followed a pseudo linear increase during the oral $^{13}C_6$-leucine pulse and first-order kinetic decay during the chase with unlabeled leucine (Figure 2B). This confirmed that our oral labeling approach achieved sufficient $^{13}C_6$-leucine incorporation into soluble SOD1 peptides with minimal variance between animals. The SOD1 labeling curves reflect tracer derivation from a direct precursor/product relationship between plasma leucine and each protein, as the SOD1 labeling curves intersect the plasma leucine enrichment at their peak

enrichments (Figure 2B). These measurements also showed that $^{13}C_6$-leucine labeled SOD1 in the CSF could be measured, that the $t_{1/2}$ of CSF SOD1 was on the order of days, and that the kinetics of CSF SOD1 closely paralleled the kinetics of SOD1 in the CNS, specifically the spinal cord. However, the changing plasma free $^{13}C_6$-leucine enrichment over the time course presented a level of complexity in the system that excluded a simple calculation of SOD1 $t_{1/2}$. Specifically, the linear rise and first order decay of the curve as well as the persistence of substantial $^{13}C_6$-leucine long after the cessation of labeled diet reflected the slow kinetics of the oral administration method and the contribution of whole-body tracer recycling to long term kinetic analysis, respectively. As such, we recognized the need to model the system in order to account for the dynamics of this tracer pool and its influence on the tissue-specific SOD1 pools to precisely quantify in vivo SOD1 kinetics.

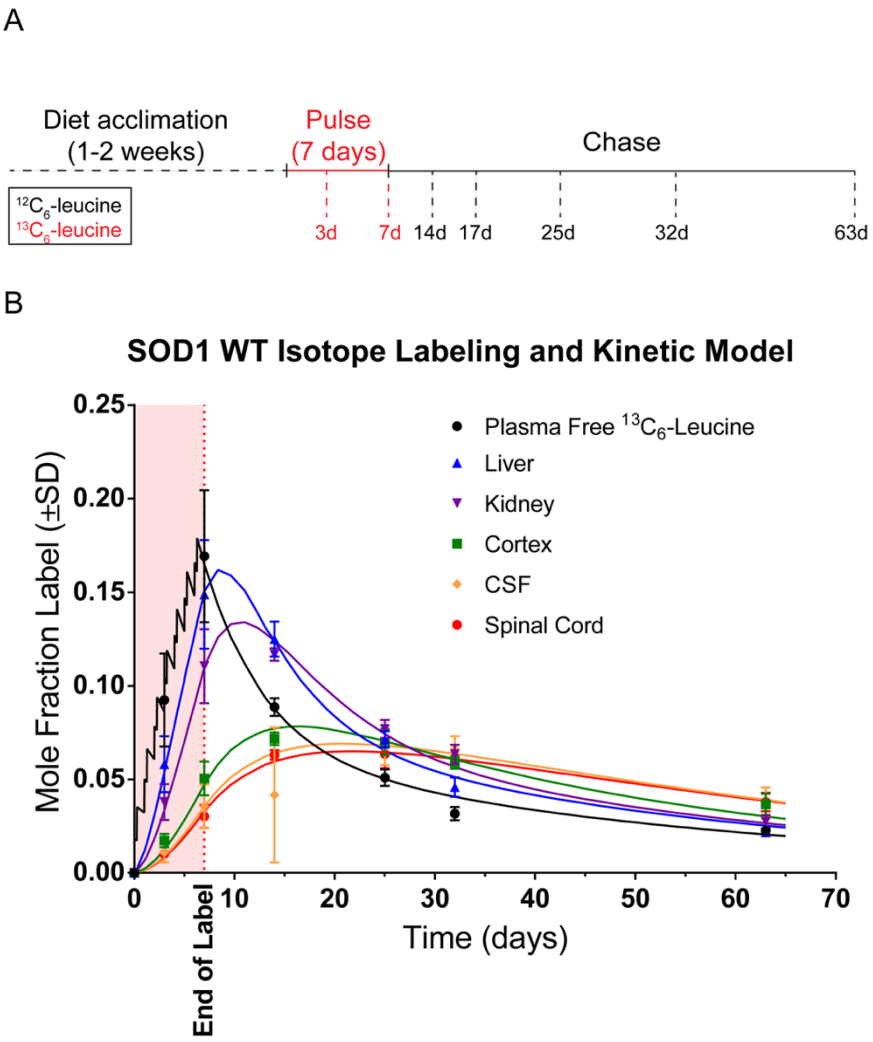

Figure 2. Kinetic data and model from SOD1 WT rats. A) Schematic of the oral labeling paradigm. SOD1 WT rats were fed $^{13}C_6$-leucine for 7 days then chased with unlabeled leucine for an additional 56 days. Tissues were collected at the indicated time points and detergent soluble SOD1 was immunoprecipitated, digested, and analyzed by LC/tandem MS. B) Mole fraction labeled (MFL) plasma free $^{13}C_6$-leucine and liver, kidney, cortex, CSF, and spinal cord SOD1 WT were plotted over time (individual points). Solid lines represent best-fit model curves. The shape of the plasma leucine curve during the $^{13}C_6$-leucine labeling period reflects the pulsatile administration of the tracer twice daily. The slower kinetics of SOD1 WT in spinal cord, cortex, and CSF are reflected in the gradual rise and fall of the curves compared to the steep slopes seen in liver and kidney. Light red shading between 0 and 7 days represents the $^{13}C_6$-leucine labeling period. n=3 for all time points with the exception of days 3 and 7 (n=6).

Kinetic modeling defined slow SOD1 kinetics

A compartmental model was developed to account for the shape of the plasma $^{13}C_6$-leucine time course and long-term whole-body tracer recycling (Supplemental Figure 2A). In this model, plasma leucine represents a central compartment where tracer freely exchanges with all other measured compartments and whole body protein or is irreversibly lost from the system. From this central compartment, forward arrows indicate the forward exchange of tracer into each tissue compartment. The reverse arrows indicate tracer return and represent the FTR, expressed as pools per day, for each compartment. Best-fit curves for free plasma $^{13}C_6$-leucine, and spinal cord, cortex, CSF, liver, and kidney SOD1 are seen overlaid the raw data in Figure 2B. The shape of the plasma $^{13}C_6$-leucine curve during labeling represents the simulated pulsatile nature of oral $^{13}C_6$-leucine tracer administered twice a day for 7 days. The model calculated a $t_{1/2}$ of 14.9 days for CSF SOD1, confirming that SOD1 is a relatively long-lived protein in this pool (Table 1). Furthermore, it showed no significant difference between SOD1 turnover rate in the CSF and the spinal cord, suggesting that the CSF pool could serve as a suitable proxy for spinal cord SOD1.

	SOD1 WT			SOD1 G93A		
	FTR (pools/d)	95% CI	Half-life (d)	FTR (pools/d)	95% CI	Half-life (d)
Whole body protein	0.063	0.057 − 0.069	11.0	0.089	0.085 − 0.093	7.8
Liver SOD1	0.397	0.379 − 0.415	1.7	0.485	0.457 − 0.514	1.4
Kidney SOD1	0.205	0.197 − 0.213	3.4	0.188	0.180 − 0.196	3.7
Cortex SOD1	0.074	0.071 − 0.078	9.3	0.104	0.098 − 0.109	6.7
CSF SOD1	0.047	0.044 − 0.050	14.9	0.074	0.070 − 0.077	9.4
Spinal cord SOD1	0.044	0.041 − 0.046	15.9	0.077	0.073 − 0.081	9.0
Liver misfolded SOD1				0.868	0.795 − 0.941	0.8
Spinal cord misfolded SOD1				0.325	0.309 − 0.342	2.1
Liver total protein	1.265	1.121 − 1.409	0.5	0.711	0.655 − 0.767	1.0
Cortex total protein	0.177	0.167 − 0.186	3.9	0.127	0.120 − 0.135	5.4
Spinal cord total protein	0.087	0.081 − 0.094	7.9	0.096	0.088 − 0.104	7.2

Table 1. Model parameters for SOD1 WT and G93A turnover in ALS rats. For each compartment in the SOD1 kinetic model, the fractional turnover rate (FTR), 95% confidence interval (95% CI), and $t_{1/2}$ were calculated. The data confirm the long $t_{1/2}$ of SOD1 in CNS tissues, with SOD1 WT approximately 9-fold and 5-fold longer-lived in the spinal cord and cortex than in the liver, respectively. For SOD1 G93A, this relationship persists, with SOD1 approximately 6- and 4.5-fold longer-lived in spinal cord and cortex than in the liver, respectively. Between groups of animals, SOD1 G93A was generally shorter-lived in each tissue than SOD1 WT.

SOD1 WT and G93A turnover

Although we were primarily concerned with using SILK to measure the turnover of SOD1 in the CSF and the CNS, our labeling method also allowed us to examine SOD1 turnover in several tissues within the same animal. As expected, the plasma free $^{13}C_6$-leucine served as the tracer source for all measured SOD1 pools. Interestingly, SOD1 turnover was significantly slower in the CNS (Figure 2B and Table 1). Specifically, the $t_{1/2}$ of SOD1 in the spinal cord (15.9 days) and cortex (9.3 days) was 2.8 – 9 times slower than the $t_{1/2}$ from the liver (1.8 days) or kidneys (3.4 days).

To better understand disease models, we also applied our SILK method to SOD1 G93A rats (Supplemental Figure 2B, Figure 3A). Similar to SOD1 WT rats, the shape of the plasma free $^{13}C_6$-leucine curve confirmed that these animals received sufficient label (Figure 3B). When comparing the SOD1 labeling curves, the same relative differences between tissues with regards to SOD1 turnover rates were evident (Table 1). When comparing between SOD1 WT and G93A in the same tissues, SOD1 G93A has a 1.1 – 1.8 fold faster turnover rate with the exception of the kidneys. This accelerated turnover rate for SOD1 G93A agrees with previous cell culture and in vivo studies, and may reflect an unstable state (Borchelt et al 1994, Hoffman et al 1996, Johnston 2000, Oeda et al 2001, Ratovitski et al 1999).

In addition to assaying total soluble SOD1 G93A, we were able to immunoprecipitate the pool of misfolded SOD1 G93A from the spinal cord in our labeled animals using the misfolded-specific SOD1 antibody B8H10. Best-fit curves showed that the misfolded G93A pool has much faster turnover rate than total soluble SOD1 G93A in each tissue measured (Figure 3C). Misfolded SOD1 G93A had extremely rapid

kinetics in the liver, faster than the total soluble SOD1 G93A pool, and much faster than the misfolded protein pool in the spinal cord. Interestingly, misfolded SOD1 G93A in the liver peaked higher than the peripheral plasma free $^{13}C_6$-leucine enrichment, which likely reflected first-pass absorption of the orally administered tracer coupled with a fast turnover rate. As expected, no misfolded SOD1 could be immunoprecipitated or detected by LC/tandem MS in either spinal cords or livers from SOD1 WT animals (data not shown). These data indicate that misfolded mutant SOD1 is not unique to the spinal cord, that its turnover rate is accelerated relative to total soluble SOD1, and suggest that its low levels in the liver may be a function of its fast turnover rate.

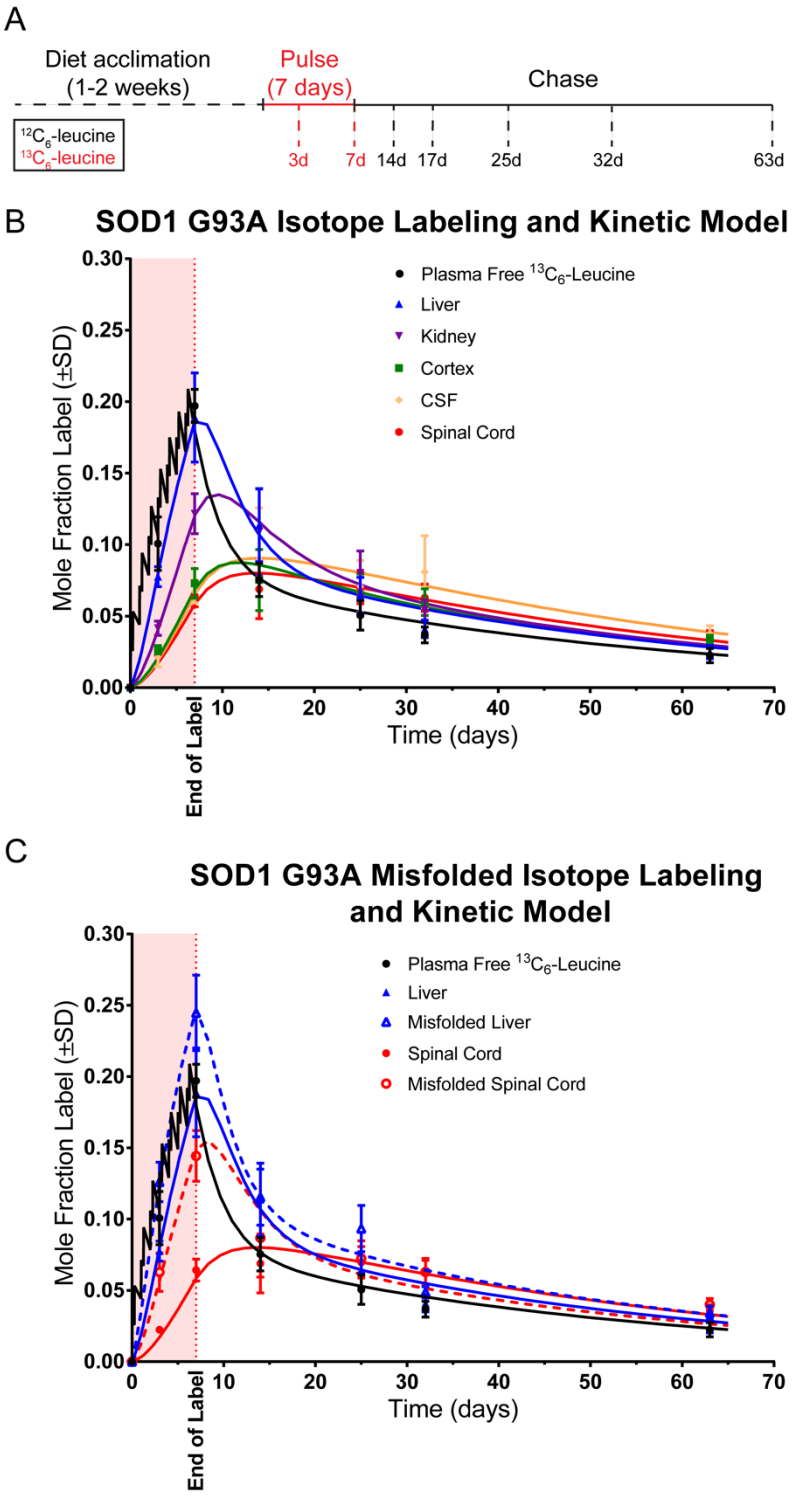

Figure 3. Kinetic data and model from SOD1 G93A rats. A) Schematic of the oral labeling paradigm. SOD1 G93A rats were fed $^{13}C_6$-leucine for 7 days then chased with unlabeled leucine for an additional 56 days. Tissues were collected at the indicated time

points and detergent soluble SOD1 was immunoprecipitated, digested, and analyzed by LC/tandem MS. B) Mole fraction labeled (MFL) plasma free $^{13}C_6$-leucine and liver, kidney, cortex, CSF, and spinal cord SOD1 G93A were plotted over time (individual points) and modeled as previously described (solid lines). The slower kinetics of SOD1 G93A in spinal cord, cortex, and CSF are reflected in the gradual rise and fall of the curves compared to the steep slopes seen in liver and kidney. C) Misfolded SOD1 G93A was immunoprecipitated from previously labeled SOD1 G93A rat tissue with the α-misfolded SOD1 B8H10 antibody, digested, analyzed by LC/tandem MS, and modeled as previously described (solid lines). Labeled misfolded pools in both spinal cord and liver reveal accelerated turnover rates when compared to total soluble SOD1 within each tissue. For both graphs, light red shading between 0 and 7 days represents the $^{13}C_6$-leucine pulse interval. n=3 for all time points with the exception of day 14 (n=2).

Determination of SOD1 turnover in human CSF using SILK

Translating this SILK method to healthy, normal human research participants allowed us to determine CSF SOD1 turnover rates as a proxy for CNS SOD1 turnover rate. In these human studies, we optimized the timing of CSF and blood sampling over a long time period because our SOD1 WT rodent studies revealed a slow CSF SOD1 turnover rate (approximately 15 days), and the major limitation in a human study was the frequency of CSF collections by lumbar puncture. Human participants consumed a reduced leucine-containing diet supplemented with $^{13}C_6$-leucine powder for 10 days. Plasma and CSF were collected at indicated time points after label administration and processed for plasma free $^{13}C_6$-leucine, total CSF protein, and labeled SOD1 (Figure 4A). The data were then modeled as previously described where plasma free $^{13}C_6$-leucine fit to a central compartment and tracer freely exchanged with all other tissue compartments (Supplemental Figure 2C).

In all subjects, plasma free $^{13}C_6$-leucine enrichment achieved ~3% at the end of label administration. This indicated that our 10-day oral labeling strategy resulted in detectable and sufficient plasma $^{13}C_6$-leucine enrichment for quantifying in vivo CSF SOD1 kinetics in the context of a controlled leucine diet. This was confirmed after quantifying $^{13}C_6$-leucine abundance in CSF total protein (Table 2). For each subject, the CSF SOD1 labeling curve displayed a slow rise and fall relative to total CSF protein labeling, indicating a much slower CSF SOD1 turnover rate of CSF SOD1 compared to CSF total protein. The average CSF SOD1 and CSF total protein $t_{1/2}$ was 25.0 ± 7.4 days and 3.6 ± 1.0 days, respectively. Thus, the human CSF SOD1 turnover rate agreed with the slow SOD1 turnover rate observed in our rodent study. Importantly,

these four human studies validated our $^{13}C_6$-leucine oral administration paradigm for quantifying long-lived protein kinetics.

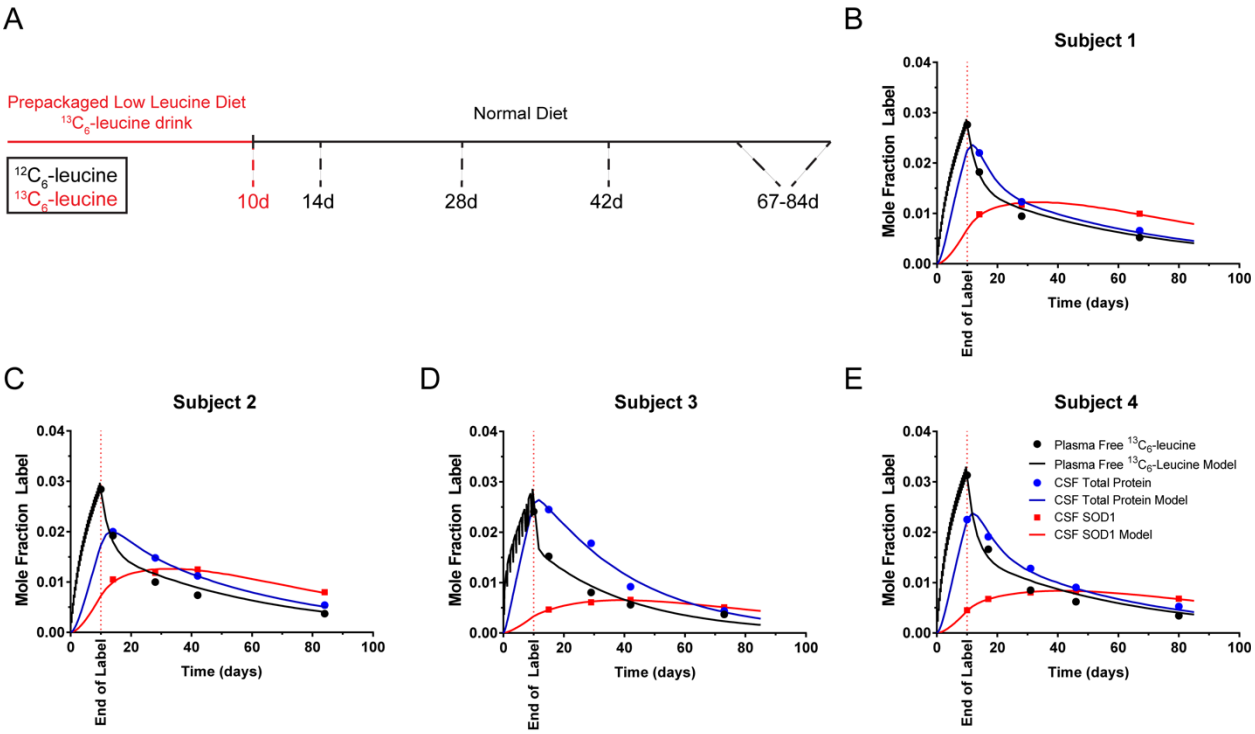

Figure 4. Modeling SOD1 kinetics in human CSF. A) Schematic of the oral labeling paradigm. Participants were placed on a prepackaged low leucine diet and administered $^{13}C_6$-leucine for 10 days, after which they resumed a normal diet. CSF and plasma were collected at the indicated time points and total protein or SOD1 were isolated, digested, and analyzed by GC-MS or LC/tandem MS, respectively. B) Data points with overlaid best fit model curves (solid lines) of plasma free $^{13}C_6$-leucine, CSF total protein, and CSF SOD1 for human subject 1, C) subject 2, D) subject 3, E) and subject 4.

	Half-life (d)				
	Subject 1	**Subject 2**	**Subject 3**	**Subject 4**	**Average (±SD)**
CSF total protein	2.4	4.9	3.7	3.45	**3.6 ± 1.0**
CSF SOD	19.2	18.3	32.9	29.8	**25.0 ± 7.4**

Table 2. CSF SOD1 and total protein half-life in human participants. Average half-life was calculated for CSF total protein and CSF SOD1 from all 4 subjects.

DISCUSSION

This approach marks the first time to our knowledge that a stable isotope of an amino acid was administered orally for the purposes of measuring the turnover of a long-lived protein in human CSF and expands the repertoire of oral tracers for studying long-lived proteins in vivo. Similar to oral administration of heavy water, our oral $^{13}C_6$-leucine administration paradigm resulted in detectable amounts of labeled amino acid in the plasma and CSF, suggesting that this approach is reliable and suitable for quantifying protein kinetics in tissues and CSF of animals and humans. The oral SILK approach presents significant advantages. First, oral administration of the tracer amino acid is technically easier than intravenous or intraperitoneal injections in humans or rodents and achieves predictable labeling in plasma and tissue protein pools. Second, it is much safer than using radioactively labeled amino acids. Third, the time scale over which the labeling and tissue collection occurs facilitates the study of other long-lived proteins. Fourth, the LC/tandem MS is highly specific for detecting and quantifying label-incorporated SOD1 peptides after immunoprecipitation and digestion of soluble SOD1. Oral administration of $^{13}C_6$-leucine was well tolerated with no adverse events reported by the participants (data not shown), achieved detectable levels in both rodents and humans, and displayed predictable kinetics. Isolation and LC/tandem MS detection of tracer-incorporated SOD1 peptides enabled a high degree of specificity as a result of both antibody specificity and predicted *m/z* ratios. Overall, this method provides a specific, quantitative, and safe approach for quantifying long-lived protein turnover in vivo with extensive applications to many areas of biology.

The development of our SILK method allowed us to measure for the first time the rate of SOD1 turnover in the CSF of human subjects. After optimization of the method in humans, we found that SOD1 $t_{1/2}$ in the CSF was approximately 25 ± 7 days, a number that reflects the long $t_{1/2}$ of SOD1 WT in the CSF of transgenic rats. We also found that the $t_{1/2}$ of CSF total protein was 3.6 ± 1.0 days. Since the CSF total protein pool is weighted heavily by few abundant proteins, this is not a representative sample of CNS protein pools. However, our rat study did show that CSF and spinal cord SOD1 turnover were not significantly different, suggesting that CSF SOD1 could be used as a proxy for the spinal cord SOD1 pool. Determination of human SOD1 turnover in the CSF has important implications for understanding SOD1 biology in ALS and for biomarker development and monitoring therapy in patients treated with SOD1 ASOs (DeVos & Miller 2013, Miller et al 2013, Winer et al 2013). By measuring the $t_{1/2}$ of SOD1 in human CSF, one can predict the optimal time to measure SOD1 CSF concentrations in patients treated with SOD1 ASOs. The data also influence the timing and frequency of dosing, as well as many other pharmacodynamic aspects of ASO therapy. Indeed, one theoretical application of this technique involves labeling during ASO treatment to monitor therapeutic effects of the drug on SOD1 clearance rates.

Although we have successfully measured SOD1 $t_{1/2}$ in healthy subjects, an important future study will need to address mutant SOD1 $t_{1/2}$ in ALS patients. Our rat data and previous cell culture studies confirm that mutant SOD1 $t_{1/2}$ is significantly shorter than WT and that the degree of $t_{1/2}$ reduction may be mutant dependent (Borchelt et al 1994, Hoffman et al 1996, Johnston 2000, Ratovitski et al 1999). The autosomal dominant nature of SOD1-ALS means that patients have one copy of both

WT and mutant SOD1. A significant advantage in our LC/tandem MS SILK approach is the ability to independently measure both WT and mutant SOD1 species in the same patient, as single amino acid changes result in detectable changes in the m/z ratios of predicted peptides. Future studies in these patients have the potential to determine SOD1 turnover as a function of age, disease status (e.g. presymptomatic versus symptomatic), and to what degree the SOD1 WT $t_{1/2}$ is or is not influenced by the presence of mutant SOD1.

In SOD1 WT and G93A rats, the tissues most affected in ALS (i.e. spinal cord and cortex) possessed the slowest rate of turnover. Slow turnover may explain the general susceptibility of the CNS in many neurodegenerative proteinopathies. Indeed, global proteomics approaches using stable isotopes have shown that brain proteins possess a slow turnover rate, even if identical proteins or protein complexes are compared between tissues. (Price et al 2010, Savas et al 2012). This relative difference between tissues agrees with our TCA-precipitated total protein data from cortex and liver and suggests, but does not prove, that slower protein turnover in the CNS tissue may result in misfolded SOD1 accumulation and pathology. Consistent with this, in primary culture, slow protein turnover correlates with susceptibility to toxicity (Barmada et al 2014, Tsvetkov et al 2013). As mutant SOD1 selectively kills motor neurons, it will be important to determine the relative rates of SOD1 protein turn over in specific cell types within the CNS.

Our SILK labeling method could be applied to study the kinetics of a wide variety of long-lived proteins in both animal models and human CSF and plasma. We hypothesize that most intracellular proteins in the CNS have a $t_{1/2}$ on the order of days

to weeks, making them ideal for the long-term labeling method developed here. Our kinetic data from TCA-precipitated total protein from spinal cord and cortex support this claim with a $t_{1/2}$ of 7.9 and 3.9 days for SOD1 WT rats, respectively (Table 1).

It should be noted that D_2O labeling has also been successfully used for understanding kinetics of proteins in the CNS (Fanara et al 2012). We used oral $^{13}C_6$-leucine in this study because of the known safety of oral leucine and the high enrichment of the label within a single M+6 isotopomer facilitating LC/tandem MS analysis.

With this study, we have demonstrated a successful SILK design that utilizes oral administration of a tracer amino acid for measuring long-lived proteins in rodents and human subjects. This technique enabled us to show that SOD1 is a long-lived protein in human CSF and that the $t_{1/2}$ of SOD1 in the CSF correlates with that in the CNS in rats. The method described here has wide ranging applications that could be applied to measure protein turnover in a number of neurodegenerative diseases in both animals and human CSF (or plasma) as well as monitor the pharmacodynamics of treatments designed to modulate protein levels, such as ASOs, small molecules, or siRNA.

ACKNOWLEDGEMENTS

We thank Carey Shaner, Amy Wegener, and Tao Shen for expert technical assistance and Pak Chan for the gift of the SOD1 WT rats. We also thank Lucy Liu and Ling Muncell for their preliminary work on this project and Rebecca Blair for designing and implementing the reduced leucine diet for the human study. Funding was provided by the ALS Association #2427, R01NS078398, U01NS084970, R21NS072584, Washington University Hope Center for Neurologic Disorders Pilot Project to TMM and 5F31NS078818-02 to MJC. Support for clinical subjects was provided by U.S.P.H.S. grant 5UL1 RR024992-02 to the Center for Applied Research Sciences (CARS) at Washington University. This study was funded by the following grants to RJB: NIH R01NS065667 and the Adler Foundation and also supported by the Glenn Foundation and Ruth K. Broadman Biomedical Research Foundation. The Washington University Biomedical Mass Spectrometry Research Facility was funded by NIH grants P41 GM103422, P30 DK056341, and P30 DK020579 to KEY. BWP gets salary support from the Nutrition Obesity Research Center and P30 DK056341.

Sequence	Precursors	Product	Collision Energy (V)
GLHGFHVHE	516.754	649.32	21
	516.754	725.336	21
	516.754	748.388	21
	519.764	655.34	21
	519.764	725.336	21
	519.764	754.409	21
KADDLGKGGNEE	616.791	543.277	24
	616.791	690.305	24
	616.791	803.389	24
	616.791	1033.443	24
	616.791	1104.48	24
	619.801	549.297	24
	619.801	690.305	24
	619.801	809.409	24
	619.801	1039.463	24
	619.801	1110.5	24
SNGPVKVWGSIKGLTE	836.457	547.308	32
	836.457	868.467	32
	836.457	990.525	32
	836.457	1089.593	32
	836.457	1125.605	32
	839.467	553.328	32
	839.467	868.467	32
	839.467	996.545	32
	839.467	1095.614	32
	839.467	1125.605	32

Supplemental Table 1. Transition ions used for LC/tandem MS

Subject	Age	Gender	Race
1	66	Male	Caucasian
2	51	Male	African American
3	72	Male	Caucasian
4	74	Male	African American

Supplemental Table 2. Demographics of human participants labeled with $^{13}C_6$-leucine.

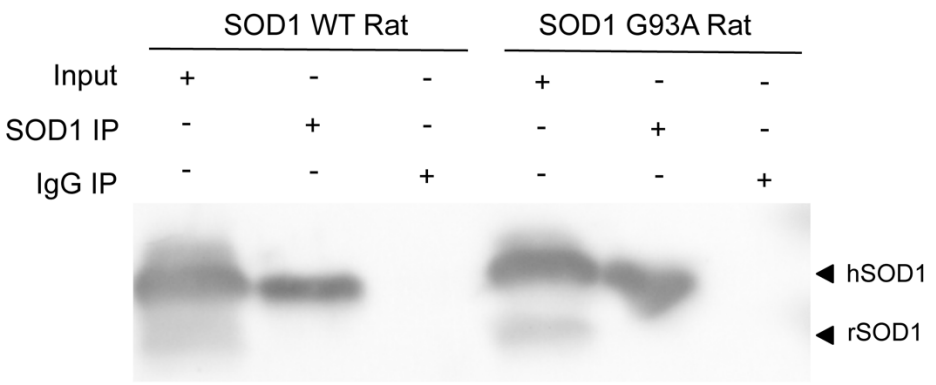

Supplemental Figure 1. Immunoprecipitation of human SOD1 transgenic rats. Western blot showing the successful immunoprecipitation of SOD1 from SOD1 WT and G93A transgenic rat spinal cord using magnetic beads covalently coupled to anti-SOD1 antibodies. hSOD1 signifies human SOD1 and rSOD1 signifies rat SOD1.

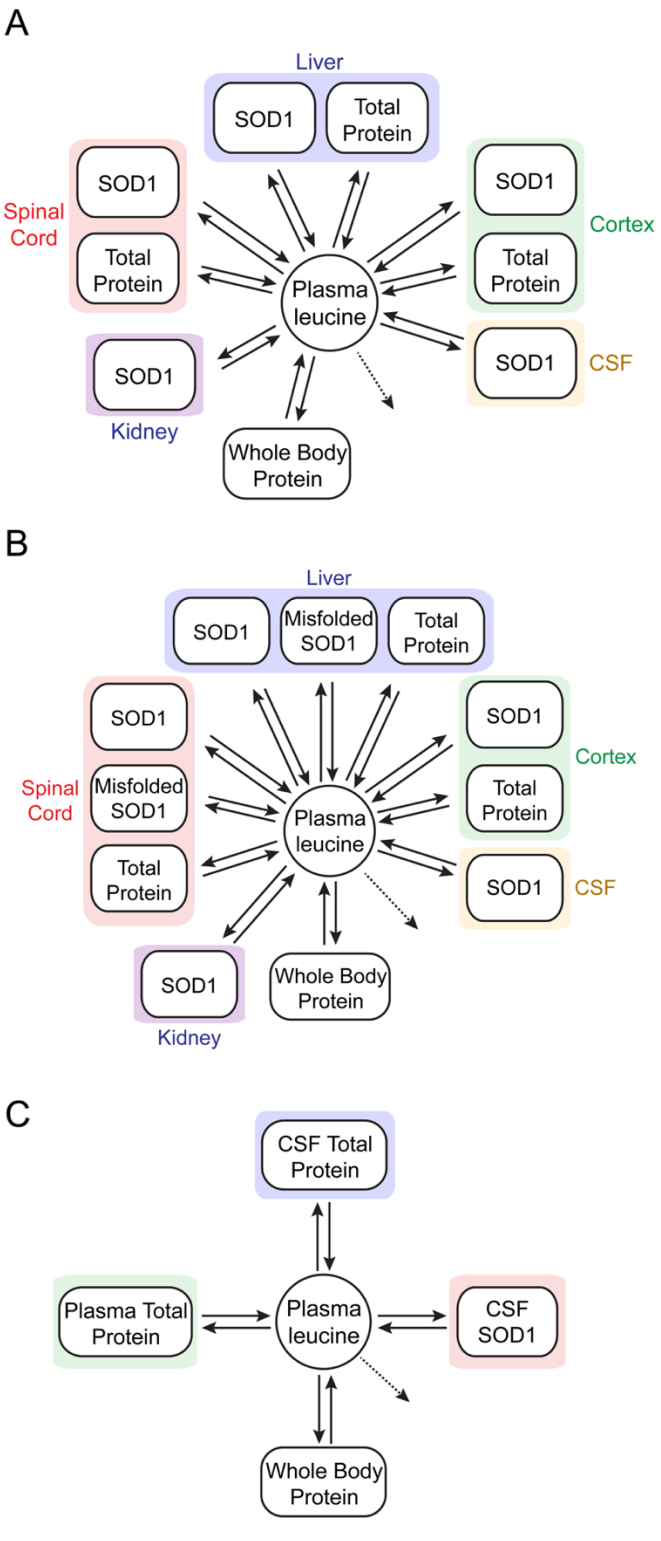

Supplemental Figure 2. Kinetic models developed for this study. In each model, plasma leucine represents a central compartment where tracer freely exchanges with all other measured compartments and whole body protein or is irreversibly lost from the

system. From this central compartment, forward arrows indicate the forward exchange of tracer into each tissue compartment. The reverse arrows indicate tracer return and represent the FTR, expressed as pools per day, for each compartment. Dotted lines represent irreversible loss of tracer from the system. A) Diagram of the compartmental model accounting for plasma $^{13}C_6$-leucine, tissue-specific soluble SOD1, and total protein over the full time course in SOD1 WT rats. B) Diagram of the compartmental model accounting for plasma $^{13}C_6$-leucine, tissue specific soluble SOD1, misfolded SOD1, and total protein over the full time course in SOD1 G93A rats. C) Diagram of the compartmental model accounting for plasma free $^{13}C_6$-leucine, CSF total protein, and CSF SOD1 over the full time course for human participants receiving a 10-day course of $^{13}C_6$-leucine followed by a normal diet.

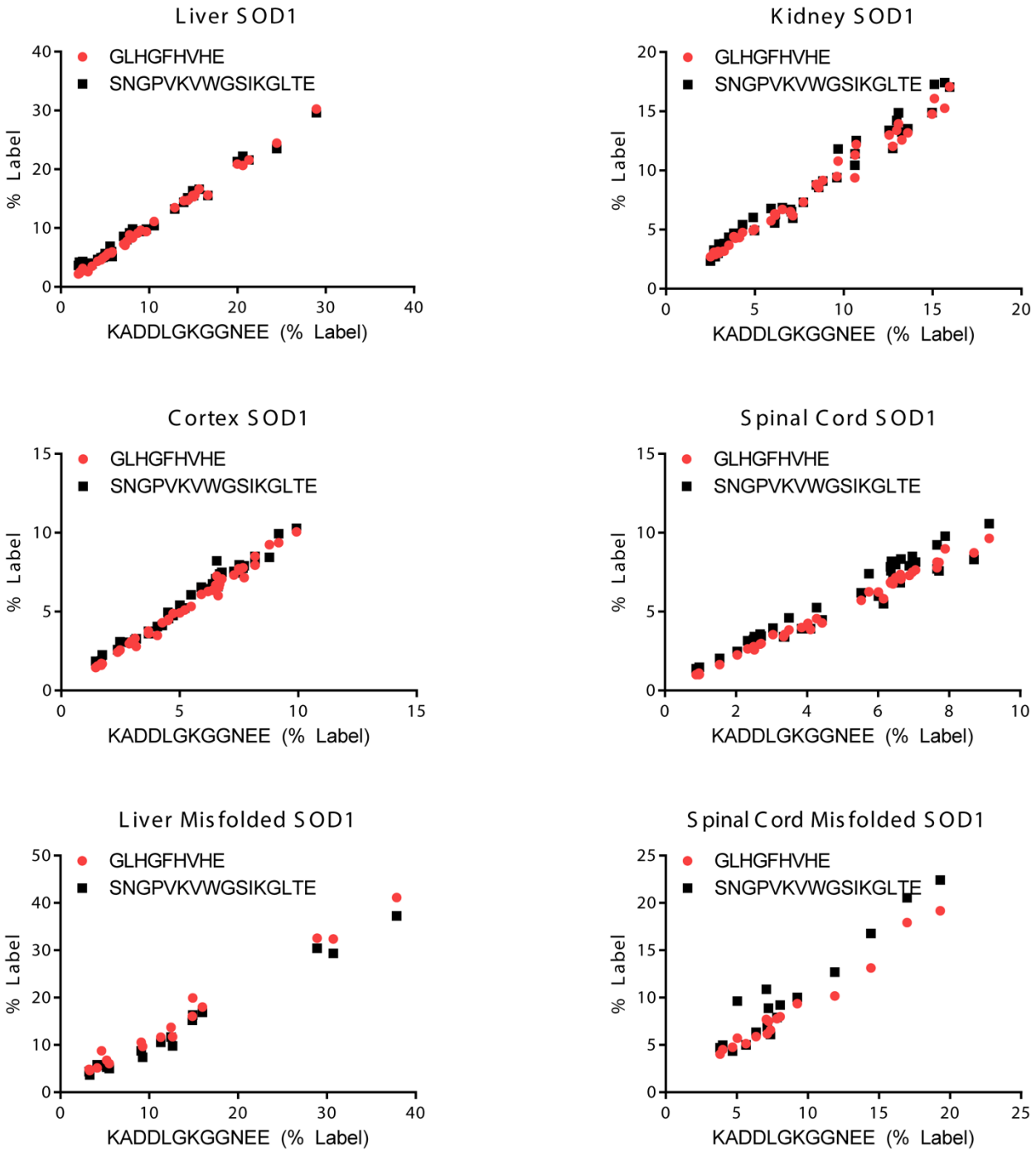

Supplemental Figure 3. Correlations between the three leucine-containing SOD1 peptides used in this study. High correlations confirm the accuracy of mass spectrometric quantification of tracer:tracee measurements for tissue-specific SOD1. $R^2 > 0.9199$ and $p < 0.0001$ for all groups.

REFERENCES

Aoki M, Kato S, Nagai M, Itoyama Y. 2005. Development of a rat model of amyotrophic lateral sclerosis expressing a human SOD1 transgene. Neuropathology 25: 365-70

Barmada SJ, Serio A, Arjun A, Bilican B, Daub A, et al. 2014. Autophagy induction enhances TDP43 turnover and survival in neuronal ALS models. Nat Chem Biol 10: 677-85

Bateman RJ, Munsell LY, Chen X, Holtzman DM, Yarasheski KE. 2007. Stable isotope labeling tandem mass spectrometry (SILT) to quantify protein production and clearance rates. J Am Soc Mass Spectrom 18: 997-1006

Bateman RJ, Munsell LY, Morris JC, Swarm R, Yarasheski KE, Holtzman DM. 2006. Human amyloid-beta synthesis and clearance rates as measured in cerebrospinal fluid in vivo. Nat Med 12: 856-61

Bateman RJ, Siemers ER, Mawuenyega KG, Wen G, Browning KR, et al. 2009. A gamma-secretase inhibitor decreases amyloid-beta production in the central nervous system. Ann Neurol 66: 48-54

Borchelt DR, Lee MK, Slunt HS, Guarnieri M, Xu ZS, et al. 1994. Superoxide dismutase 1 with mutations linked to familial amyotrophic lateral sclerosis possesses significant activity. Proc Natl Acad Sci U S A 91: 8292-6

Castellano JM, Kim J, Stewart FR, Jiang H, DeMattos RB, et al. 2011. Human apoE isoforms differentially regulate brain amyloid-beta peptide clearance. Sci Transl Med 3: 89ra57

Chan PH, Kawase M, Murakami K, Chen SF, Li Y, et al. 1998. Overexpression of SOD1 in transgenic rats protects vulnerable neurons against ischemic damage after global cerebral ischemia and reperfusion. J Neurosci 18: 8292-9

Cheah BC, Vucic S, Krishnan AV, Kiernan MC. 2010. Riluzole, neuroprotection and amyotrophic lateral sclerosis. Current medicinal chemistry 17: 1942-199

DeVos SL, Miller TM. 2013. Antisense oligonucleotides: treating neurodegeneration at the level of RNA. Neurotherapeutics 10: 486-97

Elbert DL, Mawuenyega KG, Scott EA, Wildsmith KR, Bateman RJ. 2008. Stable isotope labeling tandem mass spectrometry (SILT): integration with peptide identification and extension to data-dependent scans. J Proteome Res 7: 4546-56

Fanara P, Wong PY, Husted KH, Liu S, Liu VM, et al. 2012. Cerebrospinal fluid-based kinetic biomarkers of axonal transport in monitoring neurodegeneration. J Clin Invest 122: 3159-69

Foust KD, Salazar DL, Likhite S, Ferraiuolo L, Ditsworth D, et al. 2013. Therapeutic AAV9-mediated suppression of mutant SOD1 slows disease progression and extends survival in models of inherited ALS. Molecular therapy : the journal of the American Society of Gene Therapy 21: 2148-59

Gros-Louis F, Soucy G, Lariviere R, Julien JP. 2010. Intracerebroventricular infusion of monoclonal antibody or its derived Fab fragment against misfolded forms of SOD1 mutant delays mortality in a mouse model of ALS. J Neurochem 113: 1188-99

Gurney ME, Pu H, Chiu AY, Dal Canto MC, Polchow CY, et al. 1994. Motor neuron degeneration in mice that express a human Cu,Zn superoxide dismutase mutation. Science 264: 1772-5

Hoffman EK, Wilcox HM, Scott RW, Siman R. 1996. Proteasome inhibition enhances the stability of mouse Cu/Zn superoxide dismutase with mutations linked to familial amyotrophic lateral sclerosis. J Neurol Sci 139: 15-20

Johnston JA. 2000. Formation of high molecular weight complexes of mutant Cu,Zn-superoxide dismutase in a mouse model for familial amyotrophic lateral sclerosis. Proceedings of the National Academy of Sciences 97: 12571-76

Kiernan MC, Vucic S, Cheah BC, Turner MR, Eisen A, et al. 2011. Amyotrophic lateral sclerosis. Lancet 377: 942-55

Liu HN, Tjostheim S, Dasilva K, Taylor D, Zhao B, et al. 2012. Targeting of monomer/misfolded SOD1 as a therapeutic strategy for amyotrophic lateral sclerosis. J Neurosci 32: 8791-9

Mawuenyega KG, Kasten T, Sigurdson W, Bateman RJ. 2013. Amyloid-beta isoform metabolism quantitation by stable isotope-labeled kinetics. Anal Biochem 440: 56-62

Mawuenyega KG, Sigurdson W, Ovod V, Munsell L, Kasten T, et al. 2010. Decreased clearance of CNS beta-amyloid in Alzheimer's disease. Science 330: 1774

McCord JM, Fridovich I. 1969. Superoxide dismutase. An enzymic function for erythrocuprein (hemocuprein). J Biol Chem 244: 6049-55

Miller TM, Pestronk A, David W, Rothstein J, Simpson E, et al. 2013. An antisense oligonucleotide against SOD1 delivered intrathecally for patients with SOD1

familial amyotrophic lateral sclerosis: a phase 1, randomised, first-in-man study. Lancet neurology 12: 435-42

Nagai M, Aoki M, Miyoshi I, Kato M, Pasinelli P, et al. 2001. Rats expressing human cytosolic copper-zinc superoxide dismutase transgenes with amyotrophic lateral sclerosis: associated mutations develop motor neuron disease. J Neurosci 21: 9246-54

Oeda T, Shimohama S, Kitagawa N, Kohno R, Imura T, et al. 2001. Oxidative stress causes abnormal accumulation of familial amyotrophic lateral sclerosis-related mutant SOD1 in transgenic Caenorhabditis elegans. Hum Mol Genet 10: 2013-23

Ong SE. 2012. The expanding field of SILAC. Anal Bioanal Chem 404: 967-76

Owens FN, Shin IS, Pettigrew JE, Oltjen JW. 1994. Apportioning Leucine Requirements for Maintenance Versus Growth for Rats. Nutr Res 14: 73-82

Parise G, Mihic S, MacLennan D, Yarasheski KE, Tarnopolsky MA. 2001. Effects of acute creatine monohydrate supplementation on leucine kinetics and mixed-muscle protein synthesis. J Appl Physiol 91: 1041-7

Potter R, Patterson BW, Elbert DL, Ovod V, Kasten T, et al. 2013. Increased in vivo amyloid-beta42 production, exchange, and loss in presenilin mutation carriers. Sci Transl Med 5: 189ra77

Price JC, Guan S, Burlingame A, Prusiner SB, Ghaemmaghami S. 2010. Analysis of proteome dynamics in the mouse brain. Proc Natl Acad Sci U S A 107: 14508-13

Price JC, Holmes WE, Li KW, Floreani NA, Neese RA, et al. 2012. Measurement of human plasma proteome dynamics with (2)H(2)O and liquid chromatography tandem mass spectrometry. Anal Biochem 420: 73-83

Prudencio M, Durazo A, Whitelegge JP, Borchelt DR. 2010. An examination of wild-type SOD1 in modulating the toxicity and aggregation of ALS-associated mutant SOD1. Hum Mol Genet 19: 4774-89

Ratovitski T, Corson LB, Strain J, Wong P, Cleveland DW, et al. 1999. Variation in the biochemical/biophysical properties of mutant superoxide dismutase 1 enzymes and the rate of disease progression in familial amyotrophic lateral sclerosis kindreds. Hum Mol Genet 8: 1451-60

Reeds DN, Cade WT, Patterson BW, Powderly WG, Klein S, Yarasheski KE. 2006. Whole-body proteolysis rate is elevated in HIV-associated insulin resistance. Diabetes 55: 2849-55

Rosen DR, Siddique T, Patterson D, Figlewicz DA, Sapp P, et al. 1993. Mutations in Cu/Zn superoxide dismutase gene are associated with familial amyotrophic lateral sclerosis. Nature 362: 59-62

Savas JN, Toyama BH, Xu T, Yates JR, 3rd, Hetzer MW. 2012. Extremely long-lived nuclear pore proteins in the rat brain. Science 335: 942

Tsvetkov AS, Arrasate M, Barmada S, Ando DM, Sharma P, et al. 2013. Proteostasis of polyglutamine varies among neurons and predicts neurodegeneration. Nat Chem Biol 9: 586-92

Wang H, Yang B, Qiu L, Yang C, Kramer J, et al. 2014. Widespread spinal cord transduction by intrathecal injection of rAAV delivers efficacious RNAi therapy for amyotrophic lateral sclerosis. Hum Mol Genet 23: 668-81

Winer L, Srinivasan D, Chun S, Lacomis D, Jaffa M, et al. 2013. SOD1 in cerebral spinal fluid as a pharmacodynamic marker for antisense oligonucleotide therapy. JAMA neurology 70: 201-7

Worms PM. 2001. The epidemiology of motor neuron diseases: a review of recent studies. J Neurol Sci 191: 3-9

Chapter 4

Summary and Future Directions

Research into SOD1 ALS has been ongoing for over twenty years, resulting in numerous hypotheses of disease mechanisms, multiple models organisms, and a significant number of proposed treatments. The lack of a consensus on the pathogenesis of ALS indicates that, even after two decades, much has yet to be discovered for this multifaceted disease. This dissertation presents novel findings in two different aspects of SOD1 mediated ALS – the initial biochemical characterization of cSOD1 in canine DM and insights into the tissue specificity of the disease. The highlights of these findings and their future directions are described below.

SOD1 mutants in canine DM biochemically parallel human SOD1 and ALS

In Chapter 2, original work detailed the first characterization of cSOD1 mutants in canine DM. This was a direct extension of work done by Joan Coates' group that first identified the cSOD1 E40K mutation in dogs with canine DM (Awano et al. 2009). Two years later, a second mutation (T18S) was discovered in Bernese Mountain dogs with canine DM (Wininger et al. 2011). Prior to these discoveries, only one paper had unsuccessfully tried to link cSOD1 to canine spinal muscular atrophy, and only in terms of genetic sequence (Green et al. 2002). The work described in this dissertation marks the first characterization of the cSOD1 protein, the findings of which strengthen the parallels between human ALS and canine DM.

Similar to hSOD1 mutants in human ALS and transgenic animals, I was able to show that cSOD1 mutants exist as detergent insoluble aggregates in the spinal cords of affected animals and that they accumulate with disease (Johnston et al. 2000, Wang et al. 2003). This finding suggests that mutant cSOD1 possesses a similar mechanism to

hSOD1 in the spinal cords of these animals, as an accumulation of SOD1 aggregates is a defining pathological feature of SOD1 ALS. Using a variety of *in vitro* assays, I also found that cSOD1 mutants are intrinsically less stable and prone to aggregation compared to the wild-type protein. This finding recapitulates the reduced stability of human SOD1 mutants as measured by many different biochemical assays (Münch & Bertolotti 2010, Ratovitski et al. 1999, Tiwari & Hayward 2003). Importantly, I was able to determine that both the cSOD1 E40K and T18S mutants were functional dimers with full enzymatic activity. This was a critical finding, as, unlike human SOD1 ALS, a majority of canine DM is autosomal recessive, raising the possibility of a loss of function mechanism for pathogenesis. My findings lend strong support for the same toxic gain-of-function mechanism seen in human ALS.

Canine DM offers an unprecedented new model to study the natural progression of ALS

With the discovery of canine DM, the ALS field gained the first ever naturally occurring model of disease. The fact that this disease occurs in dogs is an added bonus, as the medical infrastructure for canine veterinary medicine in the United States is well established. This facilitates the discovery of affected dogs and affords ample opportunity for intervention and study, including canine clinical trials. Also, as the human environment is frequently shared by canines, the opportunity for studying environmental contributions to disease in a relatively controlled or quantified setting is unique. Additionally, since canine DM is largely a disease of purebred dogs, the genetics of the disease are closely monitored and a robust market for genetic testing exists. This

enables a large population of dogs to be accurately diagnosed and allows for early detection of mutations in the offspring of carriers or affected animals.

A significant advantage to studying canine DM over existing transgenic animal models is the natural occurrence of the disease in the setting of endogenous mutant SOD1 levels. This closely parallels the endogenous levels of SOD1 seen in human ALS, offering a more physiological window into the pathogenesis of disease. Even though there exist transgenic animal models with levels of mutant SOD1 expression below endogenous mouse SOD1, such as the SOD1 G85R, L126X, L126delTT, and G127X mice, these animals still require multiple copies of the hSOD1 transgene for a disease phenotype (Bruijn et al. 1997, Jonsson et al. 2004, Wang et al. 2005, Watanabe et al. 2005). Canine DM allows for the study of SOD1 disease mechanisms without the confounds of overexpression seen in transgenic models. Another advantage with canine DM is the ability to further study the effects of age and environment on disease. Although transgenic rodent models of SOD1 ALS technically develop disease with age, the significantly shorter lifespan of a rodent, coupled with the dependence on SOD1 gene copy number for a disease phenotype, creates an artificial, if not temporally convenient, system. Coupled with the biochemical similarities between human and canine SOD1 mutants described in Chapter 2, canine DM offers one of the closest approximations to human SOD1 ALS.

Dog models of disease are opportune candidates for testing therapies. This is facilitated by the limited genetic diversity of many dog breeds, the shared environment with humans, willing owners, significant veterinary infrastructure, and favorable market forces for treatments. For example, naturally occurring canine cancers have been

invaluable models for testing numerous treatments in clinical trials, as many canine cancers share similar etiologies with human cancers (Rankin et al. 2012, Rowell et al. 2011). Dogs also show age-related changes in cognition and even have deposition of β-amyloid, offering opportunities for testing amyloid-lowering therapies in these animals (Cotman & Head 2008, Head 2013). One promising therapy that has recently completed a Phase I clinical trial in humans is the use of antisense oligonucleotides (ASOs) against SOD1 (Miller et al. 2013). These drugs have shown enormous promise in animal models of ALS, but the clinical trial process in humans is long and arduous. Using these drugs in a canine DM model can expedite the search for safer, more efficacious ASOs, as well as elucidating the best time to treat (e.g. early vs. late).

As described in Chapter 2, cSOD1 and hSOD1 share approximately 80% identity and a propensity to aggregate when mutated. Coupled with overlapping clinical presentations between human ALS and canine DM, it is reasonable to assume that disease mechanisms are also shared. This paves the way for future experiments testing current theories of human disease in the canine DM model. For example, the past few years have seen the advent of work describing a prion-like spreading of mutant SOD1. Such a mechanism had been theorized based on the geographic spread of the disease through the neuroaxis, affecting motors neurons closest to the site of clinical manifestation (Ravits & La Spada 2009). One study has shown that hSOD1 mutants, once misfolded, can trigger further misfolding of intact SOD1 *in vitro* (Chia et al. 2010). Cell culture systems have shown that exogenously applied aggregates of mutant hSOD1 could be taken up by cells via macropinocytosis, causing endogenous mutant SOD1 to misfold, aggregate, and self-propagate through subsequent cell divisions

(Münch et al. 2011). Misfolded SOD1 can also be released from dying cells as a naked aggregate or from live cells as exosome and spread to neighboring cells (Grad et al. 2014). It would be interesting to determine if mutant cSOD1 aggregates possess the same properties of cellular uptake and SOD1 propagation. Additionally, further work by another lab using antibodies against misfolded-specific SOD1 epitopes demonstrated that co-expression of mutant hSOD1 with wild-type hSOD1 resulted in misfolding of the wild-type protein (Grad et al. 2011). More importantly, this group showed that the species-specific propagation of misfolding was dependent upon the tryptophan-32 residue. By mutating this residue, which is unique to hSOD1 (and equine SOD1), to serine (as is found in most other species' SOD1, including mouse, rat, and dog), the propagation of misfolding was significantly reduced. Since cSOD1 lacks a tryptophan at this residue, this implies that cSOD1 mutants will be unable to propagate within a cell. If the prion-like hypothesis of SOD1 ALS is correct, then that would signify that the mechanism for canine DM is dramatically different from human ALS. Therefore, further study into the ability of cSOD1 mutants to propagate misfolding and spread from cell-to-cell could offer support for or detract from a prion-like mechanism for disease.

SILK is a viable method for successfully measuring SOD1 protein turnover

Chapter 3 of this dissertation described original work developing a stable isotope labeling method with oral administration of $^{13}C_6$-leucine in both SOD1 transgenic rat models and healthy human subjects. As SOD1 was hypothesized to be a long-lived protein in the CNS, the labeling and chase period needed to be significantly long in order to accurately model SOD1 turnover. This study marked the first time that stable

isotopes were used to measure SOD1 turnover in multiple tissues in an ALS animal model and in human CSF. The method of administering the stable isotope $^{13}C_6$-leucine via the drinking water was validated by our ability to detect ample circulating free label in plasma and incorporated label in total protein and SOD1 with minimal variation. The pulse-chase paradigm employed for this study has significant advantages over more conventional methods. First, oral administration of the tracer amino acid is technically easier than injections in rodents and achieves predictable kinetics in plasma pools. It is also much safer than using traditional radioactive isotopes. Second, the time scale over which the labeling and tissue collection occurred (>60 days) facilitates the study of longer-lived proteins. Third, the LC-MS method for detecting and measuring label-incorporated SOD1 peptides is highly specific and quantitative.

Looking forward, this labeling method could be applied to other SOD1 mutant models or neurodegenerative proteins. Canine DM would be an ideal model to apply SILK, as this model avoids any artifacts due to transgenic overexpression that characterize rodent models. Administration of $^{13}C_6$-leucine to dogs with canine DM could be easily accomplished and the fact that most of the owners elect for euthanasia affords an amount of control over when tissues are collected. For younger or presymptomatic animals, cSOD1 turnover in the CSF could be monitored as a proxy for the CNS. SILK would be a valuable tool for studying the turnover of other neurodegenerative proteins, especially those with expression in multiple tissues, such as TDP-43, FUS, huntingtin, androgen receptor, and others (Huang et al. 2010, Li et al. 1993, Ruizeveld de Winter et al. 1991, Sephton et al. 2010).

SOD1 turnover is significantly slower in the tissues most affected in ALS

SILK revealed that the tissues most affected in ALS possessed the slowest rate of turnover. Specifically, the half-life of SOD1 WT in muscle (22.7 days), spinal cord (15.7 days), and cortex (9.3 days) were significantly different than in kidney (3.4 days) and liver (1.8 days). For SOD1 G93A, this relative difference was also seen, with SOD1 half-life in muscle (20.5 days), spinal cord (9.0 days), and cortex (6.7 days) significantly different from kidney (3.7 days) and liver (1.4 days). Interestingly, these turnover rates correlated with the pathological progression of disease noted in many ALS animal models. Some of the earliest pathological changes in SOD1 animal models are seen in muscle tissue. For example, muscle atrophy, NMJ loss, and mitochondrial vacuolization and uncoupling in muscle fibers have been found to precede motor neuron loss in zebrafish and mouse SOD1 models (Brooks et al. 2004, Dupuis et al. 2003, Leclerc et al. 2001, Ramesh et al. 2010, Sakowski et al. 2012). Interestingly, selective expression of SOD1 in muscle was found to be sufficient to cause muscle pathology and, in one study, motor neuron loss in mice (Dobrowolny et al. 2008, Wong & Martin 2010). While research into presymptomatic muscle function and pathology in human ALS patients is sparse, some studies have shown mitochondrial uncoupling and reduced cellular respiration in patients with disease (Dupuis et al. 2003, Echaniz-Laguna et al. 2006, Krasnianski et al. 2005, Wiedemann et al. 1998). After mitochondrial changes in muscle, the next tissue affected is the CNS with the majority of pathology seen in the spinal cord with motor neuron loss and reactive gliosis. By correlating turnover rate with the temporal order of pathogenesis, these data suggest that a reduced rate of protein clearance may play an important role in the tissue specificity of the disease.

Prior to this study, only one group looked at SOD1 turnover *in vivo* by administering deuterium-labeled water to mice, chasing with normal water, and measuring the clearance of labeled SOD1 WT-YFP or G85R-YFP in the spinal cord over time (Farr et al. 2011). This group did find that the SOD1 WT half-life was relatively long (approximately 22 days), which agreed with our SOD1 half-life data from SOD1 WT rat spinal cords. They also found that the G85R mutant possessed accelerated turnover, but to a much larger degree than what we found for G93A. This difference in mutant turnover reflects the correlation between SOD1 mutant stability and half-life that has been repeatedly demonstrated in cell culture, with more unstable mutants having significantly reduced half-lives (Borchelt et al. 1994, Hoffman et al. 1996, Johnston et al. 2000, Ratovitski et al. 1999). Indeed, future SILK experiments in SOD1 mouse models expressing more unstable mutants, such as G85R, G37R, and G127X, would most likely show rapid turnover in each tissue in comparison to SOD1 WT and G93A. As SOD1 ALS patients and animal models with these unstable mutations show the same tissue specificity of disease, this implies that the absolute rate of SOD1 mutant turnover is less important than the relative difference between tissues.

Misfolded SOD1 turnover is accelerated relative to total soluble SOD1

One of the advantages in using stable isotopes to examine SOD1 turnover *in vivo* is the ability to look at multiple SOD1 pools within the same animal. When we looked at mutant SOD1 in the spinal cord of SOD1 G93A rats, we found a 4.2-fold increase in the turnover rate compared to the total soluble SOD1 G93A protein. As with total soluble SOD1 G93A, this reflects the increased instability of the misfolded mutant

protein, which is rapidly targeted for degradation. However, the magnitude of the increase was surprising, as the misfolded pool in the spinal cord turned over faster than kidney SOD1. This finding prompted us to isolate and measure labeled misfolded SOD1 in the liver, which has been previously shown to exist at very low levels compared to the same pool in the spinal cord (Zetterström et al. 2007). As expected, the kinetics of this pool revealed a half-life of only 19.2 hours, the fastest measured in this study and 2.7 times faster than the misfolded pool in the spinal cord. The fact that the misfolded pool in the spinal cord is relatively slower than the same pool in the liver, despite significantly faster kinetics in both pools, further supported the hypothesis that affected tissues clear mutant protein less effectively than non-affected tissues.

The significantly faster turnover of the misfolded SOD1 G93A pool explains the low steady state levels of this pool in the spinal cord and liver. As this is thought to be the pathogenic species in SOD1 ALS, these low levels must be sufficient to cause disease. Indeed, other more unstable SOD1 mutants, such as G85R, L126X, L126delTT, and G127X, cause disease in animal models at levels below those of endogenous mouse SOD1 (Bruijn et al. 1997, Jonsson et al. 2004, Wang et al. 2005, Watanabe et al. 2005). The accelerated turnover rates of the more unstable SOD1 mutants in cell culture may reflect the relative population of these pools that is misfolded. For example, many of the metal-binding region mutants, such as G85R and H46R, exist mostly in the misfolded state as measured by proteinase K sensitivity assays (Hayward et al. 2002, Ratovitski et al. 1999). It would be reasonable to hypothesize that the relative difference between total soluble and misfolded pools with these mutants would be substantially less than the relative difference observed for the

G93A pools. This could be easily tested using the same misfolded-specific antibody immunoprecipitation utilized in our study in a $^{13}C_6$-leucine mouse SOD1 G85R or G127X model.

SOD1 is a long-lived protein in healthy human CSF

Chapter 3 also describes the development of a method to label healthy human subjects with $^{13}C_6$-leucine and measure SOD1 turnover in the CSF. SOD1 is prevalent in the CSF at measurable and stable levels, implying that measuring its turnover could be used as a proxy for CNS SOD1 turnover (Jacobsson et al. 2001, Winer et al. 2013). Since SOD1 turnover was relatively slow in rat CSF, we reasoned that human SOD1 would be at least as slow. Previous studies looking at β-amyloid turnover in the CSF, which has a half-life of a few hours, have relied on continuous or bolus intravenous infusions of $^{13}C_6$-leucine followed by CSF sample collection every hour from a catheter installed in the base of the spine (Bateman et al. 2006, 2007). As our animal studies demonstrated the success of oral administration of $^{13}C_6$-leucine and that SOD1 turnover in the CSF was on the order of days, we applied a modified version of our animal protocol to healthy human subjects. This was not without its challenges, as no study had previously used repeated oral doses of $^{13}C_6$-leucine in humans or had measured remaining labeled protein so far out, where amino acid recycling would increasingly contribute to TTR measurements. Oral administration of $^{13}C_6$-leucine in the setting of a controlled low leucine diet for 10 days resulted in sufficient concentration of the tracer in plasma, CSF proteins, and SOD1. We were able to construct a model from the data to incorporate the changing $^{13}C_6$-leucine precursor pool over time as well as the

contributions from tracer recycling. This study marks the first time that a stable isotope was administered orally for the purposes of measuring the turnover of a long-lived protein in human subjects and establishes a new labeling paradigm for studying long-lived proteins.

The data from labeled human subjects confirmed the long half-life of SOD1 seen in ALS rat CNS tissues and CSF. After optimizing our sample collection time points in subjects, the SOD1 half-life was approximately 25 days compared and between 2-5 days for CSF total protein. This is comparable to the approximately 15-day half-life calculated for SOD1 WT in rat CSF. Additionally, our animal data indicated that CSF SOD1 turnover closely approximates spinal cord SOD1 turnover, meaning that the SOD1 turnover rate measured in human subjects could be used as a proxy for turnover in the CNS. This has important implications for future studies looking at CSF SOD1 as a biomarker in disease and in potential treatments that modulate SOD1 levels, such as SOD1 antisense oligonucleotides (Miller et al. 2013).

SILK could be used to measure additional SOD1 pools and age-related changes in turnover

One pool that has yet to be measured in our labeled SOD1 G93A rat model is the SOD1 aggregates. Indeed, the accumulation of detergent-insoluble SOD1 species is a hallmark of disease in many animal models, including canine mutant SOD1 as demonstrated in Chapter 2. An interesting future experiment would involve looking at the turnover rates of mutant SOD1 in these aggregates in the spinal cord. Depending on the shape of the kinetic curve, one could learn much about the nature of these

aggregates. For example, if newly synthesized SOD1 was immediately incorporated into an aggregate, the aggregate curve should rise in line with the soluble SOD1 curve. If there was a delay in incorporation, then a delay in the appearance of labeled SOD1 species in the aggregate pool would be reflected in the curve. Additionally, the turnover rate of SOD1 aggregates could be directly measured, addressing whether these aggregates are permanent structures or exist in a state of flux. Taking this idea further, one could measure adjustments in the turnover rate of all SOD1 species in response to modulation of protein clearance mechanisms.

As mentioned previously, age is a major risk factor for the development of ALS. High molecular weight species of SOD1 mutants as well as misfolded SOD1 pools accumulate in the spinal cord with age (Crisp et al. 2013, Johnston et al. 2000, Wang et al. 2002). Indeed, proteasome activity has been shown to decrease with age in normal mice (Keller et al. 2000). One potential use of SILK is to examine the effects of age on SOD1 turnover in both ALS rodent models as well as human subjects. The simplest comparison would be between young and old animals, or between presymptomatic and symptomatic. Not only could SOD1 turnover be analyzed, but global protein turnover as well, allowing one to distinguish between a more specific or general reduction in SOD1 clearance with age.

Using SILK to measure SOD1 turnover in individual cell populations

A major limitation in analyzing SOD1 turnover in whole tissues is that the homogenous mix of cell populations prevents looking at turnover at the level of specific cell types. In ALS, motors neurons are uniquely affected, yet these cells only comprise

4% of the volume of the spinal cord (Zetterström et al. 2011). This means that the turnover rate measured for spinal cord derived SOD1 most likely reflects non-motor cell populations. It is reasonable to assume that significant differences may exist between motor neurons, non-motor neurons, and glia with respect to SOD1 turnover. In fact, such differences have been shown with mutant huntingtin protein. Recent work using optical pulse-chase labeling of huntingtin protein in primary culture has shown that cortical neurons clear mutant huntingtin faster than striatal neurons (the cells affected in Huntington's Disease) and that faster clearance correlates with longer cellular lifespan (Tsvetkov et al. 2013). This study provided the first indication of heterogeneity in neuronal populations with regard to protein clearance and then linked poor turnover of the ubiquitously expressed huntingtin protein to vulnerable cell populations.

I have already shown that the CNS, specifically the spinal cord, possesses a significantly slower turnover rate of both soluble and misfolded SOD1 than non-affected tissues. The next logical hypothesis is that different cellular populations within the spinal cord have significantly different SOD1 turnover rates. If SOD1 turnover plays a role in the cellular specificity of disease, then vulnerable motor neuron populations may have the slowest turnover rate of all. After all, motor neurons expressing SOD1 mutants are the most sensitive to proteasome inhibition and play a role in disease onset (Boillée et al. 2006, Puttaparthi et al. 2004). In order to address these questions with SILK, floxed SOD1 knock-in mice could be created and crossed to mice expressing Cre recombinase under cell type specific promoters. These double transgenic mice would then only express SOD1 in motor neurons (ChAT-Cre), all neurons (Thy1.2-Cre), astrocytes (GFAP-Cre), or microglia (Iba1-Cre). Following our established $^{13}C_6$-leucine

labeling paradigm, these animals would be labeled as described in Chapter 3. The human SOD1 immunoprecipitated from tissue lysates would only be from the specific cell types expressing the protein, enabling the measurement of SOD1 turnover in specific cells *in vivo*.

Using SILK to measure SOD1 turnover in patients with dominantly-inherited ALS

Having verified a method to measure SOD1 turnover in the CSF of healthy human subjects, the next step is to measure SOD1 turnover in patients with SOD1 mutations. This will allow us to look at the role of SOD1 turnover in disease as well as monitor SOD1 antisense oligonucleotide therapy (Miller et al. 2013). The ease of orally administering $^{13}C_6$-leucine to human patients over 10 days becomes a significant advantage to conventional intravenous methods, as mobilizing ALS patients to and from the hospital becomes very difficult with advancing disease. Also, our data indicate that we require four CSF collection time points at days 10-14, 26, 42, and 70-80, meaning infrequent trips to the clinic.

Initial studies would involve patients with the SOD1 A4V mutation, as it is the most prevalent in North America at 41% of SOD1 ALS (Andersen et al. 2003). This would enable SOD1 turnover to be measured in a homogenous patient population, as animal and *in vitro* data indicate that mutant turnover is dependent on the degree of protein instability. One potential problem is that SOD1 patients possess both a wild-type and mutant copy of SOD1. However, the A4V mutation occurs within a leucine-containing peptide generated from endoproteinase Glu-C digestion, allowing the differentiation by mass spectrometry of the A4V and WT peptides and thus

simultaneous measurement of both wild-type and A4V mutant protein in human CSF. This would allow one to investigate the role of SOD1 turnover as a function of disease state (i.e. presymptomatic versus symptomatic), age, environment, or mutation status. Although one would expect to find an accelerated turnover rate for A4V relative to wild-type protein in CSF, the more interesting questions relate to the status of the wild-type protein. Wild-type protein is present in SOD1 aggregates, can form heterodimers with certain SOD1 mutants, can be seeded to misfold in the presence of misfolded mutants, and exacerbates disease when co-overexpressed with mutant protein in animal models (Chia et al. 2010, Grad et al. 2011, Prudencio et al. 2010, Witan et al. 2008). Additionally, some groups have observed misfolded SOD1 WT in sporadic ALS patients and familial ALS due to TDP43 and FUS mutations (Bosco et al. 2010, Forsberg et al. 2010, Pokrishevsky et al. 2012). SILK would be a powerful technique to look at the role of SOD1 WT protein in the setting of ALS mutations, familial ALS due to other genes, and sporadic disease.

In closing, this dissertation has described original work in two different facets of SOD1 ALS biology. Chapter 2 detailed the first biochemical characterization of the only two cSOD1 mutants found in canine DM, drawing numerous parallels with hSOD1 mutants that further establish canine DM as an exciting new naturally occurring model for ALS. This model holds immense promise for understanding aspects of the disease that have not been forthcoming from traditional models, such as the role of age and environment on disease, and the data gathered in this dissertation will hopefully serve as a foundation for such future studies. Chapter 3 detailed the first use of SILK to measure SOD1 turnover in both rodent animal models and CSF from healthy human

subjects. In animals, the data indicate that SOD1 is a long-lived protein in the tissues most affected in disease, suggesting a role for protein turnover in the tissue specificity of ALS. In humans, applying the SILK method resulted in the first successful oral labeling approach to measuring a long-lived protein in the CNS and replicated the finding in animals that SOD1 is a long-lived protein in the CNS. Moving forward, SILK will be a powerful tool for looking at SOD1 turnover in additional animal models and human ALS patients with the goal of better understanding SOD1 biology.

REFERENCES

Andersen PM, Sims KB, Xin WW, Kiely R, O'Neill G, et al. 2003. Sixteen novel mutations in the Cu/Zn superoxide dismutase gene in amyotrophic lateral sclerosis: a decade of discoveries, defects and disputes. *Amyotroph. Lateral Scler.* 4(2):62–73

Awano T, Johnson GCGSCS, Wade CM, Katz ML, Taylor JF, et al. 2009. Genome-wide association analysis reveals a SOD1 mutation in canine degenerative myelopathy that resembles amyotrophic lateral sclerosis. *Proc Natl Acad Sci U S A*. 106(8):2794–99

Bateman RJ, Munsell LY, Chen X, Holtzman DM, Yarasheski KE. 2007. Stable isotope labeling tandem mass spectrometry (SILT) to quantify protein production and clearance rates. *J. Am. Soc. Mass Spectrom.* 18(6):997–1006

Bateman RJ, Munsell LY, Morris JC, Swarm R, Yarasheski KE, Holtzman DM. 2006. Human amyloid-beta synthesis and clearance rates as measured in cerebrospinal fluid in vivo. *Nat. Med.* 12(7):856–61

Boillée S, Yamanaka K, Lobsiger CS, Copeland NG, Jenkins N a, et al. 2006. Onset and progression in inherited ALS determined by motor neurons and microglia. *Science*. 312(5778):1389–92

Borchelt DR, Lee MK, Slunt HS, Guarnieri M, Xu ZS, et al. 1994. Superoxide dismutase 1 with mutations linked to familial amyotrophic lateral sclerosis possesses significant activity. *Proc Natl Acad Sci U S A*. 91(17):8292–96

Bosco DA, Morfini G, Karabacak NM, Song Y, Gros-Louis F, et al. 2010. Wild-type and mutant SOD1 share an aberrant conformation and a common pathogenic pathway in ALS. *Nat Neurosci*. 13(11):1396–1403

Brooks KJ, Hill MDW, Hockings PD, Reid DG. 2004. MRI detects early hindlimb muscle atrophy in Gly93Ala superoxide dismutase-1 (G93A SOD1) transgenic mice, an animal model of familial amyotrophic lateral sclerosis. *NMR Biomed.* 17:28–32

Bruijn LI, Becher MW, Lee MK, Anderson KL, Jenkins NA, et al. 1997. ALS-Linked SOD1 Mutant G85R Mediates Damage to Astrocytes and Promotes Rapidly Progressive Disease with SOD1-Containing Inclusions. *Neuron*. 18(2):327–38

Chia R, Tattum MH, Jones S, Collinge J, Fisher EMC, Jackson GS. 2010. Superoxide dismutase 1 and tgSOD1 mouse spinal cord seed fibrils, suggesting a propagative cell death mechanism in amyotrophic lateral sclerosis. *PLoS One*. 5(5):e10627

Cotman CW, Head E. 2008. The canine (dog) model of human aging and disease: dietary, environmental and immunotherapy approaches. *J. Alzheimers. Dis.* 15:685–707

Crisp MJ, Beckett J, Coates JR, Miller TM. 2013. Canine degenerative myelopathy: Biochemical characterization of superoxide dismutase 1 in the first naturally occurring non-human amyotrophic lateral sclerosis model. *Exp. Neurol.* 248:1–9

Dobrowolny G, Aucello M, Rizzuto E, Beccafico S, Mammucari C, et al. 2008. Skeletal muscle is a primary target of SOD1G93A-mediated toxicity. *Cell Metab.* 8(5):425–36

Dupuis L, di Scala F, Rene F, de Tapia M, Oudart H, et al. 2003. Up-regulation of mitochondrial uncoupling protein 3 reveals an early muscular metabolic defect in amyotrophic lateral sclerosis. *FASEB J.* 17:2091–93

Echaniz-Laguna A, Zoll J, Ponsot E, N'Guessan B, Tranchant C, et al. 2006. Muscular mitochondrial function in amyotrophic lateral sclerosis is progressively altered as the disease develops: A temporal study in man. *Exp. Neurol.* 198:25–30

Farr GW, Ying Z, Fenton W a, Horwich AL. 2011. Hydrogen-deuterium exchange in vivo to measure turnover of an ALS-associated mutant SOD1 protein in spinal cord of mice. *Protein Sci*. 20(10):1692–96

Forsberg K, Jonsson PA, Andersen PM, Bergemalm D, Graffmo KS, et al. 2010. Novel antibodies reveal inclusions containing non-native SOD1 in sporadic ALS patients. *PLoS One*. 5:

Grad LI, Guest WC, Yanai A, Pokrishevsky E, O'Neill M a, et al. 2011. Intermolecular transmission of superoxide dismutase 1 misfolding in living cells. *Proc. Natl. Acad. Sci. U. S. A.* 108(39):16398–403

Grad LI, Yerbury JJ, Turner BJ, Guest WC, Pokrishevsky E, et al. 2014. Intercellular propagated misfolding of wild-type Cu/Zn superoxide dismutase occurs via exosome-dependent and -independent mechanisms. *Proc. Natl. Acad. Sci. U. S. A.* 111(9):3620–25

Green SL, Tolwani RJ, Varma S, Quignon P, Galibert F, et al. 2002. Structure, chromosomal location, and analysis of the canine Cu/Zn superoxide dismutase (SOD1) gene. *J Hered*. 93(2):119–24

Hayward LJ, Rodriguez J a, Kim JW, Tiwari A, Goto JJ, et al. 2002. Decreased metallation and activity in subsets of mutant superoxide dismutases associated with familial amyotrophic lateral sclerosis. *J. Biol. Chem.* 277(18):15923–31

Head E. 2013. A canine model of human aging and Alzheimer's disease. *Biochim. Biophys. Acta*. 1832:1384–89

Hoffman EK, Wilcox HM, Scott RW, Siman R. 1996. Proteasome inhibition enhances the stability of mouse Cu/Zn superoxide dismutase with mutations linked to familial amyotrophic lateral sclerosis. *J Neurol Sci*. 139(1):15–20

Huang C, Xia PY, Zhou H. 2010. Sustained expression of TDP-43 and FUS in motor neurons in rodent's lifetime. *Int. J. Biol. Sci.* 6:396–406

Jacobsson J, Jonsson P a, Andersen PM, Forsgren L, Marklund SL. 2001. Superoxide dismutase in CSF from amyotrophic lateral sclerosis patients with and without CuZn-superoxide dismutase mutations. *Brain*. 124(Pt 7):1461–66

Johnston J a, Dalton MJ, Gurney ME, Kopito RR. 2000. Formation of high molecular weight complexes of mutant Cu,Zn-superoxide dismutase in a mouse model for familial amyotrophic lateral sclerosis. *Proc. Natl. Acad. Sci.* 97(23):12571–76

Jonsson PA, Ernhill K, Andersen PM, Bergemalm D, Brännström T, et al. 2004. Minute quantities of misfolded mutant superoxide dismutase-1 cause amyotrophic lateral sclerosis. *Brain*. 127(Pt 1):73–88

Keller JN, Hanni KB, Markesbery WR. 2000. Possible involvement of proteasome inhibition in aging: implications for oxidative stress. *Mech. Ageing Dev.* 113(1):61–70

Krasnianski A, Deschauer M, Neudecker S, Gellerich FN, M??ller T, et al. 2005. Mitochondrial changes in skeletal muscle in amyotrophic lateral sclerosis and other neurogenic atrophies. *Brain*. 128:1870–76

Leclerc N, Ribera F, Zoll J, Warter JM, Poindron P, et al. 2001. Selective changes in mitochondria respiratory properties in oxidative or glycolytic muscle fibers isolated from G93AhumanSOD1 transgenic mice. *Neuromuscul. Disord.* 11:722–27

Li S-H, Schilling G, Young WS, Li X-., Margolis RL, et al. 1993. Huntington's disease gene (IT15) is widely expressed in human and rat tissues. *Neuron*. 11(5):985–93

Miller TM, Pestronk A, David W, Rothstein J, Simpson E, et al. 2013. An antisense oligonucleotide against SOD1 delivered intrathecally for patients with SOD1 familial amyotrophic lateral sclerosis: A phase 1, randomised, first-in-man study. *Lancet Neurol.* 12:435–42

Münch C, Bertolotti A. 2010. Exposure of Hydrophobic Surfaces Initiates Aggregation of Diverse ALS-Causing Superoxide Dismutase-1 Mutants. *J. Mol. Biol.* 399(3):512–25

Münch C, O'Brien J, Bertolotti A. 2011. Prion-like propagation of mutant superoxide dismutase-1 misfolding in neuronal cells. *Proc. Natl. Acad. Sci. U. S. A.* 108(9):3548–53

Pokrishevsky E, Grad LI, Yousefi M, Wang J, Mackenzie IR, Cashman NR. 2012. Aberrant localization of FUS and TDP43 is associated with misfolding of SOD1 in amyotrophic lateral sclerosis. *PLoS One*. 7:

Prudencio M, Durazo A, Whitelegge JP, Borchelt DR. 2010. An examination of wild-type SOD1 in modulating the toxicity and aggregation of ALS-associated mutant SOD1. *Hum Mol Genet*. 19(24):4774–89

Puttaparthi K, Wojcik C, Rajendran B, DeMartino GN, Elliott JL. 2004. Aggregate formation in the spinal cord of mutant SOD1 transgenic mice is reversible and mediated by proteasomes. *J. Neurochem.* 87(4):851–60

Ramesh T, Lyon AN, Pineda RH, Wang C, Janssen PML, et al. 2010. A genetic model of amyotrophic lateral sclerosis in zebrafish displays phenotypic hallmarks of motoneuron disease. *Dis Model Mech*. 3(9-10):652–62

Rankin KS, Starkey M, Lunec J, Gerrand CH, Murphy S, et al. 2012. Of dogs and men: comparative biology as a tool for the discovery of novel biomarkers and drug development targets in osteosarcoma. *Pediatr Blood Cancer*. 58(3):327–33

Ratovitski T, Corson LB, Strain J, Wong P, Cleveland DW, et al. 1999. Variation in the biochemical/biophysical properties of mutant superoxide dismutase 1 enzymes and the rate of disease progression in familial amyotrophic lateral sclerosis kindreds. *Hum Mol Genet*. 8(8):1451–60

Ravits JM, La Spada AR. 2009. ALS motor phenotype heterogeneity, focality, and spread: deconstructing motor neuron degeneration.

Rowell JL, McCarthy DO, Alvarez CE. 2011. Dog models of naturally occurring cancer. *Trends Mol Med*. 17(7):380–88

Ruizeveld de Winter JA, Trapman J, Vermey M, Mulder E, Zegers ND, van der Kwast TH. 1991. Androgen receptor expression in human tissues: an immunohistochemical study. *J. Histochem. Cytochem.* 39(7):927–36

Sakowski S a, Lunn JS, Busta AS, Oh SS, Zamora-Berridi G, et al. 2012. Neuromuscular effects of G93A-SOD1 expression in zebrafish. *Mol. Neurodegener.* 7(1):44

Sephton CF, Good SK, Atkin S, Dewey CM, Mayer P, et al. 2010. TDP-43 is a developmentally regulated protein essential for early embryonic development. *J. Biol. Chem.* 285(9):6826–34

Tiwari A, Hayward LJ. 2003. Familial amyotrophic lateral sclerosis mutants of copper/zinc superoxide dismutase are susceptible to disulfide reduction. *J Biol Chem*. 278(8):5984–92

Tsvetkov AS, Arrasate M, Barmada S, Ando DM, Sharma P, et al. 2013. Proteostasis of polyglutamine varies among neurons and predicts neurodegeneration. *Nat. Chem. Biol.* 9(9):586–92

Wang J, Slunt H, Gonzales V, Fromholt D, Coonfield M, et al. 2003. Copper-binding-site-null SOD1 causes ALS in transgenic mice: aggregates of non-native SOD1 delineate a common feature. *Hum Mol Genet*. 12(21):2753–64

Wang J, Xu G, Borchelt DR. 2002. High Molecular Weight Complexes of Mutant Superoxide Dismutase 1: Age-Dependent and Tissue-Specific Accumulation. *Neurobiol. Dis.* 9(2):139–48

Wang J, Xu G, Li H, Gonzales V, Fromholt D, et al. 2005. Somatodendritic accumulation of misfolded SOD1-L126Z in motor neurons mediates degeneration: alphaB-crystallin modulates aggregation. *Hum. Mol. Genet.* 14(16):2335–47

Watanabe Y, Yasui K, Nakano T, Doi K, Fukada Y, et al. 2005. Mouse motor neuron disease caused by truncated SOD1 with or without C-terminal modification. *Brain Res. Mol. Brain Res.* 135(1-2):12–20

Wiedemann FR, Winkler K, Kuznetsov A V, Bartels C, Vielhaber S, et al. 1998. Impairment of mitochondrial function in skeletal muscle of patients with amyotrophic lateral sclerosis. *J. Neurol. Sci.* 156:65–72

Winer L, Srinivasan D, Chun S, Lacomis D, Jaffa M, et al. 2013. SOD1 in cerebral spinal fluid as a pharmacodynamic marker for antisense oligonucleotide therapy. *JAMA Neurol.* 70:201–7

Wininger FA, Zeng R, Johnson GS, Katz ML, Johnson GC, et al. 2011. Degenerative myelopathy in a Bernese Mountain Dog with a novel SOD1 missense mutation. *J Vet Intern Med*. 25(5):1166–70

Witan H, Kern A, Koziollek-Drechsler I, Wade R, Behl C, Clement AM. 2008. Heterodimer formation of wild-type and amyotrophic lateral sclerosis-causing mutant Cu/Zn-superoxide dismutase induces toxicity independent of protein aggregation. *Hum. Mol. Genet.* 17(10):1373–85

Wong M, Martin LJ. 2010. Skeletal muscle-restricted expression of human SOD1 causes motor neuron degeneration in transgenic mice. *Hum. Mol. Genet.* 19(11):2284–2302

Zetterström P, Graffmo KS, Andersen PM, Brännström T, Marklund SL. 2011. Proteins that bind to misfolded mutant superoxide dismutase-1 in spinal cords from transgenic amyotrophic lateral sclerosis (ALS) model mice. *J. Biol. Chem.* 286(23):20130–36

Zetterström P, Stewart HG, Bergemalm D, Jonsson PA, Graffmo KS, et al. 2007. Soluble misfolded subfractions of mutant superoxide dismutase-1s are enriched in

spinal cords throughout life in murine ALS models. *Proc. Natl. Acad. Sci. U. S. A.* 104(35):14157–62

CURRICULUM VITAE

M a t t h e w J . C r i s p
Washington University in St. Louis
School of Medicine
Phone: 314-616-3147
crispm@wusm.wustl.edu

Education

Washington University in St. Louis School of Medicine, St. Louis, MO
MD/PhD candidate (Expected May 2016)
Medical Scientist Training Program
Graduate Program: Neuroscience

Washington College, Chestertown, MD
Bachelor of Science (May 2006)
GPA: 3.973
Majors: Biochemistry, Behavioral Neuroscience
Minor: Chemistry

Research Experience

Medical Scientist Training Program 2008-Present
Washington University School of Medicine, St. Louis, MO
PI – Timothy Miller, MD PhD
Dissertation: Superoxide dismutase 1: Novel insights on disease models and tissue specificity in amyotrophic lateral sclerosis

Intramural Research Training Award Post-baccalaureate Fellow 2006-2008
National Cancer Institute/NIH, Bethesda, MD
PI – Munira Basrai, PhD
Project description: Determining how the centromere-specific histone variant Cse4p regulates mitotic fidelity

Interdepartmental Senior Research Thesis 2005-2006
Washington College, Chestertown, MD
PI – Michael Kerchner, PhD
Honors Thesis: Effects of a 5-HT_3 agonist and antagonist on inter-male aggression in Mus musculus

Summer Internship Program in Biomedical Research Summer 2005
National Institute of Neurological Disorders and Stroke/NIH,

Bethesda, MD
PI – Zu-Hang Sheng, PhD
Project description: The role of microtubule-associated protein 2A light chain in L-type calcium channel localization to the synapse

National Science Foundation's Research Experience for Undergraduates — Summer 2004
Davidson College, Davidson, NC
PI – Barbara Lom, PhD
Project description: Elucidating the role of fibroblast growth factor 2 on retinal ganglion cell migration to the optic tectum

Honors and Awards

2015 Alpha Omega Alpha
2014 Best Talk at Medical Scientist Training Program Annual Retreat
2012 National Institutes of Health NINDS Ruth L. Kirschstein Predoctoral National Research Service Award # F31NS078818
2006 B.S. Biochemistry and Neuroscience Summa Cum Laude, Washington College
2006 Departmental Honors in Biology, Washington College
2006 Departmental Honors in Psychology, Washington College
2006 The Biology Department Award of Special Recognition, Washington College
2006 The Psychology Department Capstone Experience Award, Washington College
2002 Advanced Placement Scholar with Honors
2002 Maryland Distinguished Scholar Honorable Mention
2002 Maryland Senatorial Scholarship
2002 Merit Scholarship, Washington College

Teaching Experience

Teaching Assistant (2012-2014) – Human Anatomy
Washington University School of Medicine, St. Louis, MO
Program in Physical Therapy

Kaplan MCAT/DAT/OAT Instructor (2007-2014)
Bethesda Kaplan Center, Bethesda, MD
St. Louis Kaplan Center, St. Louis, MO

Teaching Assistant (Fall 2010) – Human Anatomy and Development
Washington University School of Medicine, St. Louis, MO

First year medical students

Peer-Reviewed Publications

1. Sato, C., Mawuenyega, K.G., Barthelemy, N., Patterson, B.W., Jockel-Balsarotti, J., Crisp, M.J., Kasten, T., Chott, R., Yarasheski, K.E., Karch, C.M., Miller, T.M., Bateman, R.J. Tau kinetics in the human central nervous system. *In preparation*.

2. Crisp, M.J., Mawuenyega, K.G., Patterson, B.W., Reddy, N.C., Chott, R., Self, W.K. Weihl, C.C., Jockel-Balsarotti, J., Varadachary, A., Buccelli, R., Yarasheski, K.E., Bateman, R.J., Miller, T.M. In vivo kinetic approach reveals slow SOD1 turnover in the CNS. **J Clin Invest 2015**; [Epub ahead of print] PMID: 26075819

3. Choy, J., O'Toole, E., Schuster, B., Crisp, M., Karpova, T., McNally, J., Winey, M., Gardner., Basrai, M. Genome-wide Haploinsufficiency Screen Reveals a Novel Role for γ-TuSC in Spindle Organization and Genome Stability. **Mol Biol Cell**. **2013**; 24(17):2753-63 PMID: 23825022

4. Crisp, M., Beckett, J., Coates, J., Miller, T. Canine Degenerative Myelopathy: Biochemical characterization of superoxide dismutase 1 in the first naturally occurring non-human amyotrophic lateral sclerosis (ALS) model. **Exp Neurol 2013**; 248:1-9 PMID: 23707216

5. Miller, T., Pestronk, A., David, W., Rothstein, J., Simpson, E., Andres, P., Mahoney, K., Allred, P., Alexander, K., Ostrow, L., Schoenfeld, D., Macklin, E., Norris, D., Manousakis, G., Crisp, M., Smith, R., Bennett, C., Bishop, K., Cudkowicz, M. A Phase I, First-in-Human Study of an Antisense Oligonucleotide Directed Against SOD1 Delivered Intrathecally in SOD1-Familial ALS Patients. **Lancet Neurol 2013**; 12(5):435-442 PMID: 23541756

6. Stirling, P., Crisp, M., Basrai, M., Tucker, C., Dunham, M., Spencer, F., Hieter, P. Mutability and mutational spectrum of chromosome transmission fidelity genes. **Chromosoma 2012**;121(3):263-275 PMID: 22198145

7. Au, W.*, Crisp, M.*, DeLuca, S.*, Rando, O., Basrai, M. Altered dosage and mislocalization of histone H3 and Cse4p lead to chromosome loss in *Saccharomyces cerevisiae.* **Genetics 2008**;179(1):263-75 PMID: 18458100 [*co-first authors]

8. Crisp, M. & Kerchner, M. Effects of a 5-HT_3 agonist and antagonist on inter-male aggression in Mus musculus. *Impulse: The Premier Journal for Undergraduate Publications in the Neurosciences.* 2006

Conference Abstracts and Talks

Stable isotope labeling kinetics reveal tissue-specific differences in SOD1 turnover in an ALS animal model

- Medical Scientist Training Program Annual Retreat (April 2014) – Awarded Best Talk

Canine Degenerative Myelopathy: Biochemical characterization of superoxide dismutase 1 (SOD1) in the first non-human sporadic amyotrophic lateral sclerosis (ALS) model.

- New Frontiers in Neurodegenerative Disease Research, Keystone Symposium, Santa Fe, NM February 4th, 2013
- Neuroscience Retreat, Washington University in St. Louis, St. Louis, MO (Sept 2012)

Global identification of genes haploinsufficient for chromosome stability in S. cerevisiae

- Washington Area Yeast Meeting, National Institutes of Health, May 14th, 2008
- Genetics Branch Scientific Retreat, National Institutes of Health, November 15th, 2007

Chromosome transmission defect – A consequence of imbalanced expression and mislocalization of histone H3 and its variant, Cse4p

- 20th NIH Research Festival, National Institutes of Health, September 25th-28th, 2007
- Yeast Cell Biology, Cold Spring Harbor Laboratory, August 15th-19th, 2007